A SEMI-ANALYTICAL APPROACH TO OBTAIN PHYSICAL FIELDS IN HETEROGENEOUS MATERIALS

by

THANUJ S PATHAPALLI

Presented to the Faculty of the Graduate School of

The University of Texas at Arlington in Partial Fulfillment

of the Requirements

for the Degree of

DOCTOR OF PHILOSOPHY

THE UNIVERSITY OF TEXAS AT ARLINGTON

May 2013

ACKNOWLEDGEMENTS

I would like to thank my committee chair Professor Nomura, for his patience and time, not to mention his continual support and intellectual poise during the entire course of this dissertation. Without his guidance and persistent help this dissertation would not have been possible. I would also like to express my gratitude to the committee members, Professor Lawrence, Professor Haji-Sheikh, Professor Chan and Professor Dancila for their invaluable time and support. Thank you all.

April 19, 2013

ABSTRACT

A SEMI-ANALYTICAL APPROACH TO OBTAIN PHYSICAL FIELDS

IN HETEROGENEOUS MATERIALS

Thanuj S Pathapalli, PhD

The University of Texas at Arlington, 2013

Supervising Professor: Seiichi Nomura

Predicting the macroscopic response of heterogeneous materials has been the subject of extensive research in the engineering community, even more so, in the composites guild. With analytical solutions being almost impossible to obtain for such open ended problems, and numerical techniques being computationally expensive, semi-analytical methods are highly sought after. This dissertation is one such effort aimed at presenting a semi-analytical approach that serves as a confluence of effective analytical and numerical techniques, to solve for engineering fields in a heterogeneous material characterized by inclusions embedded in a matrix medium. The approach essentially involves the analytical derivation of permissible functions, in terms of geometrical and material parameters, which satisfy the peripheral and interface conditions, followed by an appropriate approximation maneuver that furnishes an expression for the physical field of interest. The semi-analytical solutions so obtained are corroborated by FEM solutions. The effectiveness of the approach is demonstrated by means of suitable examples. Two case studies have been deliberated upon – one is the 2-D Poisson type equation that essentially describes the steady state heat conduction with volumetric heat generation, and the other is the 2-D stress equilibrium equation with body forces.

TABLE OF CONTENTS

LIST OF ILLUSTRATIONS

LIST OF TABLES

CHAPTER 1

INTRODUCTION

Most of the fundamental physical processes in nature can be AMUSEd – Approximated, Modeled, Understood, Simplified and Explained using partial differential equations (PDEs) [1]. Its origin can be traced back to the 18^{th} century, amidst an era of industrial revolution, when PDEs began to be recognized as a pivotal tool in analyzing physical systems and describing continuous media. In 1752, a vibrating string model was analyzed by d'Alembert [2] that led to the development of the renowned wave equation. An extension of this work by Euler [2] in 1759, and later on by Bernoulli [2] in 1762, resulted in the two and three dimensional wave equations. In 1780, Laplace [2] studied the gravitational potential fields, a precursor to the Laplace equation. Besides the afore-mentioned paradigmatic equations, the heat equation by Fourier [2] (1810-1822) and the linear elasticity equations for solids by Navier [2] (1821) and Cauchy [2] (1822), among others, were able to describe other significant physical phenomena in the form of comprehensive and concrete mathematical models.

The physical processes, described above, and their respective models were constructed on a foundation, which assumed that the associated media is continuous rather than a composition of discrete elementary (or indivisible) particles. This kind of analysis based on the idealization (or approximation) of a material, popularly referred to as continuum mechanics [3] defines the continuum as a region (in space) of continuous matter that can be fragmented into a number of infinitesimal elements (elements large enough to accommodate a significant number of indivisible particles) that exhibit properties averaged over a given length and time scale such that engineering fields (such as temperature, stress, strain etc.) vary smoothly or tend to a definite limit. Thus continuum mechanics describes the motion of such a continuum in response to the forces influencing it and is applicable to problems in which the fine

structure of the material can be ignored. Since its inception in the latter part of the 1700s, this relatively green branch of mechanics experienced a phenomenal growth in the early 1900s and by the 1950s, continuum mechanics became a seasoned vehicle effortlessly describing the physical properties of a material in terms of constitutive equations [3] and expressing the fundamental physical laws of conservation in terms of field equations [3] while providing solutions to a wide range of practical problems on a macroscopic scale. Apart from its quintessential assumption, an underlying factor for its astonishing success in the fields of applied mathematics and engineering was its unyielding inclination towards tensors [3], with which equations governing physical processes, expressed in terms of material properties and physical fields, could be concisely represented as an identity that relates scalars and vectors bound by certain inherent properties, that allowed for the general validity of these equations irrespective of the frame of reference.

One of the initial and most successful outcomes of continuum mechanics, in conjunction with material science, was the development of fracture mechanics. In 1913, C. E. Inglis [4] examined a thin glass plate with an elliptical hole in the center, subjected to uniaxial loads perpendicular to the major axis of the ellipse, and observed that the stress at the tip of hole could be much larger than the applied stress. His work can be considered as one of the first studies into the spectrum of inhomogeneity. In the 1920s, A. A. Griffith [4] laid down the rudimentary notion of crack growth and its relation to the potential energy of the system that initiated the theory of fracture mechanics which in turn opened up a new portal for systematically examining and studying deformation and failure behavior of solids (with certain microstructures) under loading. This led to the emergence of a new domain called micromechanics [5, 6]. In contrast to continuum mechanics that deals with idealized materials made up of material elements [5], and their infinitesimal material neighborhood [5] within which the material distribution and the continuum fields are assumed to be uniform, micromechanics proposes the analysis and modeling of engineering materials in a heterogeneous framework. In

general, most materials used in structural applications and other engineering practices are rarely homogeneous, even more so in terms of their microstructure due to the presence of micro-heterogeneities such as voids and inclusions. Thus, in order to launch a fair investigation into the macroscopic behavior of these materials, it becomes necessary to describe the continuum quantities [5] associated with an infinitesimal material neighborhood in terms of its microstructural properties.

Micromechanics establishes this “macro-micro correlation” through the concept of a representative volume element (RVE) [5]. In a continuous media, an RVE for a material point represents the infinitesimal material neighborhood of that material point. The infinitesimal material neighborhood (RVE) is called a macro element and its micro-constituents are called micro elements. An RVE must include a significantly large number of micro elements for it to undergo homogenization [5] i.e. to describe the overall response and properties of the macro element in terms of the properties of its microelements. In essence, the optimum choice of an RVE is paramount in determining its effectiveness in a sense that an RVE should be small enough from a macroscopic point of view so that it can be treated as a material point in a continuum, hence yielding a simple continuous model. And at the same time it must be large enough from a microscopic perspective so as to accommodate a large number of micro constituents/inhomogeneities so as to effectively represent the microstructure of the continuum. In view of the above exposition, it is but reasonable to claim that micromechanics revolves around a pivot that essentially deals with composite (or heterogeneous) materials.

A rather simple description of a heterogeneous material is that it is a composition of two or more distinct constituents/phases at a macroscopic level. The term “distinct” implies that the constituent materials exhibit different material properties. From an engineering perspective, the definition of a composite material is best described in ASTM D 3878-95c [6]: “Composite material. A substance consisting of two or more materials, insoluble in one another, which are combined to form a useful engineering material possessing certain properties not possessed by

the constituents." Predicting the macroscopic response of such materials can be achieved by understanding their microstructure that leads to the theory of mechanics of materials, or simply micromechanics. Hence, in essence, the theory of micromechanics involves the application of continuum mechanics and numerical/analytical tools to study the response of heterogeneous materials on the basis of the geometrical and material parameters of the individual constituents, hence eliminating the need to resort to time consuming and expensive physical tests.

The formal inception of micromechanics dates back to the late 1950s when J.D. Eshelby [7, 8 , 9] laid down the conceptual framework for treating inclusion or inhomogeneity problems in an infinitely extended homogeneous elastic medium by means of an ingenious yet simple set of "imaginary cutting, straining and welding operations." His work, in 1957 [7], on the determination of the elastic field of an ellipsoidal inclusion embedded in an infinitely extended homogeneous isotropic medium is considered to be one of his most revered accomplishments. He introduced the novel concepts of equivalent inclusion and the associated eigenstrain (non-elastic strain), and found that the elastic fields within an ellipsoidal inclusion/inhomogeneity were uniform and established expressions for the same, in the form of tabulated elliptic integrals. This classical result, compounded with the versatility of the ellipsoidal geometry in approximating heterogeneities, has been extensively exercised in the modeling of macroscopic (effective) properties of fiber reinforced and random fiber reinforced composites, among other applications in metallurgy.

For this very reason, for the last sixty odd years or so, this particular work of his has been the most cited reference in micromechanics and referred to, by many, as the elasticity solution of the century. In 1959, Eshelby [8] extended the results from his previous work (1957) by primarily focusing on the elastic field outside an inclusion/inhomogeneity and was able to express it in terms of the harmonic potential of an ellipsoid. Having established expressions for the elastic fields, both inside and outside an inclusion, in a very comprehensive manner, Eshelby [9] went on to study the interaction between two inclusions embedded in a

matrix.These investigations carved out a strong basis upon which expansive studies have been carried out on elastic solids with inhomogeneities/inclusions.

In 1961, Jawson and Bhargava [10], while pointing out a major limitation of Eshelby's three-dimensional method of solution in that it involved integrals that were 'analytically intractable', provided an account of Eshelby's point force method, and of his equations of equivalent inclusion, based upon which, they applied the complex variable formalism, to obtain explicit solutions for two-dimensional elastic inclusion problems. Two years later, Bhargava and Radhakrishna [11], worked on two-dimensional elliptical inclusions to determine the elastic field in an infinite material surrounding the inclusion by applying the concepts of minimum potential energy in the classical theory of elasticity, and the previously exercised method of complex variables. In 1966, List and Silberstien [12], while addressing certain complexities involved in the two dimensional solution provided by Jawson and Bhargava [10], derived a system of equations for determining the elastic fields in an inclusion-finite matrix set up, described a method to obtain the exact solution of these system of equations, and solved a problem of a square inclusion, with rounded corners, in an infinite matrix. However, in this generalization, the inclusion (or discs) and matrix (or plate) have the same elastic constants.

The methods suggested by Jawson and Bhargava [10], and Bhargava and Radhakrishna [11], though dissimilar, essentially focused on the same problem of an elliptical inclusion in an infinite matrix, with different material properties. And each of these approaches was bound by certain restrictions. The former method [10] was unable to provide a solution unless the elastic field inside the inclusion was a constant, and the latter technique [11] was limited to an ellipse for which a relatively modest mapping function exists. These restrictions were made void by Rizzo and Shippy [13] in 1968 when they presented a novel formulation, in terms of boundary tractions and displacements, for the general non-homogeneous elastic inclusion problem, that could be administered without limitations on the number, shape or material composition of the inclusions embedded in a matrix. The formulation, based on a

fundamental solution of the equations of linear elasticity, resulted in a system of singular integral equations/boundary functional equations, the number of equations being equal to the number of the non-intersecting contours or distinct phases, that were solved numerically using the Boundary Element Method (BEM). A trial problem involving an elliptic inclusion in an infinite matrix, of a different material, was subsequently solved and compared with the results obtained from Jawson and Bhargava [10]. In addition to the test problem, two unsolved problems were considered. The first problem was that of an elliptic inclusion within a finite circular matrix and the second was that of a regular square inclusion in an infinite matrix. The results from the latter were compared with the data from List and Silberstein [12]. Though this solution procedure yields a reasonably good accuracy for a moderate approximation of the boundary, the method is more suited to treat geometrically symmetric problems and requires the prior knowledge of an appropriate fundamental solution.

List [14], in 1969, used the complex variable technique introduced by Muskhelishvili [15], and was able to determine the elastic fields in an elastic circular inclusion and its surrounding infinite dissimilar elastic matrix when either of the two phases was subjected to a concentrated force or the influence of an edge dislocation. The Muskhelishvili's technique is the same approach as employed in [10], [11], and [12] in which the stress and displacement components were expressed in terms of complex analytic functions. In 1973, the same problem, with the exception that the geometrical set up now involved two symmetrically located cracks instead of the concentrated force/edge dislocation, was solved by Bhargava and Bhargava [16] using the Muskhelishvili's technique. An interesting feature in both of the above presentations, [14] and [16], was the introduction of two sets of complex analytic functions to account for the dissimilarity in the inclusion and matrix material properties.

In 1976, as an extension of the results obtained by J.D. Eshelby [7, 8, 9], T. Mura, T. Mori and M.Kato [17, 18] investigated and obtained a solution for the elastic field throughout an ellipsoidal inclusion in an indefinitely-extended anisotropic material for the case of a periodically

distributed eigenstrain throughout the inclusion and applied the results to martensite formation. Minoru Taya and Tsu-Wei Chou [19], in 1981, as an application to a hybrid composite, studied and formulated the problem of two kinds of ellipsoidal inhomogeneities embedded in an elastic body using Eshelby's equivalent inclusion method and Mori-Tanaka's back stress analysis. In 1983, T. Iwakuma and S. Nemat-Nasser [20] studied an elastic body containing periodically distributed inhomogeneities and developed a generalized procedure for estimating the overall properties of the composite in terms of several infinite series and used the results to estimate the overall elastic moduli of composites with ellipsoidal voids or elastic inclusions.

Seiichi Nomura and Tsu-Wei Chou [21], in 1985, examined the viscoelastic behavior of short-fiber composites by approximating them using ellipsoidal elastic inclusions (fibers) embedded in a viscoelastic matrix based upon a modified version of their previous work, and provided numerical examples for various aspect ratios with the aid of the collocation approximation method. In the same year, Seiichi Nomura and Nobunori Oshima [22] addressed an analytical method to estimate the overall behavior of fiber-reinforced hybrid composites by introducing an "equivalent virtual volume fraction" to the formerly developed two-phase model. In 1986, Hiroshi Hatta and Minoru Taya [23] proposed a method based upon Eshelby's equivalent inclusion method to solve steady state heat conduction problems in composites by drawing an analogy to stress, strain and stiffness, with heat flux, temperature gradient and thermal conductivity, respectively.

Gregory J. Rodin and Yuh-Long Hwang [24], in 1991, extended the method of Kachanov, for interacting cracks, to the domain of Eshelby's equivalent inclusion method, and attacked the linear elasticity problem for an infinite region containing a finite number of non-intersecting ellipsoidal inhomogeneities. Although the adopted approach was useful in predicting the overall response of composite materials and interfacial stress concentrations, a major limitation was that the continuity conditions at the interfaces were only approximately satisfied. Muneo Hori and Sia Nemat-Nasser [25], in 1993, proposed a new averaging scheme

employing the double-inclusion model (nested inclusions embedded in an infinite uniform elastic solid) to analytically estimate the average field quantities and hence the overall moduli of multi-phase composites. Another method was proposed by Gregory J. Rodin [26], in the same year, in which a system of integral equations formulated for a representative volume element was approximated by a system of linear algebraic equations, in order to determine the overall elastic response of an isotropic matrix with non-intersecting spherical inhomogeneities. In 1994, with the application of Green's function, quasi-newtonian, quasi-biharmonic and quasi-harmonic potentials, along with the already well-established Eshelby's equivalent inclusion method, a new technique was introduced by H.Y. Yu, S.C. Sanday and C.I. Chang [27] that applied a new stress vector function called the hexagonal stress vector to obtain the induced elastic fields due to an inclusion in transversely isotropic solids.

T. Mura [17, 28], in 1997, determined the elastic field of a polygonal star shaped inclusion and confirmed his results experimentally by photoelasticity method. In 1999, Han Xueli and Wang Tzuchiang [29], illustrated the "pseudo-dislocations method" for obtaining the solution to two-dimensional elastic fields in an infinite medium containing any number of inhomogeneities under far field loadings, by reducing the inhomogeneities problem to a set of linear algebraic equations. In the same year, in an effort to compute the effective moduli of heterogeneous materials, Muneo Hori and Sia Nemat-Nasser [30] reviewed and compared two micromechanics theories, namely the average-field theory and the homogenization theory, and in turn proposed a hybrid micromechanics theory that led to a more accurate determination of the effective moduli of heterogeneous solids. S. Li, R.Sauer and G. Wang [31], in 2005, developed a novel solution procedure to determine elastic fields in a heterogeneous set-up comprising of a 2-D circular inclusion in a finite, circular RVE, subjected to displacement (Dirichlet) boundary conditions by introducing an algebraic operator called the Dirichlet-Eshelby tensor. Despite some immediate applications of this tensor, the technique is limited by its application capability to Fredholm type integral equation, geometrical symmetry and other

factors. Nicolas Brusselaars, Sofia G. Mogilevskaya, and Steven L. Crouch [32], in 2007, presented a semi-analytical approach to calculate elastic fields in a system consisting of multiple circular inhomogeneities in one of two joined infinite isotropic elastic half-planes, through the application of truncated complex Fourier series and Taylor series expansion. However, this method requires integral equations that are obtained using the corresponding fundamental solutions, a prior knowledge of which becomes imperative.

Most of the methods mentioned above are bound by certain constraints that are pertinent to the very nature of the adopted technique. However, time and again, over the past few decades, micromechanics has proven to be a very effective tool for analyzing inclusions/inhomogeneities in composite materials, and continues to do so. However, the application of micromechanics to inclusion problems is bound by an unrealistic premise that the inclusions are uniformly distributed in the medium which suggests that the heterogeneous material is homogenized, thus making it inconvenient to accurately represent general heterogeneous materials. Furthermore, most of the available literature, with regard to determining physical fields in heterogeneous materials, was conceptualized from J.D. Eshelby's pioneering work that has shaped the field of micromechanics for the last fifty odd years. Needless to say, it was his contribution, specifically, his work on ellipsoidal inclusions that provided the initial motivation behind the framework of this dissertation. However, with regard to the works of J.D. Eshelby and those of others that followed, the medium is assumed to be infinitely extended i.e. no boundaries. In actuality, the medium has a finite boundary and the distribution of inclusions is not homogeneous. Although, such media can be solved using numerical techniques such as the finite element method; numerical schemes can turn out to be a computationally expensive enterprise. Hence, analytical or semi-analytical solutions, if available, are highly sought-after. Semi-analytical solutions, which fall in a category intermediate to numerical and analytical techniques, appear to be a more practical choice since analytical solutions are virtually impossible to contrive, for such open ended problems.

Over the past, various methods have been devised by physicists and mathematicians to find solutions to boundary value problems (BVPs). For some of the simplified differential equations, analytical (exact) solutions are readily available. In conductive heat transfer, one of the well-known and commonly used analytical techniques to solve the diffusion equation is the classical separation of variables method that can be applied directly to linear homogenous boundary BVPs with homogenous boundary conditions, but this method has limited applicability with respect to the fact that it cannot solve BVPs with non-homogenous conditions.

Another method that is becoming increasingly popular in solving transient and steady-state heat conduction problems is the Green's function solution method [33]. This method can be applied to homogenous and non-homogenous materials and is independent of the coordinate system. The Fourier series method is another widely used quasi-analytical technique that allows the solution to be expressed in terms of an infinite sum of trigonometric functions (for a problem in the Cartesian coordinate system), or in terms of special functions such as the Bessel functions (for a problem in the polar coordinate system), and it can also be extended to solve problems in the spherical coordinate system, by employing Legendre polynomials. However, this method is not recommended for non-homogeneous materials or problems with complex geometries.

More often than not, it becomes absolutely imperative to adopt approximation methods, when an analytical solution does not exist. One such numerical technique that was introduced in 1915 by a Russian mathematician, Boris Galerkin, is the Galerkin method [34], which is a subclass of the Method of Weighted Residuals (MWR). This method acts as an effective tool in transforming differential equations into a problem in linear algebra, hence converting the original problem into a finite-dimensional linear system thus making the solution process more facile. Compared to other weighted residual methods (MWRs), the Galerkin method ascertains the convergence of the solution for an adequate number of terms and has been considerably used to solve problems in heat transfer and fluid flow.

This dissertation presents a semi-analytical method for solving boundary value problems (BVPs) in heterogeneous materials that makes use of both analytical and numerical techniques to obtain the mechanical/physical fields associated with the given BVP. Furthermore, the proposed approach clearly distinguishes the inclusion and matrix as two distinct phases and accommodates the existence of a finite boundary. The approach involves analytically deriving a set of continuous permissible functions, in terms of the geometrical and material constants, that satisfy the boundary conditions and continuity conditions at the matrix-inclusion interface, employing an appropriate approximation technique to obtain a set of orthonormal eigenfunctions, or a set of unknown coefficients, and finally expressing the unknown physical field as a linear combination of the eigenfunctions or permissible functions.

In order to facilitate the analytical derivation of the permissible functions in terms of the relevant material and geometrical parameters, which is a very tedious and time consuming process, a computer algebra system, *Mathematica* [35], has been extensively used. *Mathematica* is basically a symbolic computation program with a wide purview of capabilities that include number-crunching and expansive graphics options. D.K. Choi and S. Nomura [36] employed *Mathematica* to analyze a two-dimensional elasticity problem. S. Nomura and D.L. Ball [37] used symbolic algebra software to calculate the reduction in stiffness due to the presence of multiple penny-shaped cracks in transverse isotropic media. R. E. Diaz-Contreras and S. Nomura [38, 39] used *Mathematica* to construct the approximate Green's functions to solve for non-classical (Mindlin) and classical plate problems.

In the following chapters of this dissertation, certain important formulations are presented and as a preliminary case study, to better illustrate the effectiveness of the proposed method, the 2-D Poisson type equation is considered that governs the steady state heat conduction in a square shaped matrix medium with two elliptical inclusions. For given values of the geometrical and material constants, the results of the temperature profile obtained from the semi-analytical approach were favorably compared with those obtained from the finite element

method. The same approach is then extended to solve the elasticity equilibrium equation in heterogeneous materials, hence providing a potentially unified methodology to solve general boundary value problems in heterogeneous media.

Chapter 2 deals with the basic methodology involved in solving partial differential equations, using the proposed semi-analytical approach. In the first part, the procedure involved in analytically deriving a set of permissible functions is discussed in detail. The second part of this chapter describes selected variational techniques such as the Galerkin method and the Rayleigh-Ritz method. As an extension of the Galerkin method, the eigenfunction expansion method is also examined. This chapter also outlines the Sturm-Liouville theory and the Green's function solution method.

Chapter 3 contains certain related problems (2-D Poisson type equations in homogeneous mediums) that are solved using the proposed approach and compared with the corresponding FEM solution to establish the potency of the approach. The crux of this chapter deals with solving the Poisson type equation in heterogeneous materials. The procedure involved in obtaining the independent eigenfunctions for the heterogeneous material, and the final solution is outlined and discussed. Furthermore, a parametric study is launched to study the effect of varying geometrical and material constants on the resulting temperature field.

Chapter 4 forms the central part of this dissertation with emphasis on the stress equilibrium equation in heterogeneous media. Certain pertinent expressions are derived such as the relation between the traction vector and the stress tensor, the basic form of the stress equilibrium equation (SEQ), the strain-displacement relation, and a modified version of the SEQ in terms of the displacement fields. Other than that, the flow of this chapter is similar to that of Chapter 3. Finally, Chapter 5 includes the conclusion that encompasses certain discussions and recommendations that came about during the course of this dissertation. References are included at the end of this dissertation.

CHAPTER 2

FORMULATIONS AND SOLUTION PROCEDURE

This chapter presents a generalized procedure to solve two dimensional boundary value problems (BVPs), in heterogeneous materials, using the suggested semi-analytical approach in which, first, a set of permissible functions are analytically derived followed by an approximation method that delivers the final solution. The layout of this chapter is as such; in the first section, the modus operandi involved in the analytical derivation of the permissible functions will be demonstrated. The second part primarily pertains to the basic theory and methodology involved in a few of the approximation techniques used, namely the Rayleigh-Ritz method, the Galerkin method, and the Eigenfunction Expansion Method (EEM). The former two methods provide the final solution in terms of a linear combination of the permissible functions, the unknown coefficients of which are determined by minimizing the functional and residual respectively; while the more involved EEM expresses the final solution in terms of eigenfunctions procured from the analytically derived permissible functions. A brief discussion on the construction of the Green's function solution equation, from the eigenfuntions, is also presented in this section.

2.1 Analytical Derivation Of The Permissible Functions

This is the first and perhaps the most vital step in the proposed approach. The permissible functions are derived from a set of basis functions. The concept of basis functions can be best explained by drawing an analogy to base vectors. In a vector space, any arbitrary vector, $\boldsymbol{v}$, can be expressed as a linear combination of n base vectors as

$$\boldsymbol{v} = a_1\boldsymbol{e_1} + a_2\boldsymbol{e_2} + a_3\boldsymbol{e_3} + \dots\dots\dots + a_n\boldsymbol{e_n}, \tag{2.1}$$

where $\boldsymbol{e_1, e_2, e_3, \ldots\ldots e_n}$ represent a set of base vectors in the given vector space and are characterized by their linearly independent nature i.e. the right hand side of the above equation is zero if and only if all of the constants, $a_1, a_2, a_3, \ldots\ldots a_n$, are zeros. This idea, when extended to a two dimensional function space, the base vectors would now represent a set of continuous and independent basis functions, that are essentially polynomials in x and y, a linear combination of which would yield an expression for the unknown quantity of interest (such as temperature, displacement, etc.). Now, to elucidate the process involved in analytically generating the permissible functions, first, the simple case of a one-dimensional BVP is considered in which an unknown continuum quantity, $u(x)$, can be expressed as

$$u(x) = a_0 + a_1 x + a_2 x^2 + a_3 x^3 \ldots\ldots\ldots + a_n x^n. \tag{2.2}$$

Equation (2.2) is a trial function with the quantities $1, x, x^2, x^3, \ldots\ldots\ldots x^n$ representing a complete set of n continuous and independent basis functions for an n-dimensional function space. Assuming the material to be homogeneous, Equation (2.2) is subjected to the boundary conditions prescribed in the given BVP, so as to obtain a set of simultaneous equations in terms of the unknown coefficients, $a_1, a_2, a_3, \ldots\ldots\ldots a_n$. The solution to the simultaneous equations yields a set of expressions for the unknown coefficients, in terms of each other, that are substituted back into Equation (2.2). Finally, by extracting the terms (polynomials in x) associated with the unknown existing coefficients, an array of permissible functions is generated. As an illustration, the Dirichlet boundary condition is imposed on the given problem with the unknown quantity, $u(x)$, vanishing at the boundaries specified by the continuous domain, $C[-d, d]$. This results in the following set of permissible functions:

$$e(x) = \{x^2 - d^2, x(x^2 - d^2), x^4 - d^4, x(x^4 - d^4), \ldots\ldots, x^n - d^n\}. \tag{2.3}$$

In the above expression, it can be clearly observed that each of the permissible functions are continuous, independent of each other, and unconditionally satisfy the prescribed boundary

conditions. Under the same premises of homogeneity and zero boundary conditions of the first kind, the permissible functions for an equivalent problem in two dimensions can be similarly derived, only in a more simplified fashion. For a square shaped domain, $(-d, d) \times (-d, d)$, a polynomial in x and y is defined such that it satisfies all of the specified boundary conditions. Incidentally, for the problem under discussion, this polynomial happens to be the first basis function and takes the form, $(x^2 - d^2)(y^2 - d^2)$. Now, by multiplying this polynomial with the elements of the Pascal triangle, a complete set of permissible functions up to any desired order can be generated. Shown below, is a generalized expression for the permissible functions:

$$e_i(x, y) = (x^2 - d^2)(y^2 - d^2)\, x^{j-i}\, y^i \qquad (i = 0, 1, 2, \dots\dots j), \tag{2.4}$$

where j represents the order of the polynomial. From Equations (2.3) and (2.4), it can be observed that, for homogeneous materials, the permissible functions depend on the geometrical parameters and spatial coordinates.

However, for non-homogeneous materials, this dependency also includes the material properties. This is due to the introduction of the continuity conditions across the inclusion-matrix interface. In an engineering sense, continuity constraints are basically boundary conditions at the interface that define the interaction between two distinct phases of the non-homogeneous medium under consideration. To further decipher the idea of continuity conditions, the case of a two dimensional field equation is considered. The associated geometry is that of a centrally located elliptical inclusion that is introduced into the above specified square shaped domain, $(-d, d) \times (-d, d)$. This geometry represents a non-homogeneous medium with an elliptical interface that separates the inclusion material from the surrounding square shaped matrix material with different material constants. Consequently, two sets of trial functions need to be defined, each set corresponding to each of the two phases. As in the case of the two dimensional homogeneous medium, the basis functions for the heterogeneous material are defined by the constituents of the Pascal triangle i.e. $\{1, x, y, x^2, xy,\ y^2, \dots\dots\}$.

For the inclusion phase, a trial function, $f_{inc}(x,y)$ is defined as

$$f_{inc}(x,y) = \sum_{j=0}^{m}\sum_{i=0}^{j} a_{ij}^{inc}\, x^{j-i}\, y^{i}. \tag{2.5}$$

Similarly, for the matrix phase, $f_{mat}(x,y)$ is assumed to be of the form:

$$f_{mat}(x,y) = g(x,y)\sum_{j=0}^{m}\sum_{i=0}^{j} a_{ij}^{mat}\, x^{j-i}\, y^{i}, \tag{2.6}$$

where m represents the order of the polynomial and the summation ensures that the trial functions encompass all the polynomials up to the m^{th} order, a_{ij}^{inc} and a_{ij}^{mat} are unknown coefficients associated with the inclusion and the matrix phase respectively, and $g(x,y)$ is a function that categorically satisfies the boundary condition imposed on the matrix. For zero boundary conditions of the first kind applied to the given domain, this function would read

$$g(x,y) = (x^2 - d^2)(y^2 - d^2). \tag{2.7}$$

Now, for equilibrium to exist in the above described non-homogeneous medium, it is required that the above defined trial functions and their respective directional derivatives, along the surface normal, are continuous across the elliptical interface. This is achieved by subjecting the trial functions to satisfy the following conditions:

$$f_{inc}(x,y)|_{interface} = f_{mat}(x,y)|_{interface}, \tag{2.8}$$

$$C_{inc}\frac{\partial}{\partial \boldsymbol{n}}\big(f_{inc}(x,y)\big)|_{interface} = C_{mat}\frac{\partial}{\partial \boldsymbol{n}}\big(f_{mat}(x,y)\big)|_{interface}, \tag{2.9}$$

where C_{inc} and C_{mat} are material constants associated with the inclusion and matrix respectively. In relation to a Poisson type equation, this material constant would constitute the

thermal conductivity with Equations (2.8) and (2.9) representing the continuity of temperature and heat flux across the interface.

Likewise, for the stress equilibrium equation, the material would be characterized by the Lamé constants, with the above equations symbolizing the continuity of displacement and traction/stress vector, respectively. These physical quantities will be discussed in greater detail in the latter sections of this dissertation. The term, $\frac{\partial}{\partial \boldsymbol{n}}$, represents the directional derivative and in the context of Equation (2.9), it describes the rate of change of the differentiable trial function, with respect to a simultaneous change in x and y, with the direction of change being defined by a normalized vector perpendicular to the interface and pointing outward. This normalized surface normal, $\boldsymbol{n}$, for an elliptical boundary, with semi-major axis a and semi-minor axis b, can be simply obtained by partially differentiating the equation of the ellipse w.r.t. x and y separately, and dividing each of these components with the corresponding Eucledian norm, and the final form of $\boldsymbol{n}$ is obtained to be

$$\boldsymbol{n} = \begin{pmatrix} \frac{x/a^2}{\sqrt{x^2/a^4 + y^2/b^4}} \\ \frac{y/b^2}{\sqrt{x^2/a^4 + y^2/b^4}} \end{pmatrix}. \tag{2.10}$$

Mathematically, the directional derivative of any given differentiable function, $f(x,y)$, can be interpreted as the dot product between its gradient and the normalized surface normal, $\boldsymbol{n}$. i.e,

$$\frac{\partial}{\partial n}\big(f(x,y)\big) = \nabla f \cdot \boldsymbol{n}. \tag{2.11}$$

Since the interface, under study, is elliptical, it is only but more appropriate to describe the direction of the continually varying coordinates, x and y (w.r.t. every point on the ellipse), in terms of an angle, θ. In order to accommodate this transition, a parametric representation of the ellipse is resorted to, by means of the following relation:

$$\{x, y\} = \{a\ \cos\theta\,, b\sin\theta\}. \tag{2.12}$$

The above equality is imposed on the continuity constraints given by Equations (2.8) and (2.9), which results in a set of simultaneous equations involving real trigonometric polynomials, further manipulation of which yields expressions for the unknown coefficients, $a_{ij}^{inc}$and a_{ij}^{mat}, in terms of each other. Again, as discussed in the homogeneous case, substitutions and extractions are carried out to procure a set of permissible functions, $e_{inc}(x, y)$ and $e_{mat}(x, y)$, for the inclusion and matrix respectively. This plainly suggests that the permissible functions for each of the phases need to be derived separately.

Analytically derivation of the permissible functions is a very tedious and time-consuming process, especially when dealing with heterogeneous materials. However, with the use of *Mathematica*, the amount of time involved in the afore-mentioned computations is appreciably reduced. Another procedure, though not necessary, that imparts completeness to the so far derived orthogonal (independent) permissible functions is normalization. This procedure results in a set of orthonormalized permissible functions which was observed to render a certain degree of stability to the approximation methods. Orthonormality, a defining characteristic of eigenfunctions, will be dealt with in the next section.

2.2 Approximation Methods

Fundamentally, a boundary value problem represents the mathematical formulation of a physical process, in the form of a governing differential equation and the boundary/interface conditions, which describes the behavior of an engineering field, of interest, over a specified domain. In the context of heterogeneous materials, an expression for this physical field can be successfully constructed by simply understanding that this expression needs to satisfy the governing equation and the associated conditions at the boundary and the matrix-inclusion interface. The latter is precisely accounted for, through the analytical derivation of the permissible functions, as explained in the previous section. As for the approximate fulfillment of

the governing equation, the permissible functions will now act as a launch pad for a systematic numerical maneuver/s that yields a “confluent solution” for the engineering field. Of many such maneuvers, three of the most widely used variational techniques will be enumerated and discussed in the following sub-sections. Before venturing into the realm of variational techniques, it would be convenient to define an envelope within which these techniques can be comprehensively applied. This envelope constitutes the Sturm-Liouville system; an important class of problems in linear space. Hence, for completeness and better understanding, the basic ideas governing the Sturm-Liouville theory are presented below which will also serve as an introduction to the eigenfunction expansion method (EEM).

2.2.1Sturm-Liouville System

The Sturm-Liouville system (S-L problem) is a strong representative of a large class of BVPs, characterized by a homogeneous second-order linear differential equation as depicted by Equation (2.13) marginalized by a set of homogeneous boundary conditions as represented by Equation (2.14), and in its most general form reads

$$L\varphi(x) = \lambda\, \varphi(x), \qquad x_1 < x < x_2, \tag{2.13}$$

$$\begin{aligned} &\alpha_1\, \varphi(x_1) + \beta_1\, \varphi'(x_1) = 0, \\ &\alpha_2\, \varphi(x_2) + \beta_2\, \varphi'(x_2) = 0. \end{aligned} \tag{2.14}$$

The above equations collectively represent an eigenvalue problem, with λ denoting a parameter for which the above described homogeneous BVP allows for nontrivial solutions to exist. These values of λ are called eigenvalues and their corresponding nontrivial solutions, $\varphi(x)$, are referred to as eigenfuntions The S-L operator, L, is a self-adjoint differential operator defined as

$$L \equiv -\frac{1}{w(x)}\left(\frac{d}{dx}\left(P(x)\frac{d}{dx}\right) + Q(x)\right), \tag{2.15}$$

where $w(x)$ is called the weight function, and for the given function space i.e. $x_1 < x < x_2$, it is defined as a non-negative measurable quantity (analogous to density) that is used in the definition of the inner product, for that function space, as

$$\big(u(x), v(x)\big) \equiv \int_{x_1}^{x_2} u(x)v(x)w(x)dx. \tag{2.16}$$

The self-adjoint property of the differential operator, L, that ascertains the existence of a solution for a given BVP, can be summarized as

$$(Lu, v) = (u, Lv), \tag{2.17}$$

where u and v are arbitrary functions that satisfy the homogeneous boundary conditions specified by Equation (2.14). This intrinsic property of the S-L system imparts certain functional advantages, such as the symmetricity of L that renders it Hermitian, hence suggesting that in the specified domain, $x_1 < x < x_2$, all the eigenvalues, λ, are real and the corresponding eigenfunctions, $\varphi(x)$, are orthonormal. Orthonormality of eigenfunctions can be succinctly expressed as

$$\int_{x_1}^{x_2} \varphi_i(x)\ \varphi_j(x)\, dx = \delta_{ij}, \tag{2.18}$$

where δ_{ij} is called the Kronecker delta function. This is the same characteristic property that qualifies eigenfunctions as a mutually independent set of polynomials, that allows a function, in a given function space, to be expanded as a linear combination of the eigenfunctions. Furthermore, the linearity of the differential operator, L, defined by the following set of relations:

$$\begin{aligned} L(u + v) &= Lu + Lv, \\ L(c\,u) &= c\,Lu, \end{aligned} \tag{2.19}$$

accommodates the representation of the eigenfunctions in terms of a linear combination of the analytically derived permissible functions. Discussed above are a few of the quintessential features of EEM that will be dealt with, more rigorously, in the latter part of this chapter. For now, having been familiarized with certain innate properties of the S-L problem and its operator, the next logical step is to relate these concepts to the essential building blocks of BVPs, namely the governing equation and the boundary conditions. This connection is established by a rather simple linear equation that effortlessly describes a variety of physical processes, such as the heat equation, the stress equilibrium equation, etc., and the S-L system can be effectively used to solve such an equation, which is of the type

$$L[u(x)] = c(x), \tag{2.20}$$

where $c(x)$ is any given function, $u(x)$ is the unknown physical field, and L represents the linear, self-adjoint differential operator. As examples, the BVPs under investigation, specifically the Poisson type equation and the stress equilibrium equation subjected to homogeneous boundary conditions, will be used to demonstrate this connection. Substituting the definition of L, from Equation (2.15), into Equation (2.20) yields

$$-\frac{1}{w(x)}\left(\frac{d}{dx}\left(P(x)\frac{d}{dx}\right)+Q(x)\right)[\,u(x)] = c(x). \tag{2.21}$$

Further, by assigning $w(x) = 1, P(x) = k(x), Q(x) = 0, u(x) = T(x), c(x) = q(x)$ to the above formulation results in an equation of the form

$$-\frac{d}{dx}\left(k(x)\frac{d}{dx}T(x)\right) = q(x), \tag{2.22}$$

where $T(x)$ represents the temperature, $k(x)$ is the thermal conductivity of the material, and $q(x)$ denotes the internal volumetric heat generation term. On the whole Equation (2.22) represents the mathematical model for the Poisson type equation. Similarly, the equilibrium

equation in solid mechanics can be obtained, by choosing $w(x) = 1, P(x) = C(x), Q(x) = 0, u(x) = u(x), c(x) = b(x)$, as

$$-\frac{d}{dx}\left(C(x)\frac{d}{dx}u(x)\right) = b(x), \tag{2.23}$$

where $u(x)$ is the displacement, $C(x)$ represents the elastic constants of the material either in terms of the Lamé constants or the more commonly used Young's modulus and Poisson's ratio, and $b(x)$ is the body force expressed per unit volume of the material.

Furthermore, the homogeneous boundary conditions of the S-L system, as expressed by Equation (2.14), will accommodate the embodiment of the three types of boundary conditions frequently encountered in BVPs namely the Dirichlet (or first type) boundary conditions that specifies the value of the unknown function on the boundary, the Neumann (or second type) boundary conditions that stipulates a value to the normal derivative of the unknown function on the boundary, and the Robin (or third type) boundary conditions that imposes a value to the linear combination of the function and its derivative on the boundary. The homogeneous version of the afore-mentioned types of boundary conditions can be obtained from Equation (2.14) by choosing $\beta_1 = \beta_2 = 0$ for the first type, $\alpha_1 = \alpha_2 = 0$ for the second type, and $\alpha_1 \neq 0$, $\alpha_2 \neq 0$, $\beta_1 \neq 0$, $\beta_2 \neq 0$ for the third type. However, in this dissertation, for the sake of simplicity and consistency, only the homogeneous Dirichlet boundary conditions will be considered. Having set the perimeter of the BVP in terms of the governing equation and the boundary conditions, variational techniques will now be discussed within the context of this perimeter.

2.2.2 Rayleigh-Ritz Method

This method, named after Lord Rayleigh (1842-1919) and Walther Ritz (1878-1909) is one of the most fundamental and classical approximate solution techniques, for BVPs, based on the calculus of variations. This variational method, in an effort to obtain an expression for the unknown function, reduces the problem of integrating the governing differential equation to an

equivalent variational problem of seeking the extremum (maxima or minima) of a functional. A functional or variational principle is an integral expression involving a function of functions and is generally expressed as

$$I(y) = \int_{x_1}^{x_2} F(x, y, y_x) dx, \tag{2.24}$$

where $I(y)$ represents the variational principle and the integrand, $F(x, y, y_x)$, is a given function of x, y, and $y_x = dy/dx$ with x as the independent variable and y as the dependent variable. Basically, Equation (2.24) represents a variational problem of finding a function, $y(x)$, subject to the prescribed boundary conditions such that $I(y)$ is rendered stationary (or holds an extremum value) in the domain, $x_1 < x < x_2$. In this regard, a necessary condition for $I(y)$ to have an extremum is that its variation should cease to exist i.e.

$$\delta I = 0, \tag{2.25}$$

where δ is the variational symbol. The substitution of Equation (2.24) into Equation (2.25) and subsequent simplification of the resulting equation leads to

$$\frac{\partial F}{\partial y} - \frac{d}{dx}\left(\frac{\partial F}{\partial y_x}\right) = 0. \tag{2.26}$$

Equation (2.26) is widely referred to as the Euler-Lagrange equation. Hence, for $I(y)$ to have an extremum for a given function, $y(x)$, the necessary condition is that F should satisfy Equation (2.26). Extending this notion to the case where there are two independent variables, x and y, and one dependent variable, $u(x, y)$, as in the 2-D Poisson type equation, then

$$I(u) = \iint F\left(x, y, u, u_x, u_y\right) dx\, dy, \tag{2.27}$$

and the corresponding Euler-Lagrange equation is

$$\frac{\partial F}{\partial u} - \frac{\partial}{\partial x}\left(\frac{\partial F}{\partial u_x}\right) - \frac{\partial}{\partial y}\left(\frac{\partial F}{\partial u_y}\right) = 0. \tag{2.28}$$

Thus, the Poisson's equation can be solved by ascertaining an F that satisfies Equation (2.28) and hence evidently extremizes the functional, $I(u)$. One of the initial steps in the Rayleigh-Ritz method is the construction of this functional, if one does exist for the given differential equation. However, the existence of the functional need not be questioned for the Poisson type equation and stress equilibrium equation since they are a sub-class of the self-adjoint S-L system. For the stress equilibrium equation, the variational problem is not readily available in literature. Also, the procedure involved in constructing its variational principle is quite rigorous and will be discussed later in this dissertation. However, for the two dimensional Poisson equation, subjected to the homogeneous Dirichlet boundary conditions, of the type

$$\left(-\frac{\partial^2}{\partial x^2} - \frac{\partial^2}{\partial y^2}\right) u(x,y) = q(x,y), \tag{2.29}$$

the functional is defined to be

$$I(u) = \frac{1}{2}\iint \left({u_x}^2 + {u_y}^2 - 2\,u\,q\right)\, dx\, dy. \tag{2.30}$$

The equation above represents a variational problem analogous to Equation (2.27) with the integrand satisfying the corresponding Euler-Lagrange equation as described by Equation (2.28). Hence the original problem in the form of a differential equation is transformed into a variational problem, with the unknown function $u(x,y)$ approximated as a linear combination of the analytically derived permissible functions as

$$\tilde{u}(x,y) = \sum_{i=1}^{N} \alpha_i\, e_i(x,y), \tag{2.31}$$

where α_i represents the unknown coefficients associated with each of the N permissible functions $e_i(x, y)$. Substituting Equation (2.31) into Equation (2.30) yields an expression for the functional in terms of the unknown coefficients that resembles the form:

$$I(\tilde{u}) = I(\alpha_1, \alpha_2, \alpha_3, \dots\dots, \alpha_N). \tag{2.32}$$

In order for this functional to reach an extremum, its partial derivatives with respect to the unknown coefficients should vanish i.e.

$$\frac{\partial I(\tilde{u})}{\partial \alpha_i} = 0, \qquad (i = 1,2, \dots\dots, N). \tag{2.33}$$

Executing the above operation results in N simultaneous equations that are solved for the unknown coefficients that are substituted back into the approximate solution i.e., Equation (2.31), to generate the final solution. The equations above outline the generalized procedure of the Rayleigh-Ritz method that can be conveniently extended to solve for displacement fields for the stress equilibrium equation.

2.2.3 Galerkin Method

Variational methods can be broadly categorized into direct and indirect methods. While the Rayleigh-Ritz method is a direct variational approach that addresses the variational problem, the Galerkin method falls into the class of indirect methods or the method of weighted residual (MWR). As the name suggests, these methods seek to minimize the residual (error), induced due to approximation, by selecting an appropriate weight function and setting the weighted integral of the residual to zero. Depending on the definition of the weight function, other subclasses of MWR, such as the collocation method, sub-domain method, and least squares method have also been identified. Of all the indirect methods mentioned above, the Galerkin method, by far, is the most effective approximation technique that ascertains the convergence of the solution for an adequate number of terms, and is perhaps the most widely used approximation technique. Its effectiveness and versatility can be attributed to its close

affiliation to the fundamental concepts of linear space. This affiliation can be observed by examining the methodology involved in the Galerkin method. For a typical linear equation, as described by Equation (2.20), the residual $R(x)$ is defined as

$$R(x) = L[\tilde{u}(x)] - c(x), \tag{2.34}$$

where, as before, L is the linear differential operator and $\tilde{u}(x)$ denotes the approximate solution as stated earlier. Substituting the approximate solution into Equation (2.34) yields

$$R(x) = \sum_{i=1}^{N} \alpha_i \, L[e_i(x)] - c(x). \tag{2.35}$$

Since the vector space is analogous to the linear space, by extending one of the concepts that holds true in vector space, namely a vector that is perpendicular to all the base vectors that span the entire vector space must be a zero vector; the idea that governs the Galerkin method can be explored. The above rule translates into the following expression in linear space:

$$\Big(R(x), e_j(x)\Big) = 0 \qquad (j = 1,2, \dots, N). \tag{2.36}$$

The above equation basically suggests that if N is chosen such that the entire linear space is populated with permissible functions$e_i(x)$, then a function that is orthogonal to all the permissible functions must be zero, or their inner products must be zero. Substituting Equation (2.35) into Equation (2.36) yields

$$\sum_{i=1}^{N} \alpha_i \Big(L[e_i(x)], e_j(x)\Big) = \Big(c(x), e_j(x)\Big). \tag{2.37}$$

The above expression results in N equations for the N unknown coefficients that are solved for and substituted back into Equation (2.31) to obtain the approximate solution for the unknown function $u(x)$. Alternately, a matrix representation can also be employed. The expression also

suggests that the Galerkin method proposes using the permissible functions as weights in an effort to minimize the residual. In many ways, the Galerkin method can be considered to be an extension of the Rayleigh-Ritz method, especially when dealing with even order linear differential operators.

2.2.4 Eigenfunction Expansion Method (EEM)

Unlike the Rayleigh-Ritz method or the Galerkin method that approximates the unknown function as a linear combination of the permissible functions, EEM expresses the unknown function in terms of the eigenfunctions (or non-trivial solutions) of the S-L problem. This method mainly involves solving a generalized eigenvalue problem, or Sturm-Liouville (S-L) problem using the Galerkin method to obtain a set of eigenfunctions, and subsequently formulating the final solution by expressing it as a linear combination of these eigenfunctions. As mentioned earlier, the linearity of the S-L operator as shown by Equation (2.19) allows the non-trivial solutions or the eigenfucntions to be expressed as a linear combination of the analytically derived permissible functions as

$$\phi_k(x) = \sum_{i=1}^{N} c_{ki}\, e_i(x), \tag{2.38}$$

where $e_i(x)$represents each of the N permissible functions and c_{ki} is the coefficient of $e_i(x)$ corresponding to k^{th} component of the i^{th} normalized eigenvector. In order to determine this set of unknown coefficients, the eigenvalue problem, described by Equation (2.13), needs to be solved. An effective modus operandi to solve such a system would be one that will permit the differential equation to be minimized into a finite dimensional linear algebraic system (or a weak formulation). The Galerkin method, a sub-class of (MWR) is one such generalized approximation technique that fits the bill. Enumerated below, are the steps involved in determining the eigenfunctions using the Galerkin method. To begin with, the approximate

expression of the eigenfunctions as described by Equation (2.38) is substituted into the eigenvalue problem i.e., Equation (2.13) that yields

$$\sum_{i=1}^{N} c_{ki}\, L[e_i(x)] = \lambda_k \sum_{i=1}^{N} c_{ki}\, e_i(x). \tag{2.39}$$

Introducing the permissible functions, $e_j(x)$, as the weights, and integrating over the prescribed domain by imposing the inner product definition as indicated by Equation (2.16), the above equation takes the form:

$$\sum_{i=1}^{N} c_{ki} \int_{x_1}^{x_2} L[e_i(x)]\, e_j(x) dx = \lambda_k \sum_{i=1}^{N} c_{ki} \int_{x_1}^{x_2} e_i(x)\, e_j(x)\, dx. \tag{2.40}$$

In a simplified tensorial form, the above equation reads

$$\sum_{i=1}^{N} A_{ij} c_{ki} = \lambda_k \sum_{i=1}^{N} B_{ij} c_{ki}, \tag{2.41}$$

with

$$A_{ij} = \int_{x_1}^{x_2} L[e_i(x)]\, e_j(x) dx, \tag{2.42}$$

$$B_{ij} = \int_{x_1}^{x_2} e_i(x)\, e_j(x) dx. \tag{2.43}$$

The tensorial representation as shown in Equation (2.41) can be further simplified into an algebraic form that represents a generalized eigenvalue problem as

$$A\, c = \lambda\, B\, c. \tag{2.44}$$

Equation (2.44) represents a system of linear equations, thus emphasizing the transformation from the original differential equation format to an N-dimesional linear system. Further simplification results in

$$P\,c = \lambda\,c, \qquad (P = B^{-1}\,A). \tag{2.45}$$

The components of the matrices, A and B, are obtained using Equations (2.42) and (2.43). The solution to Equation (2.45) results in the eigenvalues, λ_k, and the corresponding set of unknown coefficients or eigenvectors, c_{ki}. The eigenvectors, so obtained, are normalized as

$$[c_k]^T[B][c_k] = 1. \tag{2.46}$$

The normalized eigenvectors, so evaluated, are substituted into Equation (2.38) that results in a set of orthonormal eigenfunctions, a linear combination of which will produce the final solution.

In order to formulate an expression for the final solution or the unknown physical field, $u(x)$, the linear form of the equation as depicted by Equation (2.20) is considered. An equation of this nature, that is analogous to the S-L problem, can be solved using eigenfunctions, in which all the quantities involved can be expanded, or at least assumed to be expanded using the eigenfunctions. In view of this assumption, the unknown function $u(x)$ can be expanded in terms of the eigenfunctions, $\phi_i(x)$, as

$$u(x) = \sum_{i=1}^{N} u_i \phi_i(x), \tag{2.47}$$

where u_i represents a set of unknown coefficients. In a similar fashion, the given function, $c(x)$, can be expressed in the form of a series expansion as

$$c(x) = \sum_{i=1}^{N} c_i \phi_i(x), \tag{2.48}$$

where the unknown coefficients, c_i, can be evaluated using the following relation, obtained from the principles that constitute the Fourier series expansion:

$$c_i = \int_{x_1}^{x_2} c(x)\, \phi_i(x) dx. \tag{2.49}$$

Substituting Equations (2.47) and (2.48) into Equation (2.20) yields

$$\sum_{i=1}^{N} u_i\, L[\phi_i(x)] = \sum_{i=1}^{N} c_i \phi_i(x). \tag{2.50}$$

Now, imposing Equation (2.13) to Equation (2.50) results in

$$\sum_{i=1}^{N} u_i\, \lambda_i\, \phi_i(x) = \sum_{i=1}^{N} c_i \phi_i(x). \tag{2.51}$$

Taking advantage of the independent nature of the eigenfunctions from the above equation, an expression for u_i can be obtained as

$$u_i = \frac{c_i}{\lambda_i}. \tag{2.52}$$

By substituting the above equation into Equation (2.47), an expression for $u(x)$ is obtained as

$$u(x) = \sum_{i=1}^{N} \frac{c_i\, \phi_i(x)}{\lambda_i}. \tag{2.53}$$

An alternative means to arrive at the solution to Equation (2.20) is by employing the Green's function approach in which a numerical Green's function is constructed as a linear combination of the procured eigenfunctions. With regard to mechanics, a Green's function, G, of a linear operator, L, is the solution to an equation of the form:

$$L[G] = \delta, \tag{2.54}$$

where δ is called the Dirac delta function. The Green's function is constructed based on a complete set of independent eigenfunctions. A set of eigenfunctions, $\phi_i(x)$, is said to be complete if it satisfies the following relation:

$$\delta = \sum_{i=1}^{N} \phi_i(x)\ \ \phi_i(x'). \tag{2.55}$$

It can be observed that Equation (2.54) bears resemblance to Equation (2.20).This analogy suggests that the Green's function can be expressed by a series of eigenfunctions as

$$G = \sum_{i=1}^{N} \alpha_i\ \phi_i(x). \tag{2.56}$$

Substitution of Equations (2.55) and (2.56) into Equation (2.54) yields

$$\sum_{i=1}^{N} \alpha_i\ L[\phi_i(x)] = \sum_{i=1}^{N} \phi_i(x)\ \ \phi_i(x'). \tag{2.57}$$

As before, applying Equation (2.13) to Equation (2.57) results in

$$\sum_{i=1}^{N} \alpha_i\ \lambda_i\ \phi_i(x) = \sum_{i=1}^{N} \phi_i(x)\ \ \phi_i(x'). \tag{2.58}$$

The equation above can be simplified by employing the orthornormal property of the eigenfunctions that results in an expression for the unknown coefficients as

$$\alpha_i = \frac{\phi_i(x')}{\lambda_i}. \tag{2.59}$$

Substituting the above expression into the initially assumed expression for the Green's function i.e., Equation (2.56), the final form of the Green's function is obtained as

$$G = \sum_{i=1}^{N} \frac{\phi_i(x)\,\phi_i(x')}{\lambda_i}. \tag{2.60}$$

The expression for the unknown coefficients as shown in Equation (2.59) can also be derived by implementing the definition of the inner product, i.e., multiplying both sides of Equation (2.54) with $\phi_i(x)$ and integrating the resulting equation over the prescribed domain. This results in

$$\sum_{i=1}^{N} \alpha_i\, \lambda_i\big(\, \phi_i(x), \phi_i(x)\big) = \big(\delta, \phi_i(x)\big). \tag{2.61}$$

Imposing the orthonormal property of eigenfunctions and the characteristic definition of the Dirac delta function, the above equation reduces to a form as shown in Equation (2.59). The solution $u(x)$ can now be obtained by incorporating the expression for G i.e. Equation (2.60) into the following representation:

$$u(x) = (c(x'), G) \tag{2.62}$$

It should be noted that the inner product, specified, in the above expression is defined with respect to the associated dummy variable, x'.

CHAPTER 3

HEAT EQUATION IN HETEROGENEOUS MATERIALS

The primary focus of this chapter is to solve the 2-D Poisson type equation (PTE) that describes the steady state heat conduction over a given region with internal heat generation in heterogeneous materials using the proposed semi-analytical approach. However, in order to establish the general validity and a measure of efficiency of this semi-analytical method, first, the 2-D steady state heat equation, with internal heat generation, in a homogeneous medium will be considered, for which series solutions in the form of Fourier series are readily available in literature. Homogeneous materials, being relatively simple compared to their heterogeneous counterparts, will aid in distinctly understanding the solution process involved, on a more basic level. Furthermore, once a generalized solution process has been established for homogeneous materials; one that favorably agrees with the documented results, the approach can be suitably extended to satisfy and accommodate the requirements/complexities associated with the solution process for heterogeneous materials.

Thus, the first section of this chapter will act as a primer to solving Poisson type equations in heterogeneous materials, namely single inclusion and multiple inclusion problems. Also, all of the above cases will be corroborated with their respective finite element results, obtained using ANSYS.

Most of the computations involved in the semi-analytical method, such as derivation of the permissible functions, integration of higher order polynomials over a prescribed domain, matrix operations, etc., are innately tedious and time consuming. As a favorable outcome, *Mathematica* will be extensively used to facilitate these computations. Suffice it to say that, hereon, almost all of the results and plots that are demonstrated in this dissertation have been obtained using *Mathematica.*

3.1 2-D Steady State Heat Equation In Homogeneous Media

In its most general form, the 2-D steady state heat equation with internal (volumetric) heat generation reads

$$\nabla.\big(k(x,y)\,\nabla T(x,y)\big) + q(x,y) = 0, \tag{3.1}$$

where $k(x,y)$ represents the thermal conductivity, $T(x,y)$ is the unknown temperature field that needs to be determined and $q(x,y)$ represents the heat generation per unit volume. Since the material under consideration is homogeneous, the thermal conductivity, $k(x,y)$, does not change with respect to the spatial coordinates, and hence remains a constant, k, throughout the medium. This simplification yields

$$-k\,\nabla^2 T = q, \tag{3.2}$$

where ∇^2 is the Laplacian operator defined as the divergence $(\nabla.)$ of the gradient (∇).The geometry is a square shaped homogeneous medium with dimensions specified by a parameter, d; and the boundaries of the stipulated region are subjected to the Dirichlet (or first kind) boundary conditions with the temperature vanishing at the boundaries i.e. $T(x,y) = 0$. Having delineated all the necessary elements required to study the behavior of the temperature field under steady state conditions, the boundary value problem (BVP) is now successfully defined; a graphical representation of which is shown in Figure 3.1.

As discussed in the previous chapter, the first step in this semi-analytical method is to obtain a set of characteristically continuous and independent permissible functions (polynomials in x and y) that satisfy the prescribed homogeneous boundary conditions. For the given geometry and boundary conditions, the generalized expression of the permissible functions takes the form as shown in Equation (2.4). As an illustration, for $j = 2$, the following six permissible functions are obtained:

$$e_1(x,y) \;=\; (x^2 - d^2)\;(y^2 - d^2),$$

$$e_2(x,y) = (x^2 - d^2)(y^2 - d^2)\, x,$$

$$e_3(x,y) = (x^2 - d^2)(y^2 - d^2)\, y,$$

$$e_4(x,y) = (x^2 - d^2)(y^2 - d^2)\, x^2,$$

$$e_5(x,y) = (x^2 - d^2)(y^2 - d^2)\, x\, y,$$

$$e_6(x,y) = (x^2 - d^2)(y^2 - d^2)\, y^2$$

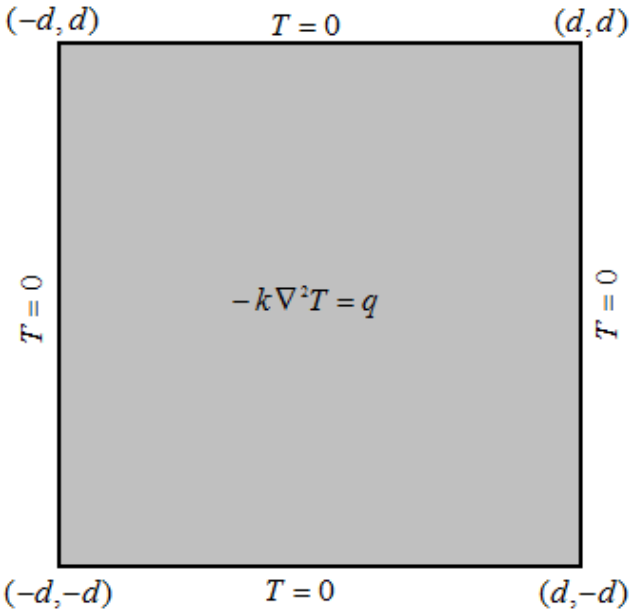

Figure 3.1 Steady state heat equation with internal heat generation in a homogeneous medium.

The set of permissible functions, derived above, are relatively simple in their structure. However, when dealing with heterogeneous media, irrespective of the simplicity in geometry, the complex structure and explicitness of the permissible functions will be revealed. The permissible functions are now subjected to one of the variational techniques discussed earlier; as default, EEM will be used, unless otherwise specified. As a result, the Galerkin method is employed to obtain a generalized eigenvalue problem, as shown in Equation (2.44), which symbolizes the transformation of the original problem to a linear system of equations. The matrix elements are represented by A_{ij} and B_{ij} respectively, and are computed as

$$A_{ij} = k \int_{-d}^{d} \int_{-d}^{d} L[e_i(x,y)]\, e_j(x,y)\, dx\, dy, \qquad L \equiv \left(-\frac{\partial^2}{\partial x^2} - \frac{\partial^2}{\partial y^2} \right), \tag{3.3}$$

$$B_{ij} = \int_{-d}^{d} \int_{-d}^{d} e_i(x,y)\, e_j(x,y)\, dx\, dy, \tag{3.4}$$

where L is the self adjoint Laplacian operator. The generalized eigenvalue problem is solved to obtain the eigenvalues λ_i, and their corresponding orthonormal eigenfunctions as

$$\varphi_i(x,y) = \sum_{j=1}^{N} v_{ij} e_j(x,y) \qquad (i = 1, 2, 3, \dots\dots\dots, N), \tag{3.5}$$

where v_{ij} represents the normalized eigenvectors and N denotes the number of permissible functions considered for the solution approximation, or simply the dimension of the linear algebraic system. The coefficients, c_i as defined in Equation (2.48), associated with the heat generation term q are obtained as

$$c_i = \int_{-d}^{d} \int_{-d}^{d} q\, \phi_i(x,y)\, dx\, dy. \tag{3.6}$$

Finally, the temperature field for the given homogeneous medium, $T(x,y)$, can be obtained from

$$T(x,y) = \sum_{i=1}^{N} \frac{c_i\, \phi_i(x,y)}{\lambda_i}. \tag{3.7}$$

For illustration purposes, the following values, $k = 1, q = 1, d = 1$, are assigned to the quantities that define the material, heat generation and geometry respectively. The number of permissible functions, N, considered for the approximation is 28 that results from $j = 6$. For the same BVP (steady state heat equation with internal heat generation in a homogeneous medium

subjected to homogeneous Dirichlet boundary conditions), the series solution for the temperature field, using the classical separation of variables, is

$$T(x,y) = \frac{(d^2 - x^2)}{2} - \frac{16}{\pi^3} \sum_{n=1}^{N} \frac{\sin\left(\frac{n\,\pi\,(d+x)}{2}\right)}{n^3\ \sinh(n\,\pi)} \times \left(\sinh\left(\frac{n\,\pi(d+y)}{2}\right) + \sinh\left(\frac{n\,\pi(d-y)}{2}\right)\right). \tag{3.8}$$

The eigenfunctions, depicted in Figure 3.2, were obtained using the semi-analytical approach and represent six (out of 28) of the arbitrarily chosen, orthonormal non-trivial solutions. The figure clearly depicts the independent nature of the eigenfunctions, hence validating

$$\int_{-d}^{d} \int_{-d}^{d} \phi_i(x,y)\ \phi_j(x,y) dx\ dy = \delta_{ij}. \tag{3.9}$$

An inference that can be drawn from these eigenfunction illustrations is that they essentially represent a variety of functions such as the trigonometric functions, the Bessel functions and the Legendre functions depending on the definition of the S-L operator. In this case, it's a combination of sine and/or hyperbolic sine functions. Another observation worth mentioning is that among all the eigenfunctions generated, the first eigenfunction is the most dominant and significantly controls the outcome of the temperature solution. Figures 3.3 and 3.4 respectively depict the 3-D profile and contour plot of the temperature solution obtained using EEM that conform to an eighth order approximation.

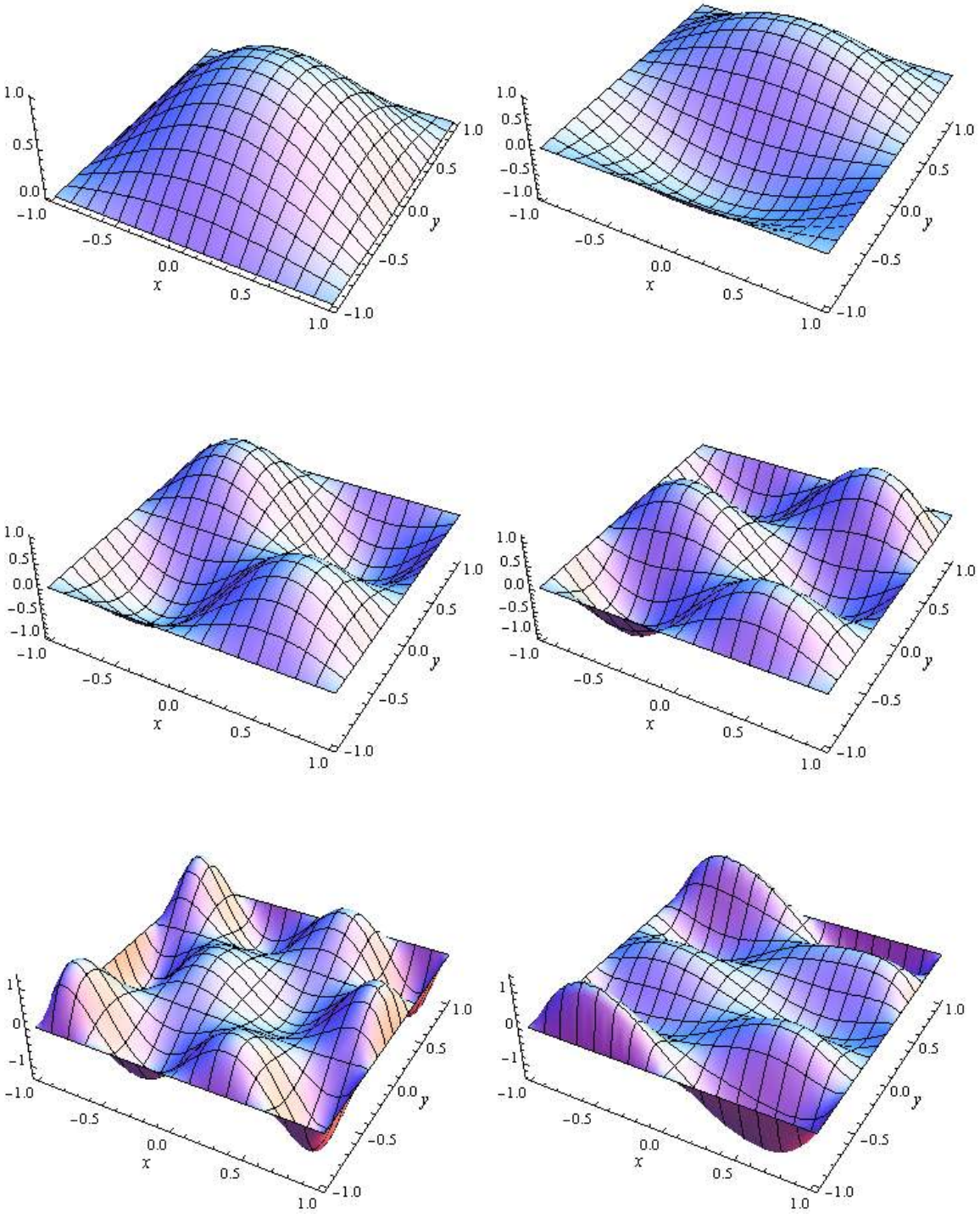

Figure 3.2 Arbitrarily chosen eigenfunctions for the PTE in a homogeneous medium.

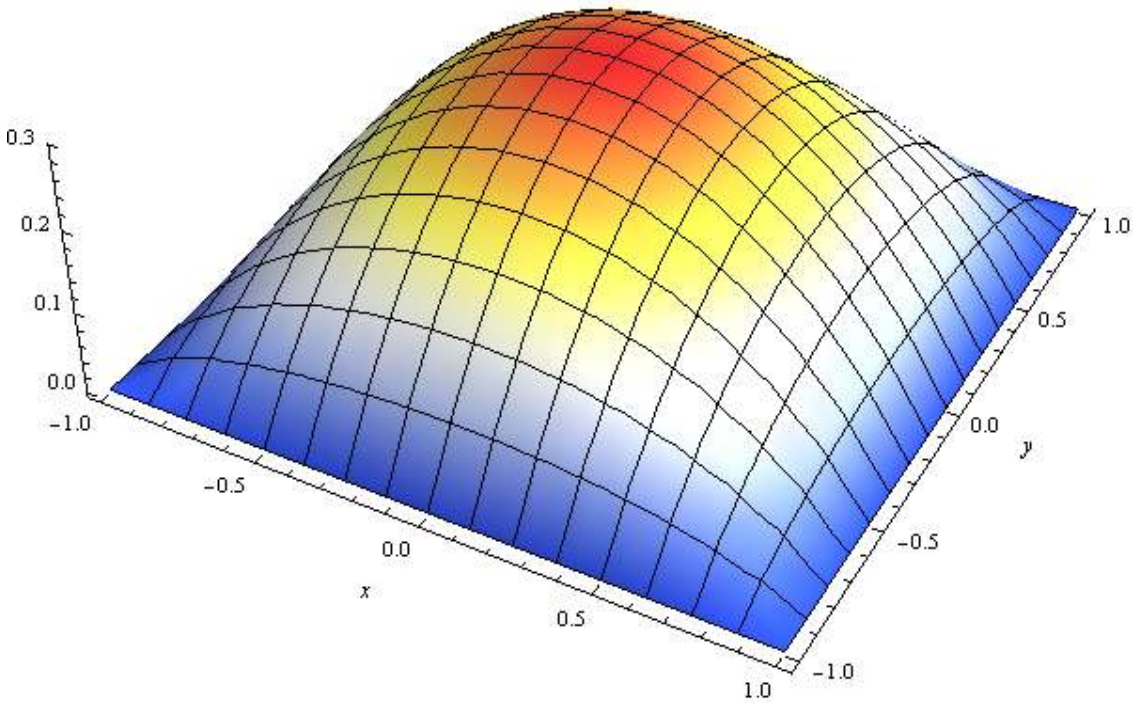

Figure 3.3 3-D Temperature profile for the PTE in a homogeneous medium.

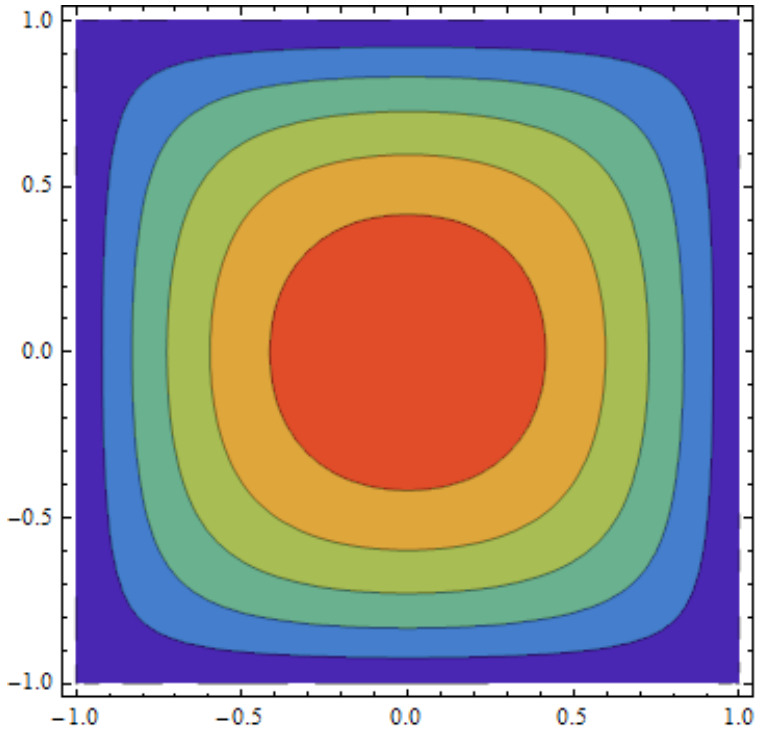

Figure 3.4 Temperature contour plot for the PTE in a homogeneous medium.

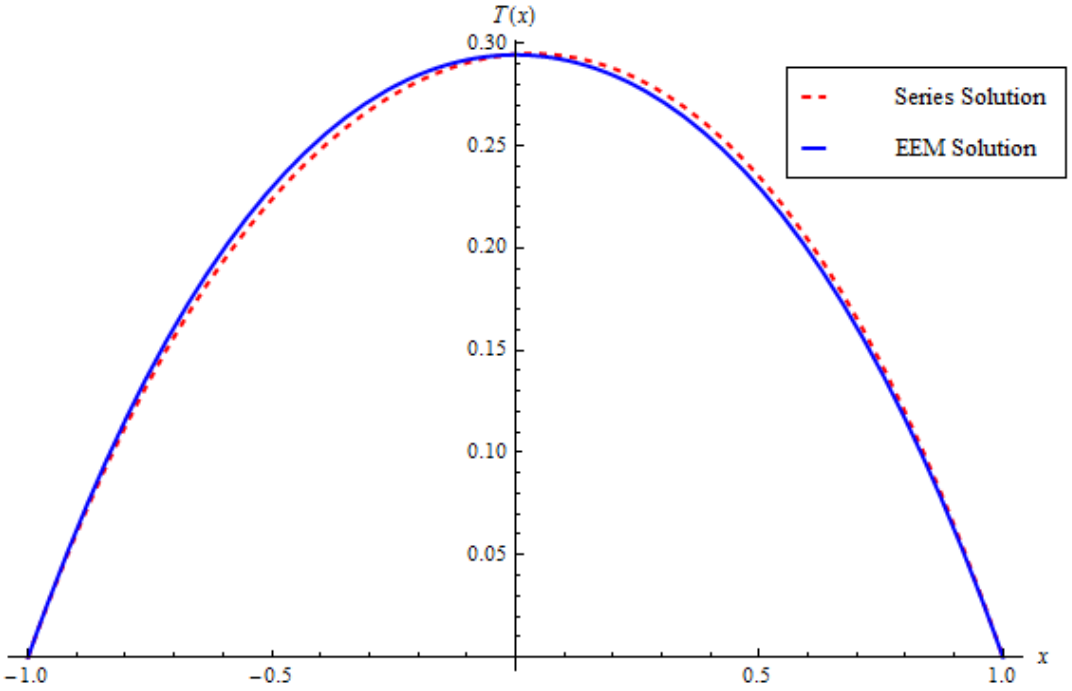

Figure 3.5 Comparison between the EEM solution and the series solution for the PTE in a homogeneous medium.

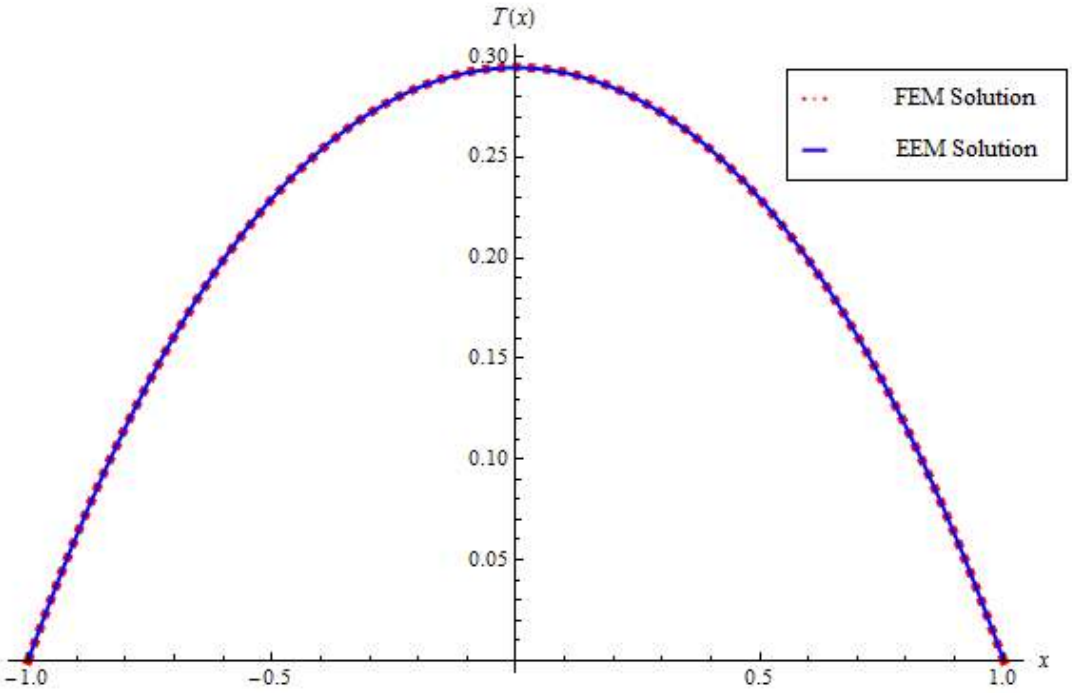

Figure 3.6 Comparison between the EEM solution and the FEM solution for the PTE in a homogeneous medium.

Figure 3.5 provides a comparison of the cross-sectional temperature profile of the EEM solution, with the series solution. The comparison corresponds to a 28 term approximation, along the x-axis, and a good agreement is observed between the two sets of results. Figure 3.6 provides additional corroboration for the EEM solution by comparing it with the FEM solution. Once again, it can be seen that the results are in good accord with each other. All the non-zero values of the coefficients associated with the internal heat generation, c_i, and their corresponding eigenvalues, λ_i, obtained from EEM are provided in the table below (Table 3.1). The table also indicates that out of the 28 permissible functions, only six of them contributed to the final solution. Table 3.2 furnishes a measure of convergence for the semi-analytical approach (EEM) for values of N corresponding to j ranging from 1 to 6. The table also provides a comparison of the EEM solution with that obtained from the series and FEM solution.

Table 3.1 EEM coefficients and eigenvalues for the PTE in a homogeneous medium

i	1	6	11	15	22	28
c_i	1.62114	0.764335	-0.182631	-0.493325	0.220957	0.517356
λ_i	4.9348	24.6749	44.8795	66.0915	116.196	222.223

Table 3.2 Comparison of the temperature solutions for the PTE in a homogeneous medium

$T(x,y)$ at $(x=0, y=0)$					
j	N	EEM	Series Solution	Percentage Error	FEM Solution
1	3	0.312500	0.294689	6.04415	0.29483
2	6	0.292193	0.294685	0.845723	
3	10	0.292193		0.845723	
4	15	0.295405		0.244121	
5	21	0.295405		0.244121	
6	28	0.294424		0.088572	

The results discussed so far, in the form of a comparative study and convergence, for the 2-D steady state heat equation in homogeneous materials demonstrate the effectiveness of the proposed semi-analytical approach. In the next section, this method will be employed to solve a similar equation in non-homogeneous materials (matrix with inclusion/s), for which closed form solutions do not exist; and the results will be corroborated using FEM.

.*3.2 2-D Steady State Heat Equation in Heterogeneous Media*

The heterogeneous media under consideration is an inclusion/s embedded in a matrix having different material constants. The objective is to solve the Poisson type equation for such a media. The mathematical model of the governing equation is equivalent to Equation (3.1); subjected to homogeneous Dirichlet conditions. First, the case of a single inclusion in a square-shaped matrix medium is examined, and an expression for the temperature field is determined using the semi-analytical method; following a convergence study. Subsequently, a parametric study is conducted to investigate the effect of varying aspect ratios, material constants, surface areas, and position of the inclusion on the temperature field. In the second instance; a similar investigation is carried out for a square-shaped matrix medium consisting of multiple elliptical inclusions. Additionally, the effect on the temperature field due to the change in the length of separation between the inclusions is studied. The results for each of the preliminary cases are compared with the FEM solutions obtained from Ansys.

3.2.1Single Inclusion Problems (SIPs)

Figure 3.7 depicts the geometry of the heterogeneous media under consideration with a centrally located elliptical inclusion and the surrounding finite matrix having different thermal conductivities; k_1 and k_2 respectively. To start with, two sets of trial functions – one for the inclusion, $f_1(x,y)$, and the other for the matrix, $f_2(x,y)$, are defined separately as described by Equations (2.5) and (2.6) respectively; explicit representations of which would read

$$f_1(x,y) = c_0 + c_1\,x + c_2\,y + c_3\,x^2 + c_4\,x\,y + c_5\,y^2 + \ldots\ldots\ldots + c_{k-1}(\ldots), \tag{3.10}$$

$$f_2(x,y) = (x^2 - d^2)(y^2 - d^2)\left(c_k + c_{k+1}\,x + c_{k+2}\,y + c_{k+3}\,x^2 + \ldots\ldots\ldots + c_{2k-1}(\ldots)\right), \quad (3.11)$$

where c_0, c_1, c_2,....., c_{2k-1} are the coefficients associated with the trial functions for the inclusion and matrix phases of the given heterogeneous medium.

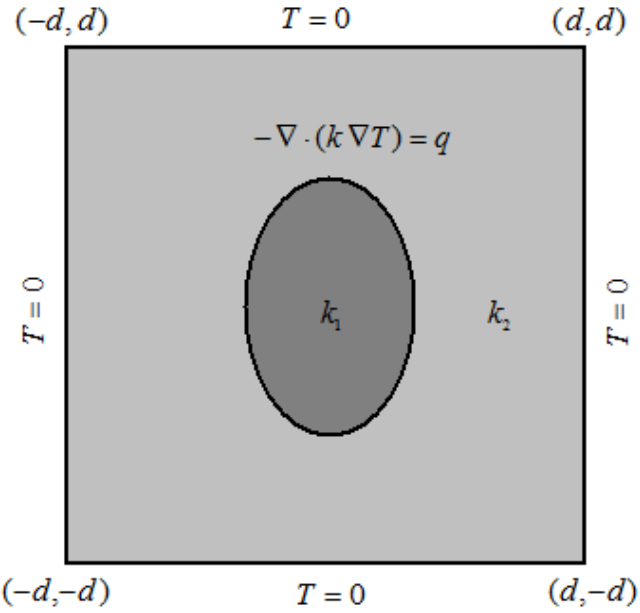

Figure 3.7 Steady state heat equation with internal heat generation for a SIP.

It is evident from Equation (3.11) that the homogeneous Dirichlet boundary conditions have been accounted for. In order for equilibrium to exist between the two distinct phases, it is required that the above trial functions also satisfy the continuity conditions of temperature and heat flux across the inclusion-matrix interface as described by Equations (2.8) and (2.9) respectively. In terms of the permissible functions, $f_1(x,y)$ and $f_2(x,y)$ defined above, the continuity conditions take the form:

$$f_1(x,y)|_{interface} = f_2(x,y)|_{interface}. \quad (3.12)$$

$$k_1 \frac{\partial}{\partial \boldsymbol{n}}\big(f_1(x,y)\big)|_{interface} = k_2 \frac{\partial}{\partial \boldsymbol{n}}\big(f_2(x,y)\big)|_{interface}, \tag{3.13}$$

where $\frac{\partial}{\partial \boldsymbol{n}}$, as discussed in Chapter 2, represents the directional derivative and in the context to Equation (3.13), it describes the rate of change of the trial functions, w.r.t a simultaneous change in x and y, with the direction of its change being defined by a normalized surface normal, $\boldsymbol{n}$. Equation (3.13) can be expanded in a more explicit fashion, by employing the formerly defined expression for the directional derivative as described by Equation (2.11), as

$$k_1 \left(\nabla f_1 \cdot \boldsymbol{n}\right)|_{interface} = k_2 \left(\nabla f_2 \cdot \boldsymbol{n}\right)|_{interface}.$$

Further, employing the definition of $\boldsymbol{n}$ for an elliptical interface, as described by Equation (2.10), to the above expression yields

$$k_1 \begin{pmatrix} \frac{\partial f_1}{\partial x} \\ \frac{\partial f_1}{\partial y} \end{pmatrix} \cdot \begin{pmatrix} \frac{x/a^2}{\sqrt{x^2/a^4 + y^2/b^4}} \\ \frac{y/b^2}{\sqrt{x^2/a^4 + y^2/b^4}} \end{pmatrix} |_{interface} = k_2 \begin{pmatrix} \frac{\partial f_2}{\partial x} \\ \frac{\partial f_2}{\partial y} \end{pmatrix} \cdot \begin{pmatrix} \frac{x/a^2}{\sqrt{x^2/a^4 + y^2/b^4}} \\ \frac{y/b^2}{\sqrt{x^2/a^4 + y^2/b^4}} \end{pmatrix} |_{interface},$$

where a and b are the semi-major and semi-minor axis of the elliptical inclusion (or interface). Application of the dot product definition and further simplification of the resulting expression yields the final form of the heat flux continuity condition that reads

$$k_1 \left(\frac{x}{a^2}\frac{\partial f_1}{\partial x} + \frac{y}{b^2}\frac{\partial f_1}{\partial y}\right)|_{interface} = k_2 \left(\frac{x}{a^2}\frac{\partial f_2}{\partial x} + \frac{y}{b^2}\frac{\partial f_2}{\partial y}\right)|_{interface}. \tag{3.14}$$

As explained in the previous chapter, solving the continuity conditions for c_i, where $i = 0, 1, 2, \ldots\ldots\ldots\ldots, (2k-1)$, followed by back-substitution into Equations (3.12) and (3.14), and extraction of the polynomials corresponding to each of the residual coefficients will result in a set of permissible functions. For illustration purposes, one of the computer generated permissible functions for the inclusion ($e_1(x,y)$) and the matrix ($e_2(x,y)$) are presented below:

$$e_1(x,y) = -\frac{a^6b^2k_2}{3k_1} + \frac{a^6d^2k_2}{k_1} + \frac{a^4b^2d^2k_2}{k_1} - \frac{2a^4d^4k_2}{k_1} - \frac{2a^2b^2d^2x^2k_2}{k_1} + \frac{2a^2d^4x^2k_2}{k_1} + \frac{a^2b^2x^4k_2}{k_1}$$
$$- \frac{a^2d^2x^4k_2}{k_1} + \frac{b^2d^2x^4k_2}{k_1} - \frac{2b^2x^6k_2}{3k_1} - \frac{2a^6d^2y^2k_2}{b^2k_1} + \frac{2a^4d^4y^2k_2}{b^2k_1} + \frac{a^6y^4k_2}{b^2k_1}$$
$$+ \frac{a^6d^2y^4k_2}{b^4k_1} - \frac{a^4d^2y^4k_2}{b^2k_1} - \frac{2a^6y^6k_2}{3b^4k_1},$$

$$e_2(x,y) = \frac{(d-x)(d+x)(d-y)(d+y)(b^4x^4 + 2a^2b^2x^2y^2 + a^4(-b^4+y^4))}{b^4}.$$

The functions, $e_1(x,y)$ and $e_2(x,y)$, represent one of the fourteen sets of permissible functions that result from an eighth order polynomial approximation; and the expressions clearly indicate that the permissible functions for heterogeneous materials depend on the geometrical parameters i.e. a, b and d, as well as the material constants, k_1 and k_2, of its constituent phases. The permissible functions, so derived, are now subjected to EEM that requires the determination of the A and B matrices; and they are constructed based on geometrical superposition as indicated in Figure 3.8.

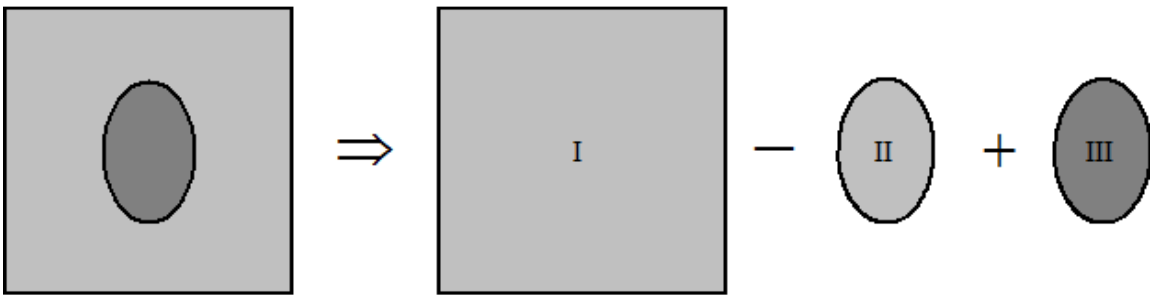

Figure 3.8 Geometrical decomposition of the SIP into its constituent phases.

$$A_{ij} = k_2\left(\iint_{\mathrm{I}} L[e_2\langle i\rangle]\, e_2\langle j\rangle\, dx\, dy - \iint_{\mathrm{II}} L[e_2\langle i\rangle]\, e_2\langle j\rangle\, dx\, dy\right)$$
$$+ k_1 \iint_{\mathrm{III}} L[e_1\langle i\rangle]\, e_1\langle j\rangle\, dx\, dy, \tag{3.15}$$

$$B_{ij} = \iint_{\mathrm{I}} e_2\langle i\rangle\, e_2\langle j\rangle\, dx\, dy \;-\; \iint_{\mathrm{II}} e_2\langle i\rangle\, e_2\langle j\rangle\, dx\, dy \;+\; \iint_{\mathrm{III}} e_1\langle i\rangle\, e_1\langle j\rangle\, dx\, dy, \tag{3.16}$$

where e_1 and e_2 are the permissible functions corresponding to the inclusion and matrix, respectively with i and j representing the i^{th} and j^{th} component of the N permissible functions. The resulting generalized eigenvalue problem is solved to obtain the eigenfuntions as

$$\varphi_i(x,y) = \begin{cases} \varphi_1\langle i\rangle \left(= \sum_{j=1}^{N} v_{ij} e_1\langle j\rangle \right), & 0 \le \dfrac{x^2}{a^2} + \dfrac{y^2}{b^2} \le 1 \\ \varphi_2\langle i\rangle \left(= \sum_{j=1}^{N} v_{ij} e_2\langle j\rangle \right), & \text{otherwise} \end{cases} . \tag{3.17}$$

The coefficients associated with the internal volumetric heat generation, q, are computed from

$$c_i = q\left(\iint_{\mathrm{I}} \varphi_2\langle i\rangle\, dx\, dy - \iint_{\mathrm{II}} \varphi_2\langle i\rangle\, dx\, dy + \iint_{\mathrm{III}} \varphi_1\langle i\rangle\, dx\, dy \right) \tag{3.18}$$

Finally, the expression for the temperature field is determined using Equation (3.7). The results associated with the single inclusion problem will be presented in the form of figures and tables. Essentially, two specimens will be studied separately; a centrally located circular and elliptical inclusion with $k_1 = 100,\ k_2 = 1,\ q = 1,\ d = 4, a = 1$, and their respective aspect ratios. First, a convergence study of the EEM solution for varying orders of the permissible functions is presented. Figure 3.9 shows the convergence of the temperature solution along the x-axis for an aspect ratio of 1 (or b =1) with even polynomial orders ranging between 6 and 12. Figure 3.10 presents a similar study for an aspect ratio of 0.6667 (or b = 1.5) with even orders ranging between 6 and 14. Tables 3.3 and 3.4 summarize the results of the convergence study for the single circular inclusion problem (SCIP) and single elliptical inclusion problem (SEIP), respectively. The study is based on a comparison of the number of permissible functions N, the dominating eigenvalue λ_1, the corresponding coefficient associated with internal heat generation c_1 and the temperature $T(x,y)$ at the origin; for each of the orders mentioned above.

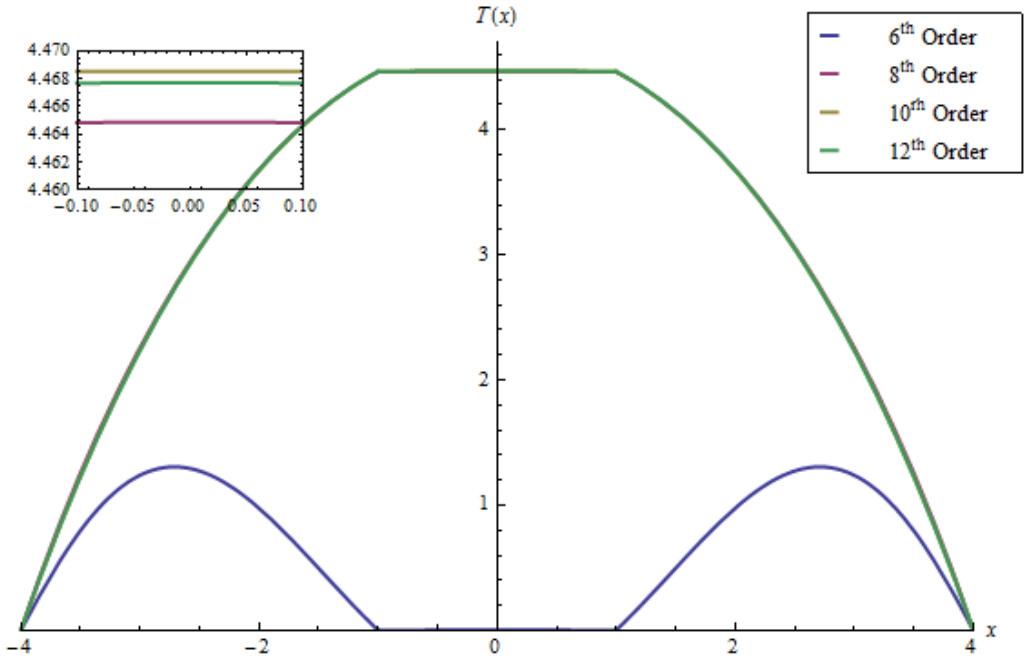

Figure 3.9 Convergence study of the temperature solution for the SCIP.

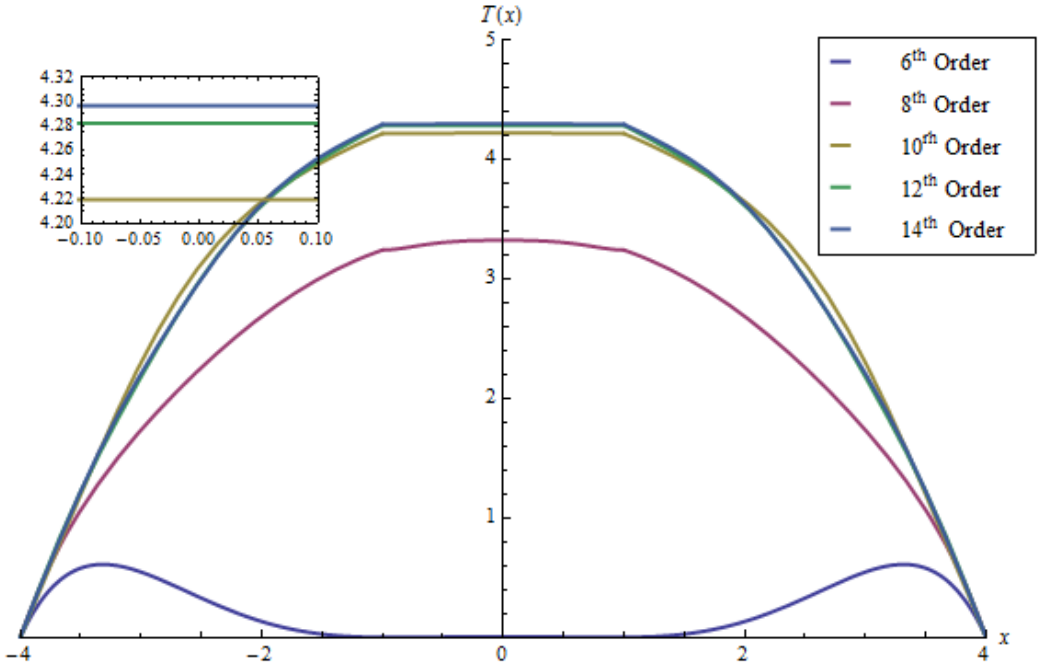

Figure 3.10 Convergence study of the temperature solution for the SEIP.

Table 3.3 Summary of the convergence study of the temperature solution for SCIP

Order	N	λ_1	c_1	$T(x,y)$ at $(x=0,\, y=0)$
6	3	0.91027	6.73748	0.00478
8	18	0.31056	6.50506	4.46487
10	44	0.31055	6.50518	4.46854
12	78	0.31054	6.50513	4.46771

Table 3.4 Summary of the convergence study of the temperature solution for SEIP

Order	N	λ_1	c_1	$T(x,y)$ at $(x=0,\, y=0)$
6	2	2.40086	6.00486	0.00346
8	14	0.38005	6.69399	3.32248
10	40	0.31868	6.53864	4.21954
12	74	0.31543	6.54107	4.28180
14	116	0.31472	6.53791	4.29610

The above illustrations and tabulations suggest that the convergence of the temperature solution is faster for a circular geometry than for the elliptical. Also, it can be observed that an 8^{th} order polynomial for the circular inclusion and a 12^{th} order polynomial for the elliptical inclusion are sufficient to provide a reasonable approximation of the final solution without a compromise on the computational efficiency.

Figures 3.11 and 3.12 show a few arbitrarily chosen eigenfunctions for each of these aspect ratios. A noticeable feature in all of these representations, besides the independent nature of the eigenfunctions, is the shape of the inclusions being clearly reflected in each of the eigenfunctions. Figures 3.13 to 3.20 present the EEM temperature solution for SCIP and SEIP, and their cross-sectional comparison with the corresponding FEM solutions.

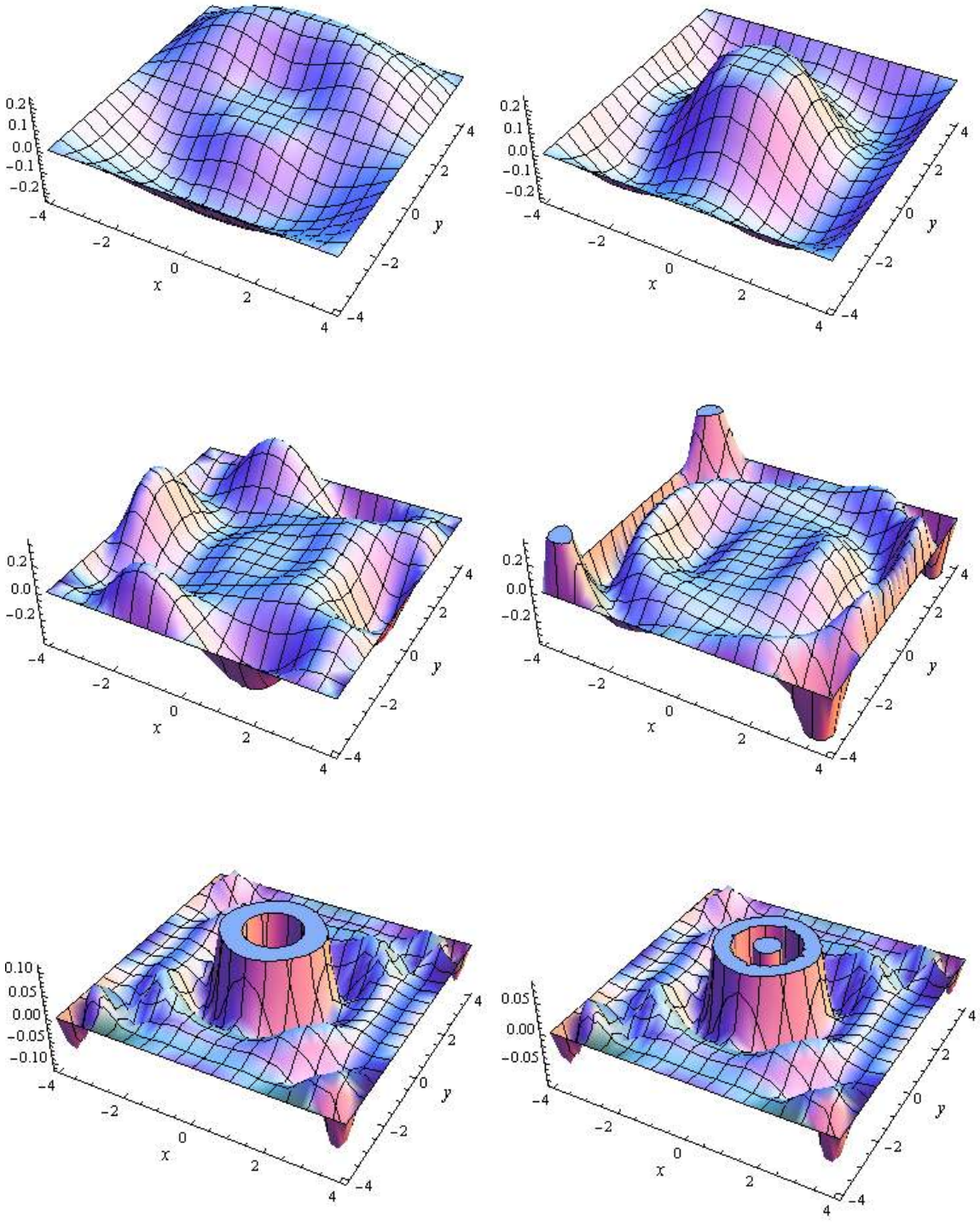

Figure 3.11 Arbitrarily chosen eigenfunctions for the PTE in the SCIP.

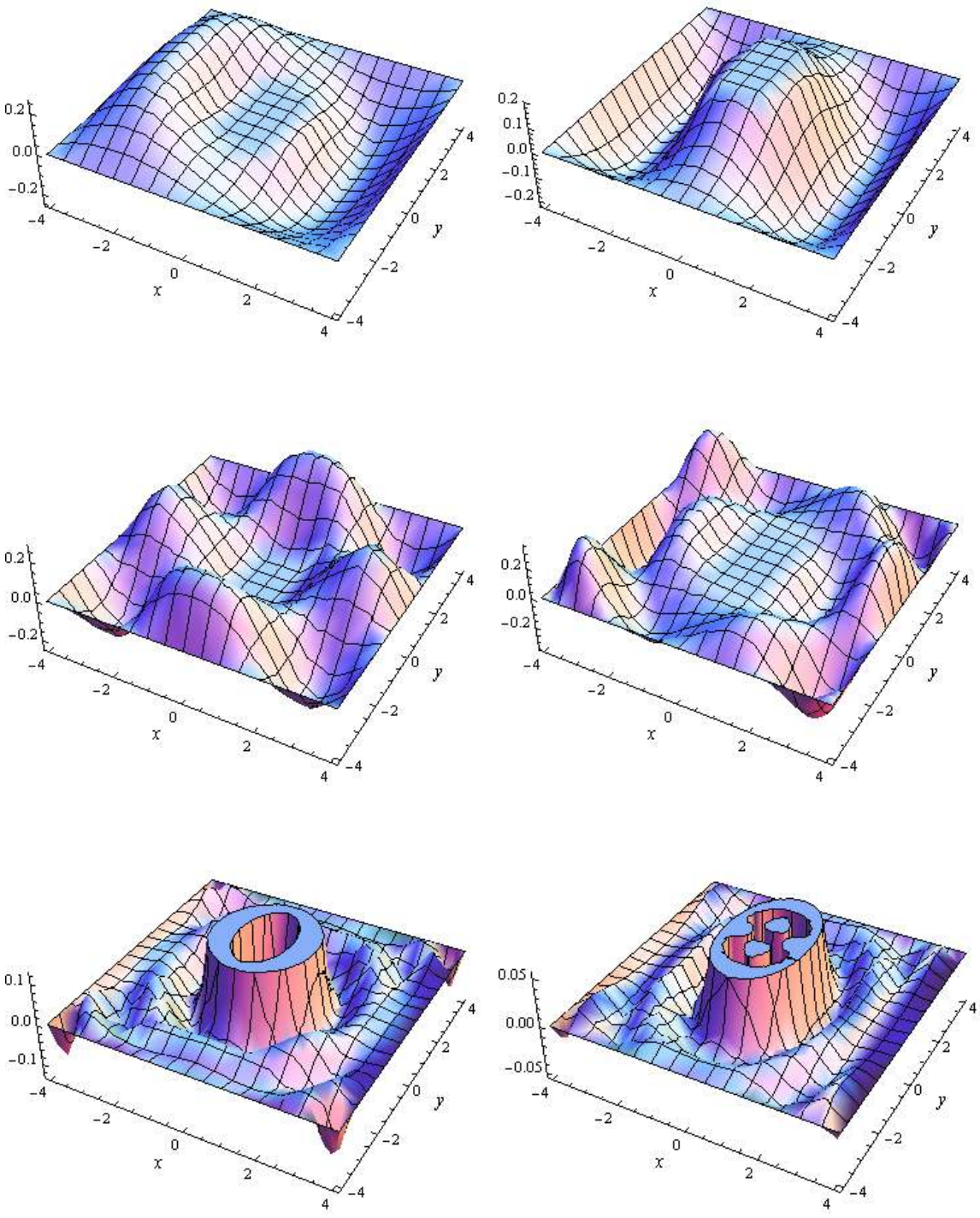

Figure 3.12 Arbitrarily chosen eigenfunctions for the PTE in the SEIP.

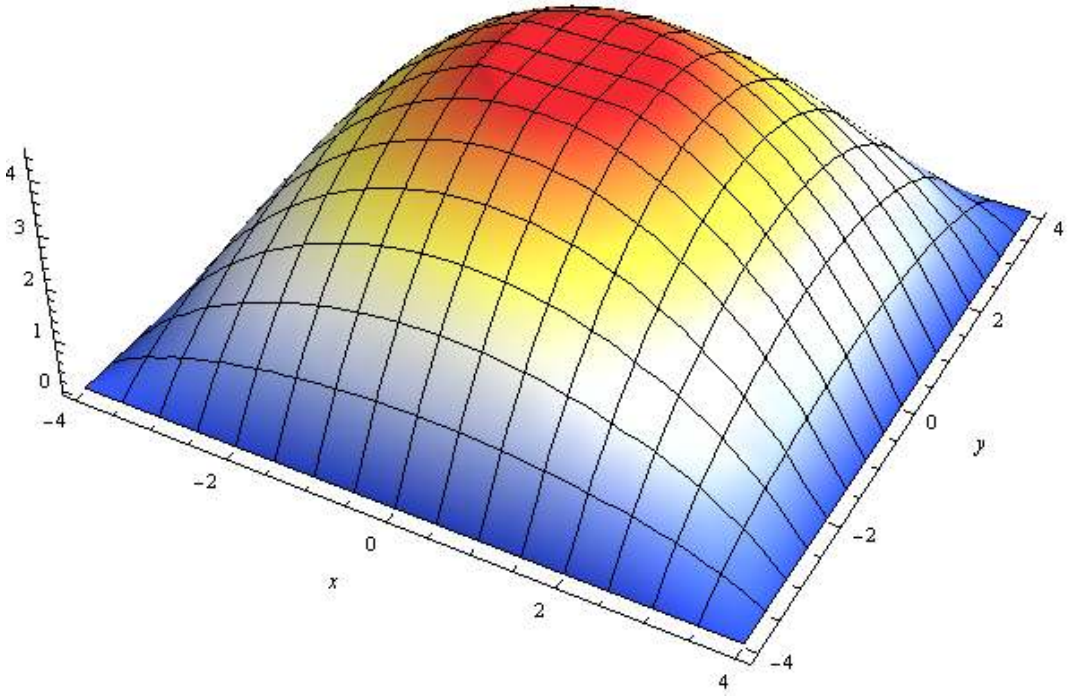

Figure 3.13 3-D Temperature profile for the PTE in the SCIP.

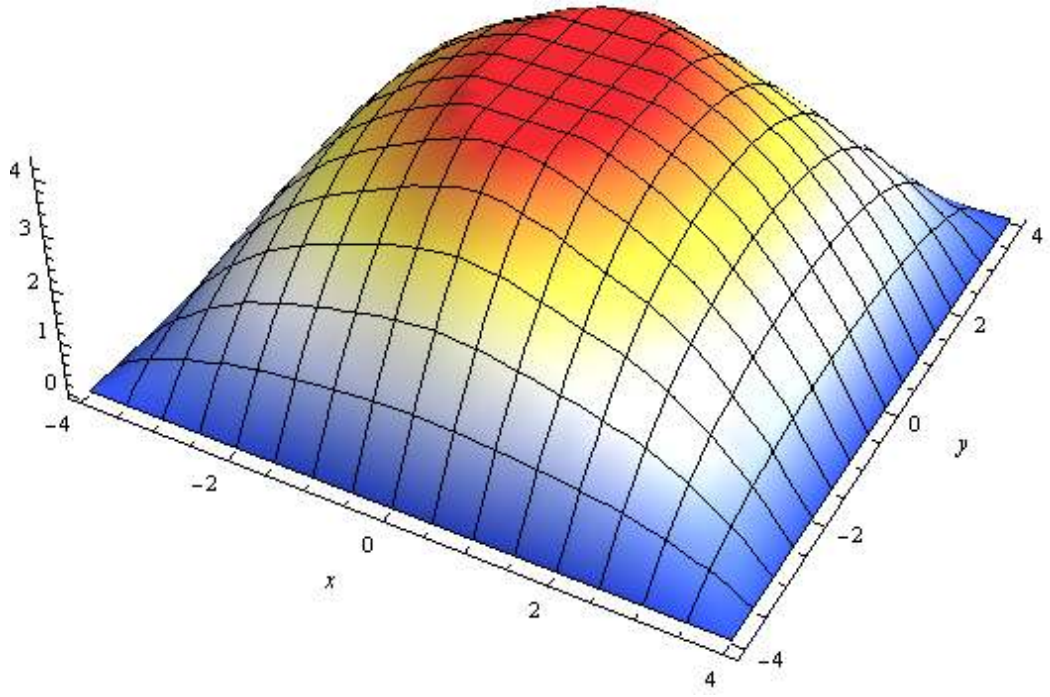

Figure 3.14 3-D Temperature profile for the PTE in the SEIP.

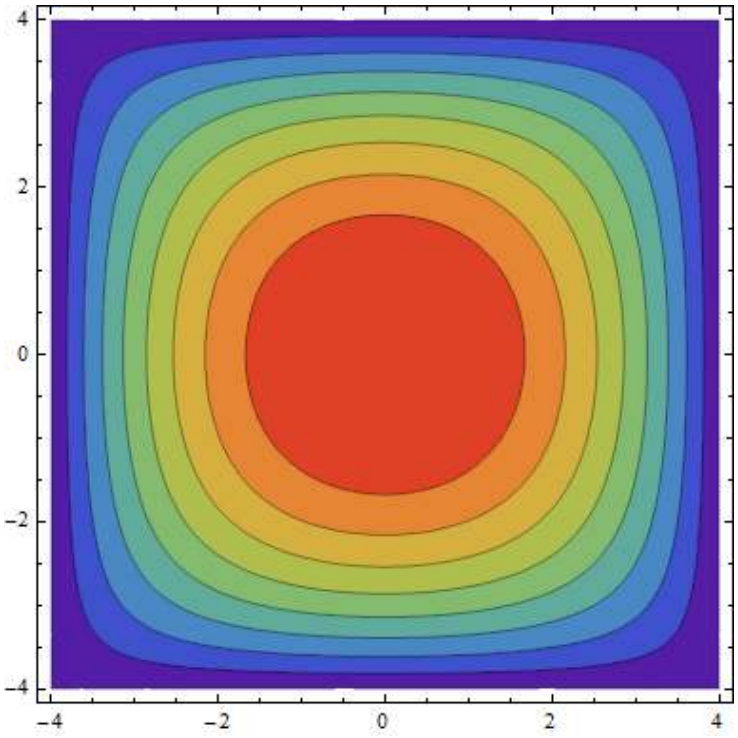

Figure 3.15 Temperature contour plot for the PTE in the SCIP.

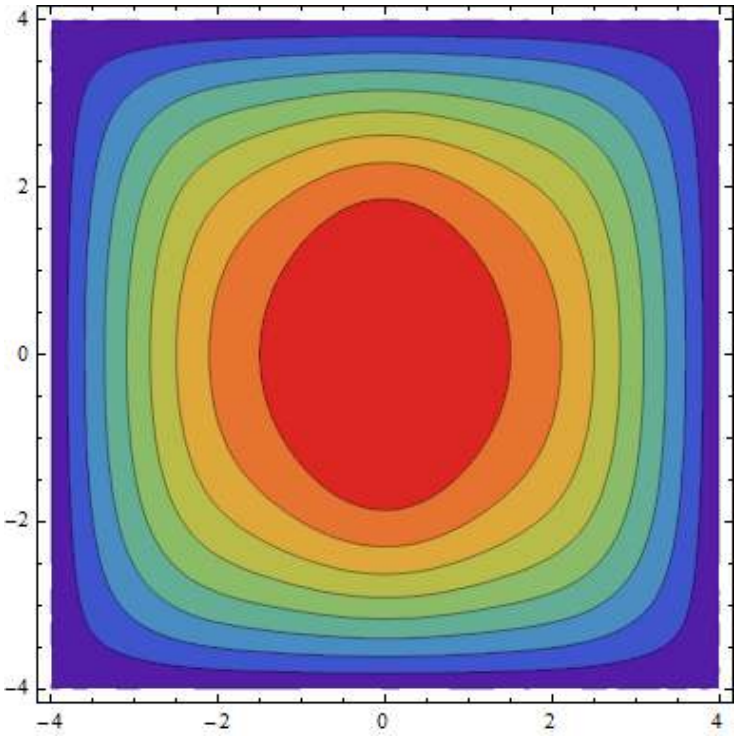

Figure 3.16 Temperature contour plot for the PTE in the SEIP.

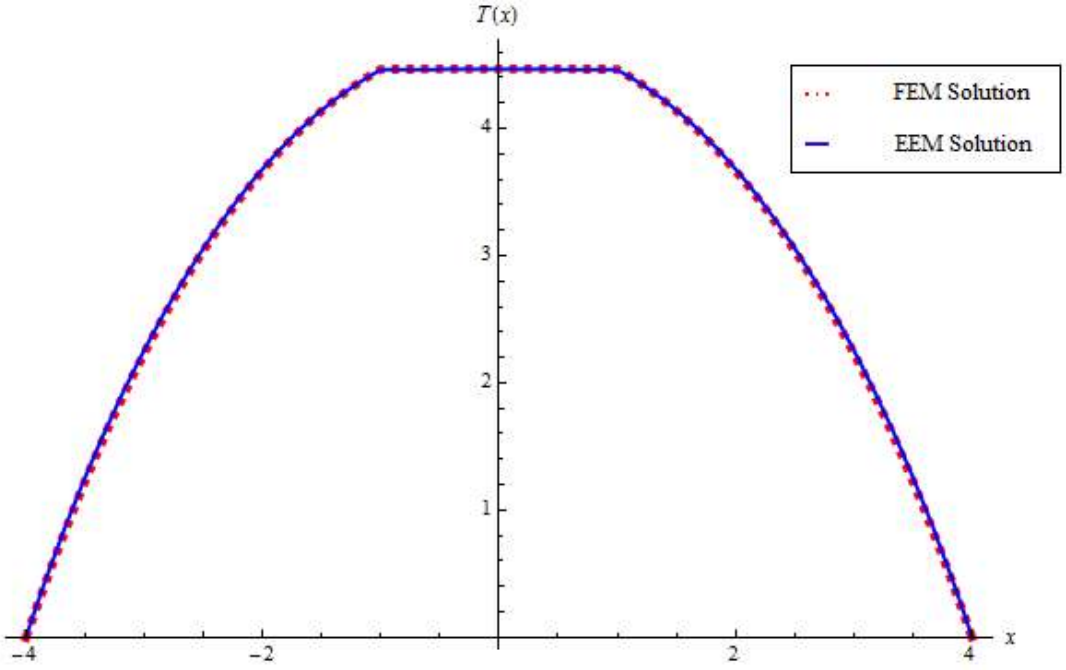

Figure 3.17 Comparison between the EEM solution and the FEM solution for the PTE along the x-axis for the SCIP.

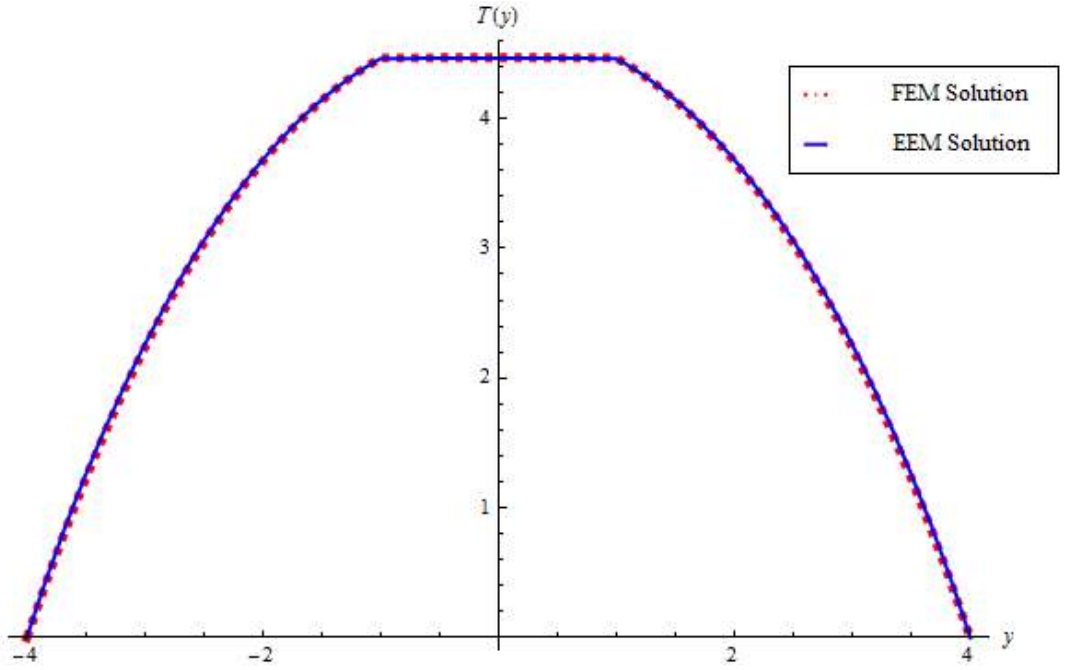

Figure 3.18 Comparison between the EEM solution and the FEM solution for the PTE along the y-axis for the SCIP.

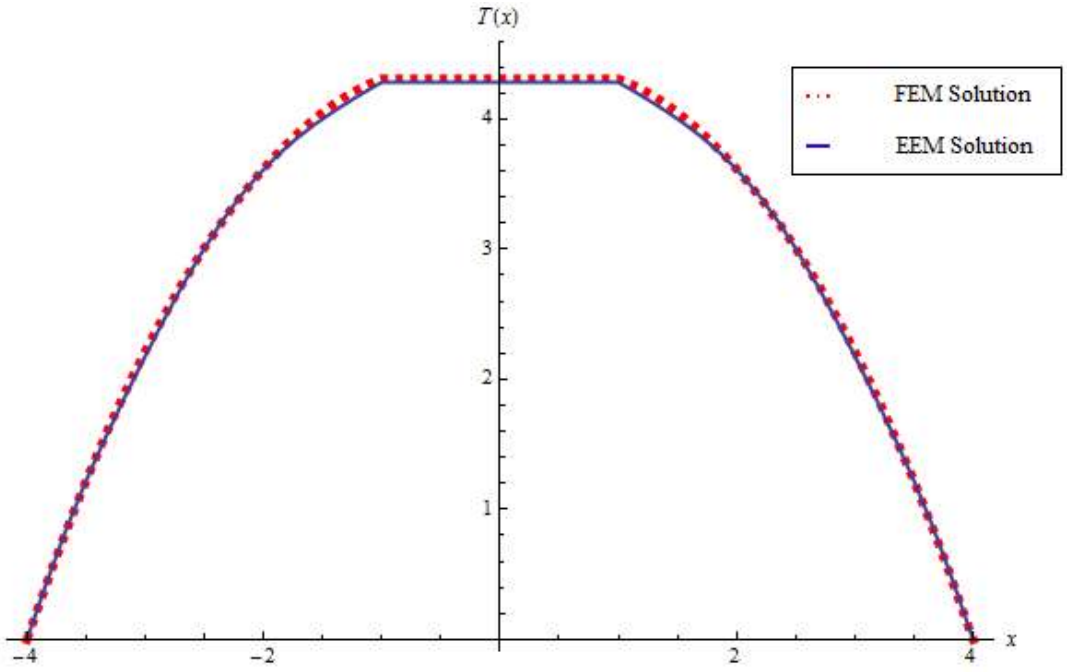

.

Figure 3.19 Comparison between the EEM solution and the FEM solution for the PTE along the x-axis for the SEIP.

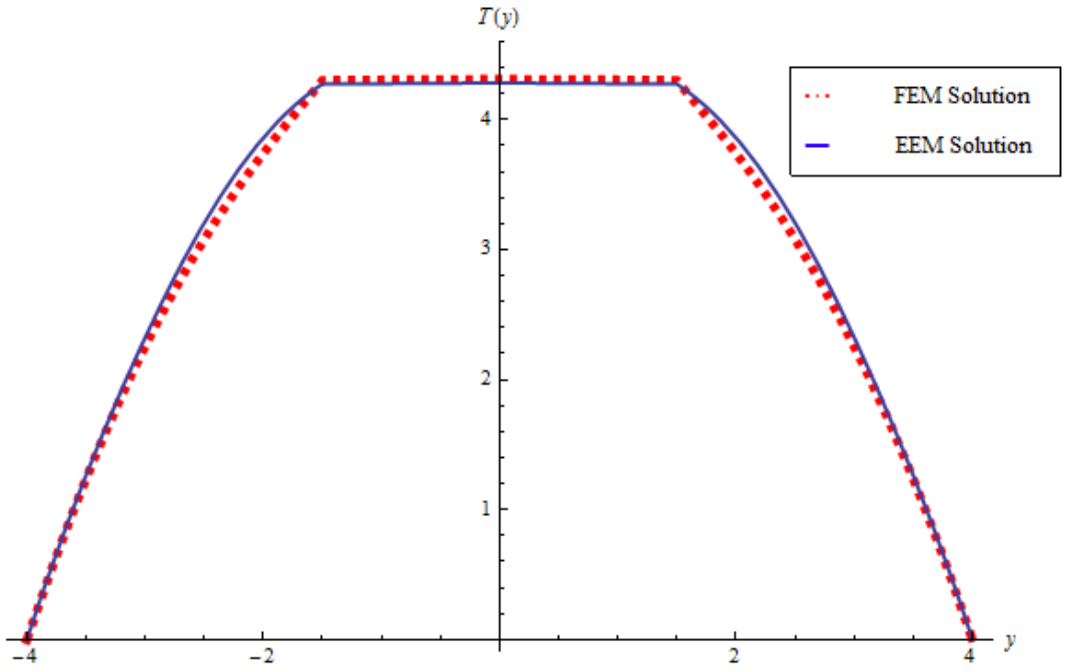

Figure 3.20 Comparison between the EEM solution and the FEM solution for the PTE along the y-axis for the SEIP.

Figures 3.13 and 3.14 depict the 3-D temperature profile for the SCIP and SEIP conforming to an 8^{th} and 12^{th} order approximation, respectively. The impact of the inclusion on the temperature profile is evident in these illustrations. The temperature contour plots (Figures 3.15 and 3.16) also exhibit a similar shape effect of the inclusion; while also portraying the distribution of temperature in the heterogeneous domain. Figures 3.17 - 3.20 provide a comparison between the EEM and FEM solutions; along the x and y axes of the inclusion for aspect ratios of 1 and 0.67. Table 3.5 substantiates the results of the comparison plots.

Table 3.5 Comparison between the EEM and FEM solutions for the SIPs

$T(x,y)$ at $(x=0,\ y=0)$				
Inc. Aspect Ratio	Inclusion Area	EEM Solution	FEM Solution	Percentage Diff.
1	π	4.4648	4.4675	0.0605
0.667	1.5 π	4.2818	4.3112	0.6866

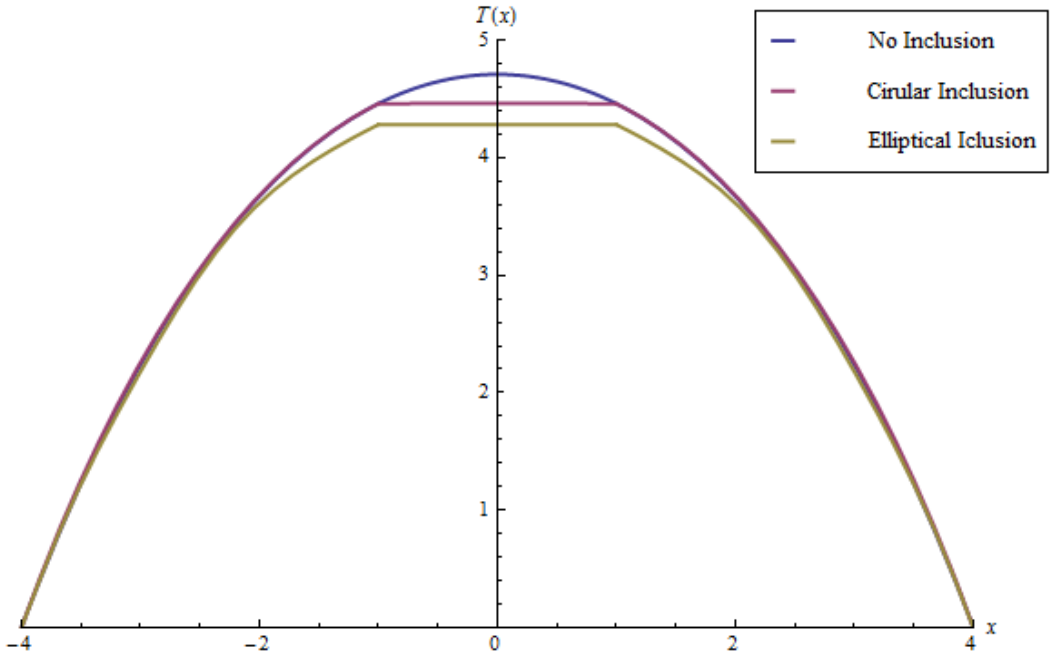

Figure 3.21 Effect on temperature due to the presence of single inclusions.

Figure 3.21 provides a comparison of the cross-sectional temperature profile between the homogeneous and heterogeneous cases studied heretofore. The effect of a more thermally conductive inclusion can be noticed that translates into a reduction in temperature. Thus, it is clear that an inclusion, with a thermal conductivity greater than the surrounding matrix, will act as a heat sink thus initiating a cooling process; a much desired necessity in electronic paraphernalia. On the same lines, an inclusion, with a thermal conductivity lower than the matrix, would serve as a thermal insulator. Hence based on the application, by varying the geometrical parameters such as the aspect ratio, position (or location), and area of the inclusion; and material properties namely thermal conductivity, an optimum temperature level, at any desired location, can be achieved. In an effort to better comprehend the effect of the afore-mentioned variables on the resulting temperature profile, a parametric study is presented below. More specifically, a sensitivity analysis will be carried out by varying the geometrical and material constants and predicting the respective temperature response, hence facilitating an optimum and cost effective design. The semi-analytical approach is a reasonable choice for an investigation of this nature since the analytically derived permissible functions retain the geometrical and material parameters in its most generic form.

First, an analysis based on varying aspect ratios (Figure 3.22) is presented in which the aspect ratio of a centrally located inclusion i.e. at $(x_1, y_1) \equiv (0,0)$ with a constant surface area ($\pi\, a\, b$), is varied by appropriate permutations of the major and minor axis of the elliptical inclusion. In the second instance (Figure 3.23), while maintaining the same aspect ratio, the area of the centrally located inclusion is varied, again by suitably altering the axes of the inclusion. Thirdly (Figure 3.24), for a fixed measure of the major and minor axes, the position of the inclusion is varied along the x-axis. In all of the above mentioned analysis scenarios, the effect on the temperature profile is examined while preserving a constant inclusion to matrix thermal conductivity ratio (k_1/k_2). In the final analysis (Figure 3.25) for the SIPs, the influence of varying conductivity ratios on the resulting temperature field is examined.

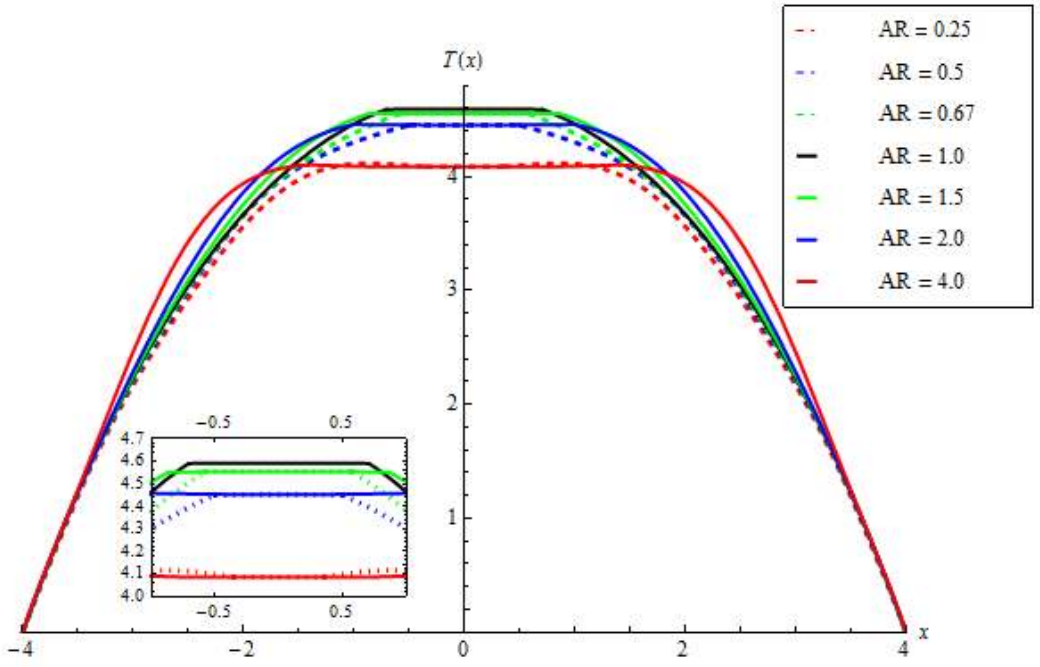

Figure 3.22 Effect of varying inclusion aspect ratios on the temperature field for SIPs.

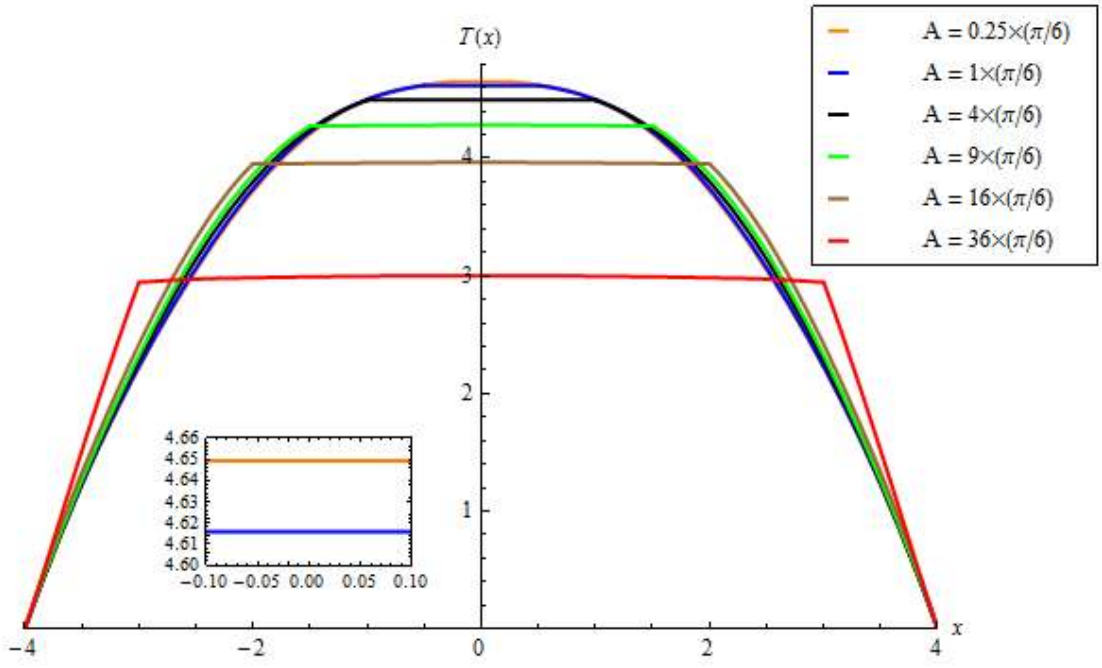

Figure 3.23 Effect of varying inclusion surface areas on the temperature field for SIPs.

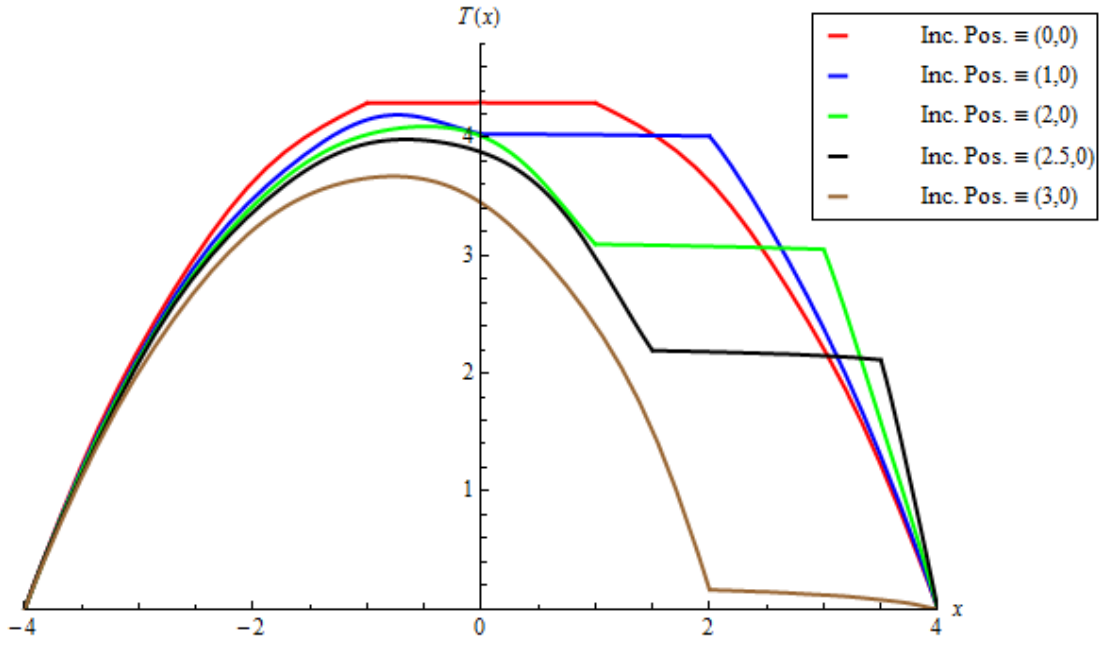

Figure 3.24 Effect of varying inclusion positions on the temperature field for SIPs.

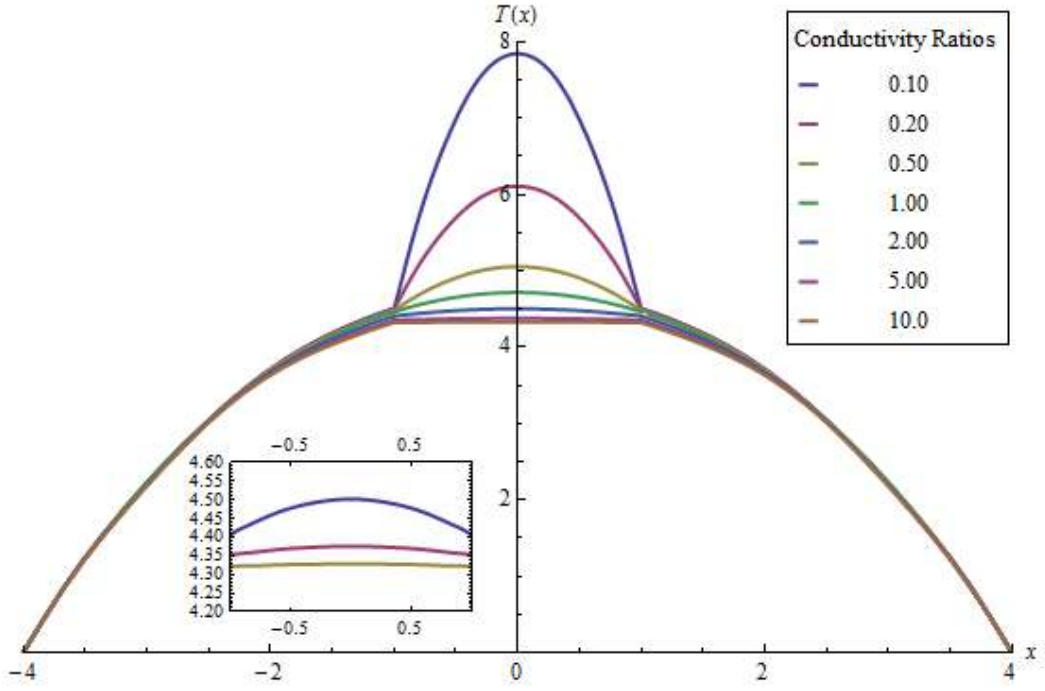

Figure 3.25 Effect of varying conductivity ratios on the temperature field for SIPs.

Table 3.6 Effect of varying aspect ratio of the inclusion on the temperature field for SIPs

Constant parameters for the inclusion			Varying parameters for the inclusion			
$\pi\ a\ b$	(x_1, y_1)	k_1/k_2	a	b	a/b	T_{max}
$\frac{\pi}{2}$	$(0,0)$	$\frac{100}{1}$	0.35355	1.41421	0.25	4.08588
			0.50000	1.00000	0.50	4.45147
			0.57735	0.86603	0.67	4.55313
			0.70711	0.70711	1.00	4.59108
			0.86603	0.57735	1.50	4.55313
			1.00000	0.50000	2.0	4.45147
			1.41421	0.35355	4.0	4.08552

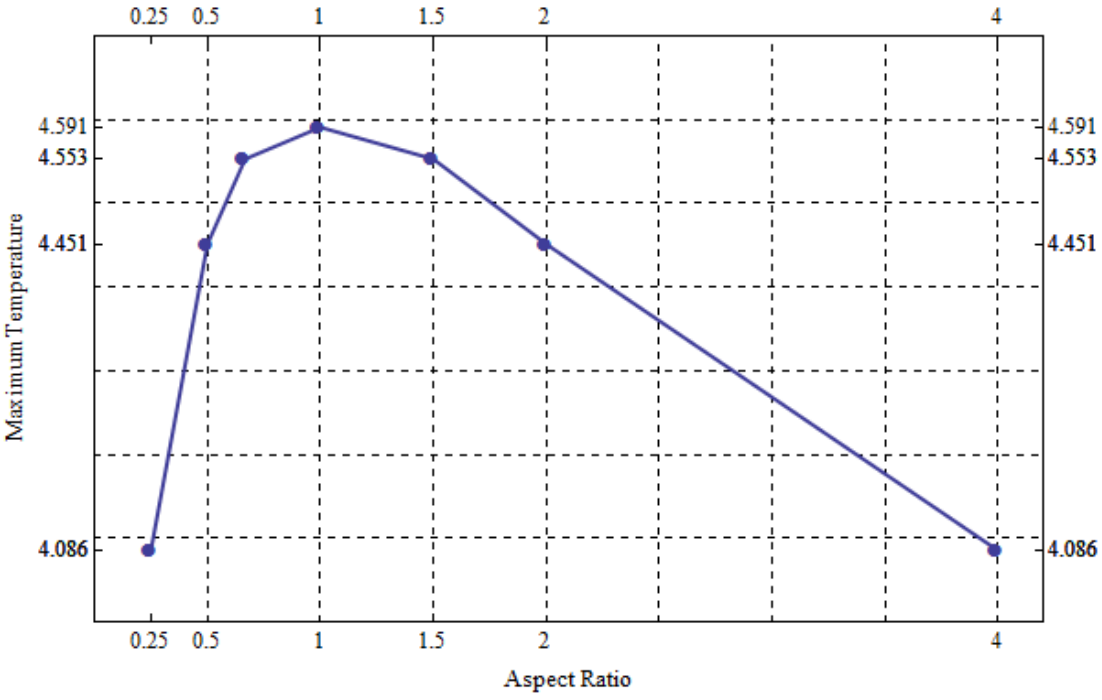

Figure 3.26 Variation of maximum temperature w.r.t the inclusion aspect ratio for SIPs.

Table 3.7 Effect of varying surface area of the inclusion on the temperature field for SIPs

Constant parameters for the inclusion			Varying parameters for the inclusion			
a/b	(x_1, y_1)	k_1/k_2	a	b	$\pi\ a\ b$	T_{max}
$\frac{3}{2}$	$(0,0)$	$\frac{100}{1}$	0.25	0.1667	0.1309	4.64935
			0.50	0.3334	0.5236	4.61579
			1.00	0.6667	2.0944	4.49674
			1.50	1.00	4.7124	4.28180
			2.00	1.3334	8.3776	3.96395
			3.00	2.00	18.8496	3.00160

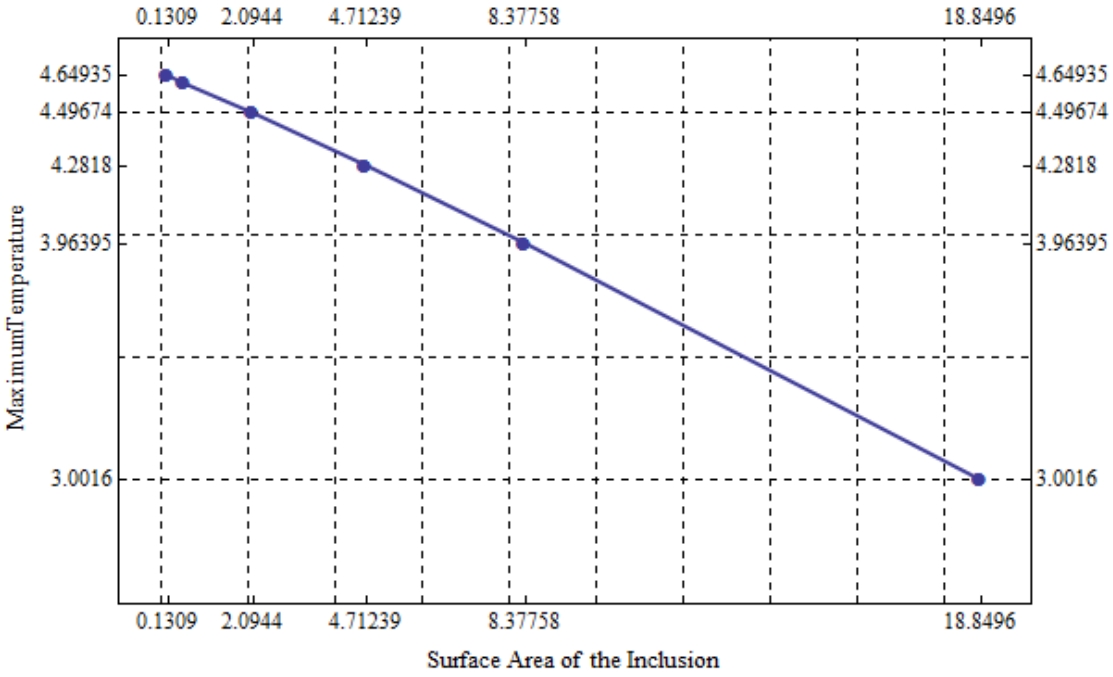

Figure 3.27 Variation of maximum temperature w.r.t the inclusion area for SIPs.

Table 3.8 Effect of varying position of the inclusion on the temperature field for SIPs

Constant parameters for the Inclusion					Varying parameters for the inclusion	
a/b	a	b	$\pi\ a\ b$	k_1/k_2	(x_1, y_1)	Maximum Temperature
$\frac{2}{3}$	1	1.5	$\frac{3\pi}{2}$	$\frac{100}{1}$	$(0,0)$	4.2961
					$(1,0)$	4.1928
					$(2,0)$	4.0944
					$(2.5,0)$	3.9844
					$(3,0)$	3.6712

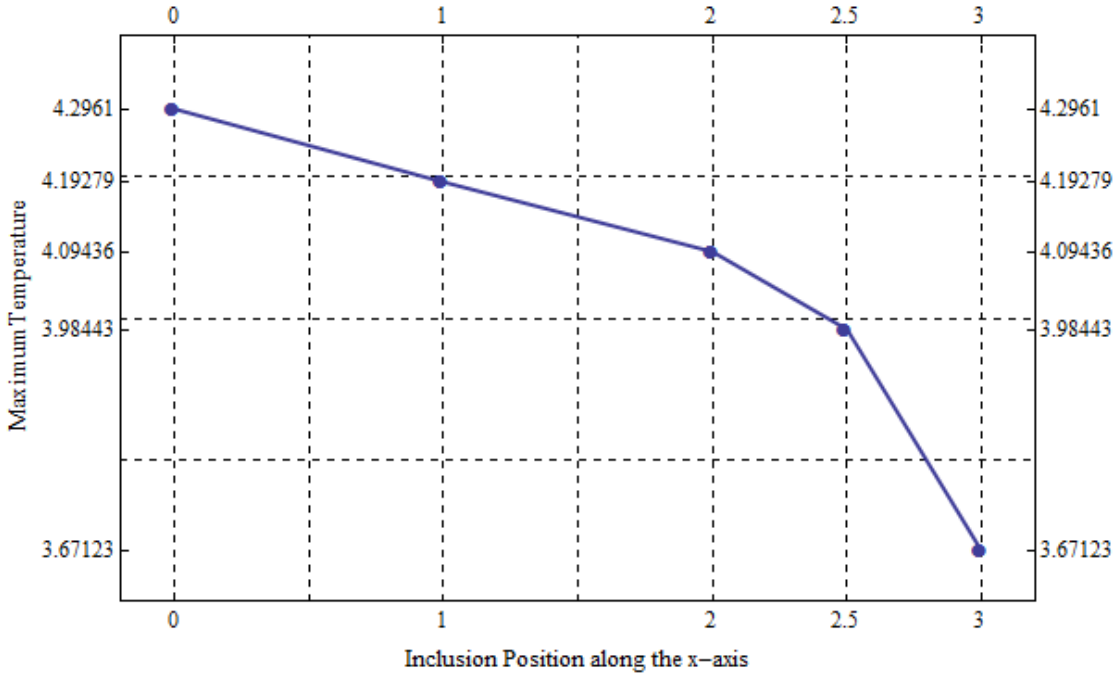

Figure 3.28 Variation of maximum temperature w.r.t the inclusion position for SIPs.

Table 3.9 Effect of varying inclusion-matrix conductivity ratio on the temperature field for SIPs

Constant Parameters for the inclusion					Varying Parameters for the inclusion	
a/b	a	b	$\pi\ a\ b$	(x_1, y_1)	k_1/k_2	Maximum Temperature
$\frac{2}{3}$	1	1.5	$\frac{3\pi}{2}$	$(0,0)$	0.1	7.84086
					0.2	6.10417
					0.5	5.05295
					1	4.71466
					2	4.50174
					5	4.37550
					10	4.32848

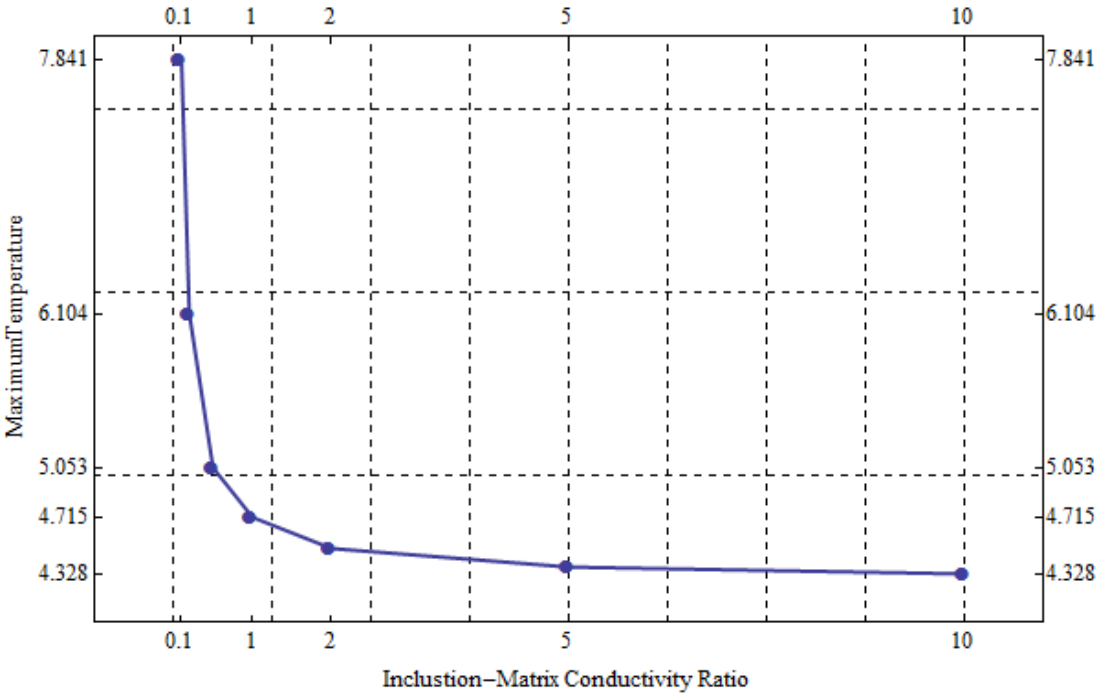

Figure 3.29 Variation of maximum temperature w.r.t the thermal conductivity ratio for SIPs.

Figure 3.22 and Table 3.6 suggest that for the same amount of inclusion material, the temperature field in a centrally located elliptical inclusion experiences a reduction in temperature as the aspect ratio increases for $\frac{a}{b} > 1$. An anti-symmetrical behavior is observed for $\frac{a}{b} < 1$ in which case the temperature undergoes a proportionate reduction with the aspect ratio. Figure 3.26 further delineates this observation.

Again, for a centrally located inclusion with a constant conductivity ratio, Figure 3.23 and Table 3.7 demonstrate the inversely proportional relationship between the surface area of an elliptical inclusion and the maximum temperature in the heterogeneous media, while maintaining a constant aspect ratio. Figure 3.27 provides a more elaborate representation of the above statement. Thus, from the analysis carried out, so far, it can be pointed out that for a given inclusion position and conductivity ratio, the inclusion axes can be optimally altered to meet the temperature requirements.

Figure 3.24 and Table 3.8 provide the results of the temperature field with varying position of the inclusion along the positive direction of the x-axis, while retaining the same values for a and b of the elliptical inclusion. It can be observed that as the inclusion moves from the center towards the boundary of the matrix medium, there is a reduction in the maximum temperature of the heterogeneous material. A closer observation would also reveal a faster rate of reduction in the maximum temperature (Figure 3.28) as the inclusion approaches the boundary A similar behavior can be anticipated along the negative x-axis.

Figure 3.25 and Table 3.9 demonstrate the effect on the temperature field as a result of varying the thermal conductivity of the inclusion (k_1) while maintaining the conductivity of the matrix to be a constant i.e. $k_2 = 1$. Setting k_1 equal to 1 represents a homogeneous medium and using this as a reference point, it can be noticed that for all $k_1 < 1$; as the value of k_1 decreases, the maximum temperature increases substantially. For $k_1 > 1$, the maximum temperature decreases gradually with an increase in k_1, almost approaching a constant value for large values of k_1. Figure 3.29 graphically illustrates this effect.

3.2.2 Multiple Inclusion Problems (MIPs)

For this class of problems, the geometry, as in the single inclusion problems, comprises of a matrix, but with two (or more) inclusions; each phase carrying different material properties. Figure 3.30, below, illustrates one such geometrical configuration (two inclusions problem - TIP) of a square-shaped matrix with two inclusions (equally spaced from the origin) having thermal conductivities, k_1 and k_2, but different from that of the matrix i.e. k_3.

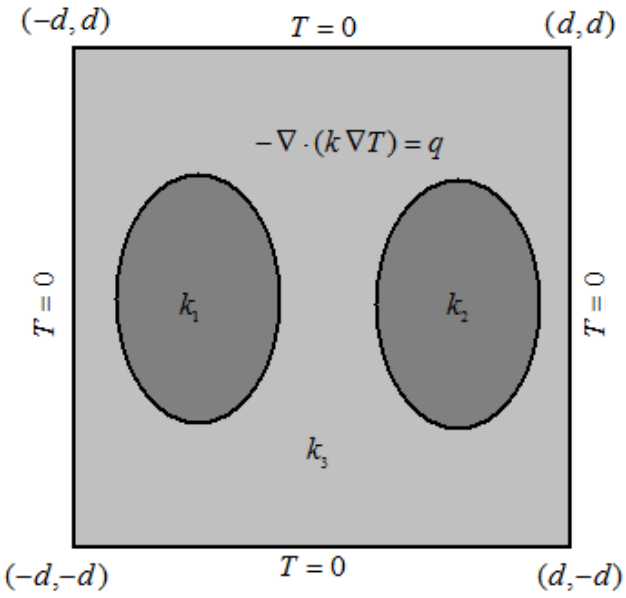

Figure 3.30 Steady state heat equation with internal heat generation for a TIP.

Three basis functions corresponding to the three distinct phases of the heterogeneous medium, $f_1(x,y)$ and $f_2(x,y)$ for the two inclusions, and $f_3(x,y)$ for the matrix that also satisfies the Dirichlet boundary conditions, are defined separately as

$$f_1(x,y) = \alpha_0 + \alpha_1(x) + \alpha_2(y) + \alpha_3(x^2) + \alpha_4(xy) + \alpha_5(y^2) + \ldots\ldots\ldots + \alpha_{k-1}(\ldots), \quad (3.19)$$

$$f_2(x,y) = \alpha_k + \alpha_{k+1}(x) + \alpha_{k+2}(y) + \alpha_{k+3}(x^2) + \alpha_{k+4}(xy) + \ldots\ldots\ldots + \alpha_{2k-1}(\ldots), \quad (3.20)$$

$$f_3(x,y) = (x^2 - d^2)(y^2 - d^2)\,(\alpha_{2k} + \alpha_{2k+1}(x) + \alpha_{2k+2}(y) + \ \ldots\ldots\ldots + \alpha_{3k-1}(\ldots)), \qquad (3.21)$$

where $\alpha_0, \alpha_1, \ldots\ldots\ldots, \alpha_{3k-1}$ are the unknown coefficients that are solved for, in terms of each other, by subjecting the above expressions to the following continuity conditions

$$f_1(x,y)|_{interface} = f_3(x,y)|_{interface}. \qquad (3.22)$$

$$f_2(x,y)|_{interface} = f_3(x,y)|_{interface}. \qquad (3.23)$$

$$k_1 \frac{\partial}{\partial \boldsymbol{n}}\big(f_1(x,y)\big)|_{interface} = k_3 \frac{\partial}{\partial \boldsymbol{n}}\big(f_3(x,y)\big)|_{interface}, \qquad (3.24)$$

$$k_2 \frac{\partial}{\partial \boldsymbol{n}}\big(f_2(x,y)\big)|_{interface} = k_3 \frac{\partial}{\partial \boldsymbol{n}}\big(f_3(x,y)\big)|_{interface}, \qquad (3.25)$$

Equations (3.22) and (3.23) represent the continuity of temperature across the elliptical interface; while Equations (3.24) and (3.25) denote the heat flux continuity across the interface. As discussed earlier, $\boldsymbol{n}$ represents the normal to the interface, which dictates the direction of the heat flux; an expression for which is obtained from the equation that describes the shape of the interface. Hence, for an elliptical interface, the surface normal is obtained as follows, starting with the equation of an ellipse.

$$\frac{x^2}{a^2} + \frac{y^2}{b^2} = 1.$$

Administering the total derivative of the above equation yields

$$\left(\frac{x}{a^2}\right) dx + \left(\frac{y}{b^2}\right) dy = 0.$$

The above expression can be expressed in the vector form as the dot product of two vectors as

$$\begin{pmatrix} x/a^2 \\ y/b^2 \end{pmatrix} \cdot \begin{pmatrix} dx \\ dy \end{pmatrix} = 0.$$

The above relation suggests that the vector $\begin{pmatrix} x/a^2 \\ y/b^2 \end{pmatrix}$ is orthogonal to the surface described by the vector $\begin{pmatrix} dx \\ dy \end{pmatrix}$ and hence, $\begin{pmatrix} x/a^2 \\ y/b^2 \end{pmatrix}$ represents the normal vector to the surface; the normalized form of which yields the following expression for $\boldsymbol{n}$ as described by Equation (2.10). Essentially, the heat flux continuity condition is based on the Fourier's law of heat conduction which states that the heat flux $\boldsymbol{h}$ (or the rate of heat energy transfer through a surface) is proportional to the negative temperature gradient ($-\nabla T$); with the constant of proportionality being defined by the material's ability to conduct heat which in turn is measured in terms of the material's thermal conductivity k. Hence,

$$\boldsymbol{h} = -k\,\nabla T, \tag{3.26}$$

is the mathematical representation of the Fourier's law. The negative sign in Equation (3.26) suggests that the heat transfer takes place in the direction of decreasing temperature. Since the surface of interest is the elliptical interface across which the continuity of heat flux must be preserved; and the defining parameter of this surface is the normal ($\boldsymbol{n}$) that continually changes at each point of the interface, it is but appropriate to define the heat flux in terms of the directional derivative of temperature in the direction of $\boldsymbol{n}$. Hence, for the elliptical inclusion on the left with thermal conductivity k_1, it's heat flux continuity with the surrounding matrix of thermal conductivity k_3 would read

$$k_1(\nabla_{\boldsymbol{n}} T_1)|_{interface} = k_3(\nabla_{\boldsymbol{n}} T_3)|_{interface}, \tag{3.27}$$

where T_1 and T_3 are the temperatures corresponding to the inclusion and matrix phase respectively, and $\nabla_{\boldsymbol{n}}$ represents the directional derivative of temperature in the direction of $\boldsymbol{n}$, mathematically expressed as

$$\nabla_{\boldsymbol{n}} T(x,y) = \frac{\partial}{\partial n}\big(T(x,y)\big) = \nabla T(x,y) \cdot \boldsymbol{n}. \tag{3.28}$$

Replacing T_1 and T_3 in Equation (3.27) with their respective trial functions $f_1(x,y)$ and $f_3(x,y)$, and imposing Equations (3.28) and (2.10) yields

$$k_1 \begin{pmatrix} \frac{\partial f_1}{\partial x} \\ \frac{\partial f_1}{\partial y} \end{pmatrix} \cdot \begin{pmatrix} \frac{x/a^2}{\sqrt{x^2/a^4 + y^2/b^4}} \\ \frac{y/b^2}{\sqrt{x^2/a^4 + y^2/b^4}} \end{pmatrix} |_{interface} = k_2 \begin{pmatrix} \frac{\partial f_2}{\partial x} \\ \frac{\partial f_2}{\partial y} \end{pmatrix} \cdot \begin{pmatrix} \frac{x/a^2}{\sqrt{x^2/a^4 + y^2/b^4}} \\ \frac{y/b^2}{\sqrt{x^2/a^4 + y^2/b^4}} \end{pmatrix} |_{interface}.$$

Further simplification of the above expression yields

$$k_1 \left(\frac{x}{a^2} \frac{\partial f_1(x,y)}{\partial x} + \frac{y}{b^2} \frac{\partial f_1(x,y)}{\partial y} \right) |_{interface} = k_3 \left(\frac{x}{a^2} \frac{\partial f_3(x,y)}{\partial x} + \frac{y}{b^2} \frac{\partial f_3(x,y)}{\partial y} \right) |_{interface} \tag{3.29}$$

On similar lines, the heat flux continuity condition at the elliptical interface that separates the inclusion of thermal conductivity k_2 and the surrounding matrix, can be expressed as

$$k_2 \left(\frac{x}{a^2} \frac{\partial f_2(x,y)}{\partial x} + \frac{y}{b^2} \frac{\partial f_2(x,y)}{\partial y} \right) = k_3 \left(\frac{x}{a^2} \frac{\partial f_3(x,y)}{\partial x} + \frac{y}{b^2} \frac{\partial f_3(x,y)}{\partial y} \right) \tag{3.30}$$

Thus, in totality, Equations (3.22), (3.23), (3.29), and (3.30) represent the continuity conditions for the given geometry; the solution to which results in expressions for the unknown coefficients of the trial functions. Described below is a more detailed version of a computationally efficient procedure involved in procuring the permissible functions. Equations (3.22) and (3.29) correspond to the continuity conditions across the elliptical interface that separates the matrix and the inclusion on the left, positioned at $(x_1, 0)$. As discussed in Chapter 2, the continually varying coordinates, x and y, along every point on the elliptical interface can be best described in terms of an angle, θ. Thus, Equations (3.22) and (3.29) are subjected to the following parametric relation:

$$\{x, y\} = \{a\ \cos\theta - x_1, b \sin\theta\} \tag{3.31}$$

In a similar fashion, Equations (3.23) and (3.30) corresponding to the inclusion on the right, positioned at $(x_2, 0)$, are subjected to

$$\{x, y\} = \{a\ \cos\theta + x_2, b \sin\theta\} \tag{3.32}$$

The afore-mentioned substitutions result in a set of simultaneous equations that involve an array of trigonometric polynomials. Shown below is a sample part of one such equation:

$$\begin{aligned} \dots\dots\dots + \frac{1}{8}a^2b^3g[8]\mathrm{Sin}[\theta] + \frac{1}{4}a^2bd^2g[8]\mathrm{Sin}[\theta] + \frac{3}{4}b^3d^2g[8]\mathrm{Sin}[\theta] - bd^4g[8]\mathrm{Sin}[\theta] \\ - \frac{1}{16}a^2b^3g[8]\mathrm{Sin}[3\theta] + \frac{1}{4}a^2bd^2g[8]\mathrm{Sin}[3\theta] - \frac{1}{4}b^3d^2g[8]\mathrm{Sin}[3\theta] \\ + \frac{1}{16}a^2b^3g[8]\mathrm{Sin}[5\theta] + g[4]x_2 - \frac{1}{2}ab^2\mathrm{Cos}[\theta]g[6]x_2 + 2ad^2\mathrm{Cos}[\theta]g[6]x_2 + \cdots \end{aligned}$$

Regrouping of the above expression and extracting the terms associated with each of the independent trigonometric polynomials and equating them to zero will result in a larger set of simultaneous equations that are solved to obtain expressions for $\alpha_0, \alpha_1, \dots\dots\dots, \alpha_{3k-1}$ in terms of each other. Further maneuvering through back substitution and extraction results in three sets of permissible functions; each set representing each of the distinct phases in the heterogeneous geometry under deliberation. In a generic form, the permissible functions would resemble

$$e_i = e_i(x, y, k_1, k_2, k_3, a, b, d, x_1, x_2), \qquad (i = 1,2,3) \tag{3.33}$$

where i represents each of the distinct phases; x_1 and x_2 indicate the positions of the inclusions along the x-axis and together with a, b, d, these parameters collectively represent the geometry, while k_1, k_2 and k_3 are the thermal conductivities of the two inclusions and matrix, respectively. As in SIPs, the matrix elements, A_{ij} and B_{ij} are evaluated based on the following schematic:

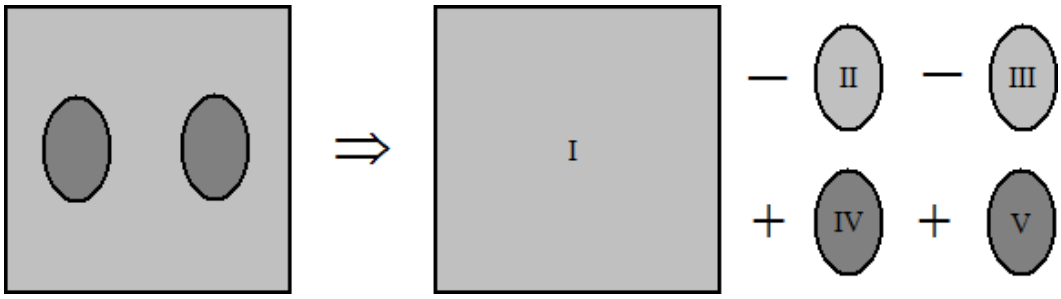

Figure 3.31 Geometrical decomposition of the TIP into its constituent phases.

$$A_{ij} = k_3\left(\iint_{\mathrm{I}} L[e_3\langle i\rangle]\, e_3\langle j\rangle\, dx\, dy - \iint_{\mathrm{II}} L[e_3\langle i\rangle]\, e_3\langle j\rangle\, dx\, dy - \iint_{\mathrm{III}} L[e_3\langle i\rangle]\, e_3\langle j\rangle\, dx\, dy\right) + k_1\left(\iint_{\mathrm{IV}} L[e_1\langle i\rangle]\, e_1\langle j\rangle\, dx\, dy\right) + k_2\left(\iint_{\mathrm{V}} L[e_2\langle i\rangle]\, e_2\langle j\rangle\, dx\, dy\right), \tag{3.34}$$

$$B_{ij} = \left(\iint_{\mathrm{I}} e_3\langle i\rangle\, e_3\langle j\rangle\, dx\, dy - \iint_{\mathrm{II}} e_3\langle i\rangle\, e_3\langle j\rangle\, dx\, dy - \iint_{\mathrm{III}} e_3\langle i\rangle\, e_3\langle j\rangle\, dx\, dy\right) + \iint_{\mathrm{IV}} e_1\langle i\rangle\, e_1\langle j\rangle\, dx\, dy + \iint_{\mathrm{V}} e_2\langle i\rangle\, e_2\langle j\rangle\, dx\, dy, \tag{3.35}$$

where e_1 and e_2 are sets of N permissible functions corresponding to the two inclusions, while e_3 represents the permissible functions for the matrix. Presented below is an effective scheme to perform integration of the permissible functions (that are a combination of polynomials of the form $x^m\, y^n$) over an elliptical region. Let I denote a definite integral defined as

$$I = \iint_{\partial E} x^m\, y^n\, dx\, dy,$$

where ∂E represents an elliptical region, positioned at (x_1, y_1) with a and b as the semi-major and semi-minor axes respectively, defined by the equation

$$\frac{(x-x_1)^2}{a^2}+\frac{(y-y_1)^2}{b^2}=1.$$

Applying change of variables, by letting $x' = x - x_1/a$ and $y' = y - y_1/b$, results in

$$I = ab\iint_{\partial C}(ax'+x_1)^m\,(by'+y_1)^n\,dx'\,dy',$$

where ∂C represents a circular region, positioned at the origin having unit radius, that reads

$$(x')^2+(y')^2=1.$$

Based on the above relation, the integral I can be written in terms of the polar coordinates as

$$I = ab\int_0^{2\pi}\int_0^1 (a\,r\cos\theta+x_1)^m\,(b\,r\,\sin\theta+y_1)^n\,r dr\,d\theta$$

The trigonometric quantities in the above integral can be reduced to basic trigonometric polynomials that eventually zero out due to the intervals of the independent variable θ. This simplification yields an expression of the form:

$$I = 2\pi\,a\,b\int_0^1 f(r)\,r\,dr,$$

where $f(r)$ is some polynomial in r. Evaluating the above integral can be further simplified by employing the following substitution rule, that expedites integration with respect to r over the interval 0 to 1, that reads

$$r^i=\begin{cases}\dfrac{1}{1+i}, & i>1\\ \dfrac{1}{2}, & i=1\end{cases}$$

The matrix elements of A and B are evaluated based on the afore-mentioned integration strategy, after which the eigenfunctions are determined using

$$\varphi_i(x,y) = \begin{cases} \varphi_1\langle i\rangle \left(= \sum_{j=1}^{N} v_i\langle j\rangle e_1\langle j\rangle \right), & 0 \le \dfrac{(x-p_1)^2}{a^2} + \dfrac{y^2}{b^2} \le 1, \\ \varphi_2\langle i\rangle \left(= \sum_{j=1}^{N} v_i\langle j\rangle e_2\langle j\rangle \right), & 0 \le \dfrac{(x-p_2)^2}{a^2} + \dfrac{y^2}{b^2} \le 1, \\ \varphi_3\langle i\rangle \left(= \sum_{j=1}^{N} v_i\langle j\rangle e_3\langle j\rangle \right), & \text{otherwise}, \end{cases} \tag{3.36}$$

where v_i denotes the set of normalized eigenvectors resulting from solving the generalized eigenvalue problem; φ_1 and φ_2 represent the separate set of eigenfunctions for the two inclusions while φ_3 is the set of eigenfunctions corresponding to the matrix phase. The coefficients associated with the volumetric heat generation are evaluated using

$$c_i = q\left(\left(\iint_{\mathrm{I}} \varphi_3\langle i\rangle \, dx\, dy - \iint_{\mathrm{II}} \varphi_3\langle i\rangle \, dx\, dy - \iint_{\mathrm{III}} \varphi_3\langle i\rangle \, dx\, dy \right) + \left(\iint_{\mathrm{IV}} \varphi_1\langle i\rangle \, dx\, dy + \iint_{\mathrm{V}} \varphi_2\langle i\rangle \, dx\, dy \right) \right) \tag{3.37}$$

All of the above expressions can be generalized to accommodate any number of inclusions. Ultimately, the temperature field is determined, using Equation (3.7); the results of which will be presented and discussed in the subsequent pages. First, a convergence study is carried out for chosen values of the geometrical and material parameters i.e. $k_1 = k_2 = 100,\ k_3 = 1, a = 1,$ $b = 1.5,\ d = 4$, and $x_1 = x_2 = 2$, with $q = 1$.

Figure 3.32 demonstrates the convergence of the EEM solution for temperature, along the x-axis, for even orders ranging between 8 and 14. For completeness, the convergence study for the resulting temperature field, along the y-axis is also presented (Figure 3.33). The cross-sectional plots of the convergence study are supported by tabulations (Table 3.10) that itemize and compare the number of permissible functions (N) used, the dominant eigenvalue λ_1

and the corresponding heat generation coefficient c_1, and the temperature at the center of the heterogeneous medium for each of the polynomial orders mentioned above. For the above-mentioned cross-sectional temperature plots and the table, it can be observed that a reasonable degree of convergence, for the eigenvalues, the coefficients of the volumetric heat generation term and the temperature at the origin, is achieved for a 14^{th} order approximation. Figure 3.34 depicts a few of the eigenfunctions that conform to the 14^{th} order temperature solution approximation. It can be observed that the impression of the two elliptical inclusions is clearly evident in these eigenfunction illustrations; so is the orthonormal nature of the independent non-trivial solutions (or eigenfucntions).

To corroborate the EEM temperature solution; its cross-sectional profile is superposed with the corresponding FEM solution (from Ansys). Figures 3.35 and 3.36 illustrate this comparison along the x and y axes respectively. Also, a table (Table 3.11) is provided that summarizes the solutions obtained from the semi-analytical (EEM) and the numerical (FEM) method. It is observed that the two results are in favorable agreement with each other. Furthermore, Figures 3.37 and 3.38 provide the 3-D temperature profile obtained from EEM and the corresponding temperature contour plot respectively. Once again, a distinctive feature in these depictions is the impact of the two inclusions on the temperature profile.

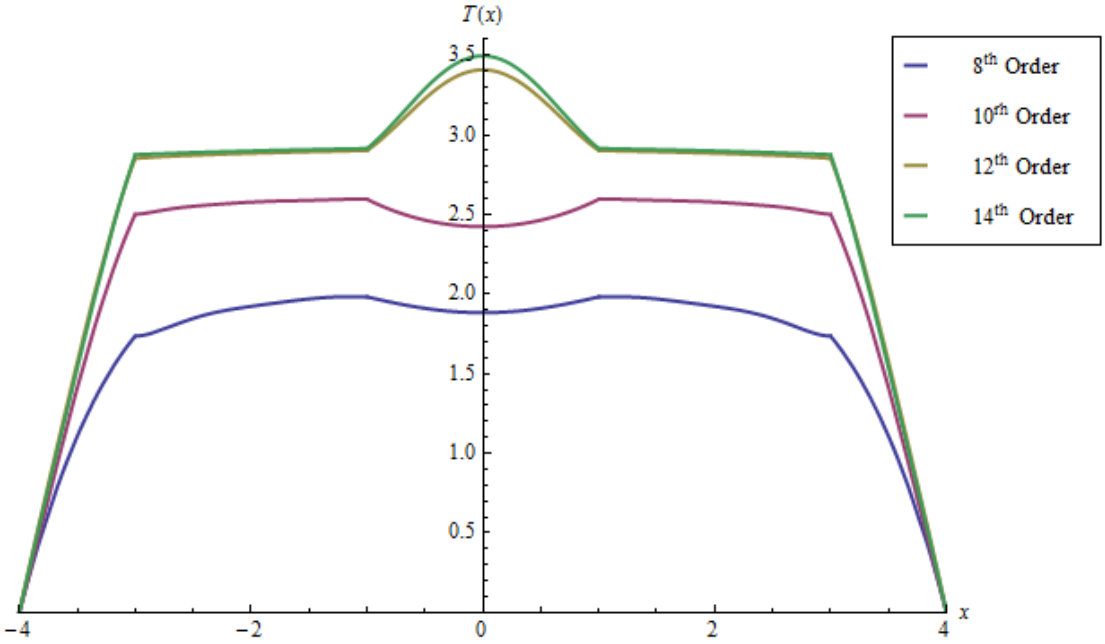

Figure 3.32 Convergence study of the temperature solution along the x-axis for the TIP.

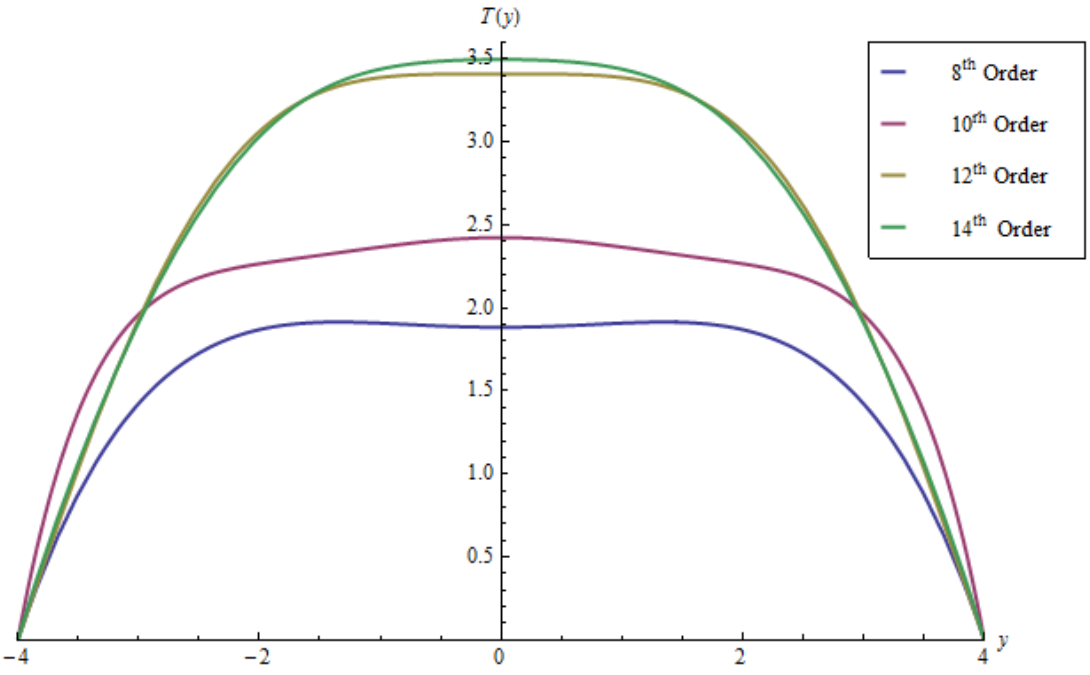

Figure 3.33 Convergence study of the temperature solution along the y-axis for the TIP.

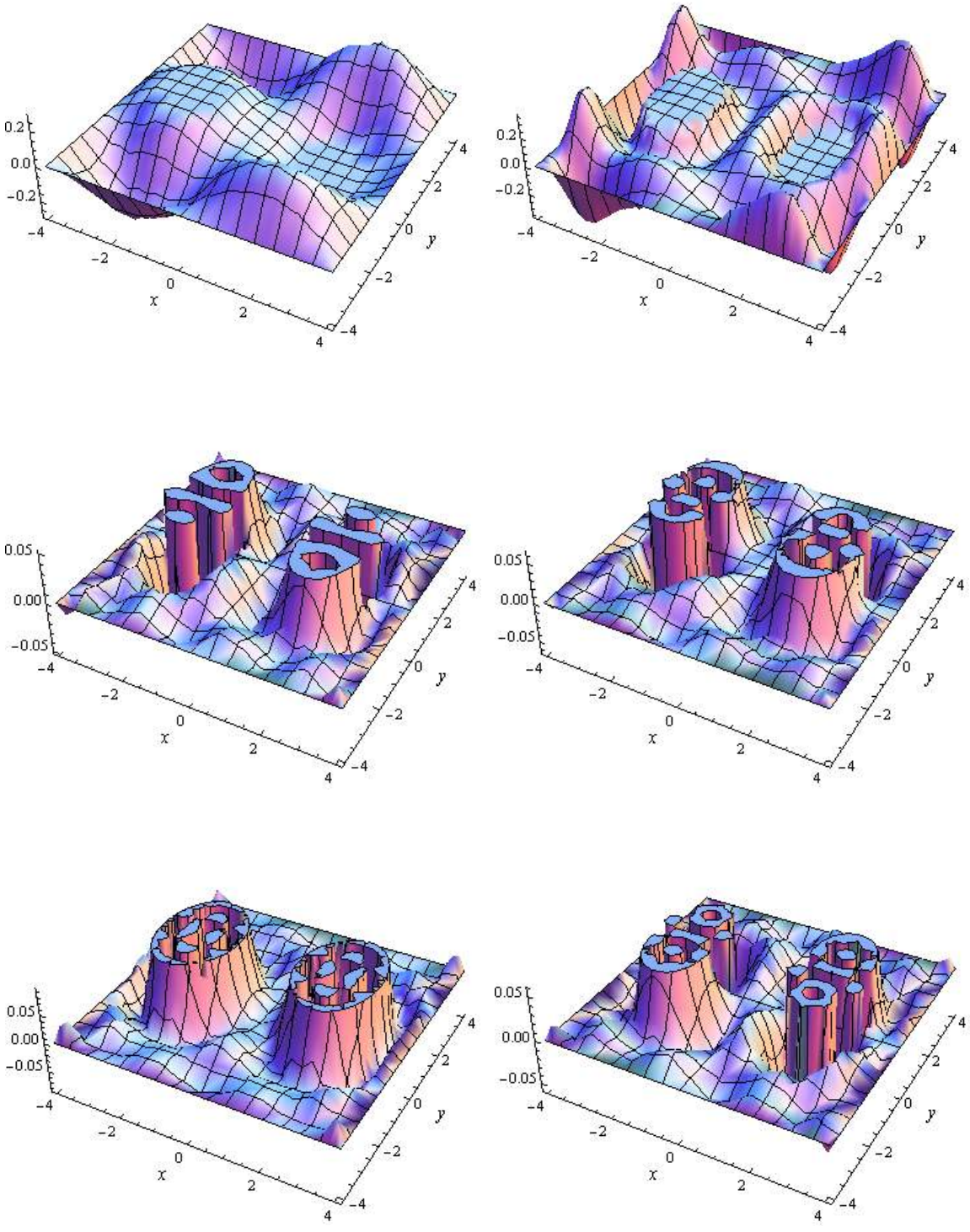

Figure 3.34 Arbitrarily chosen eigenfunctions for the PTE in the TIP.

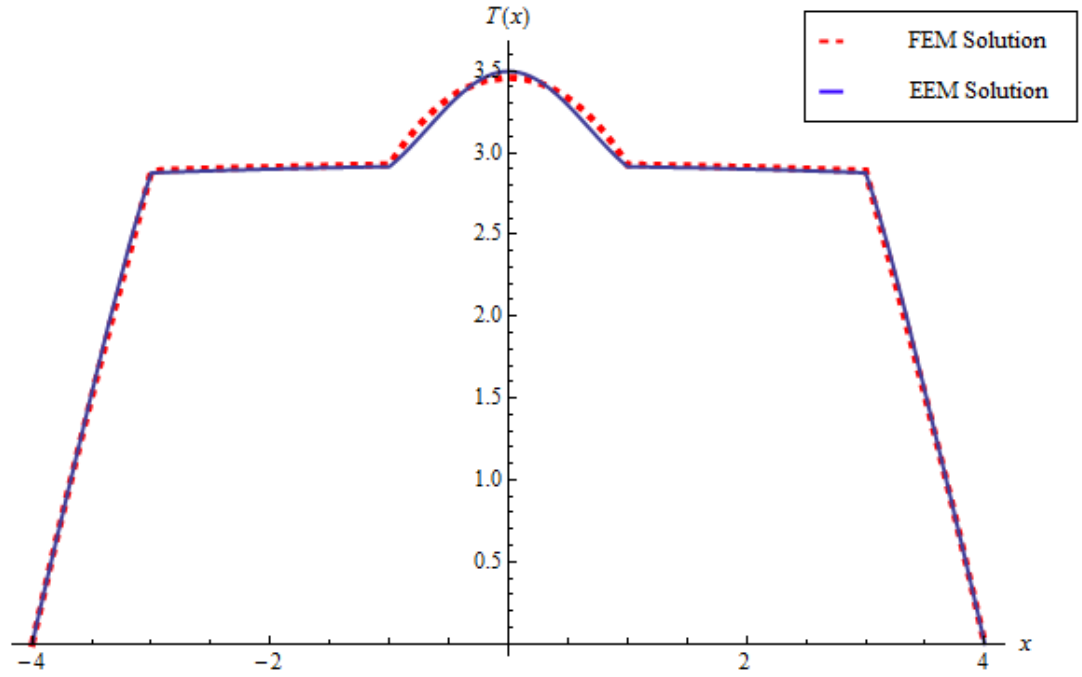

Figure 3.35 Comparison between the EEM solution and the FEM solution for the PTE along the x-axis for the TIP.

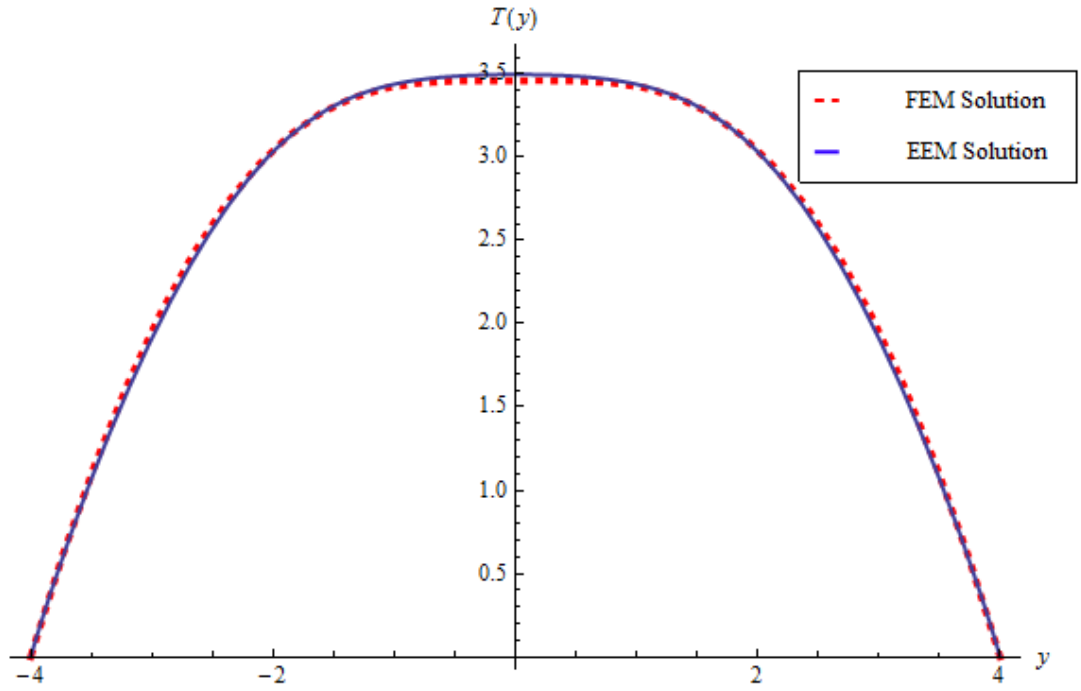

Figure 3.36 Comparison between the EEM solution and the FEM solution for the PTE along the y-axis for the TIP.

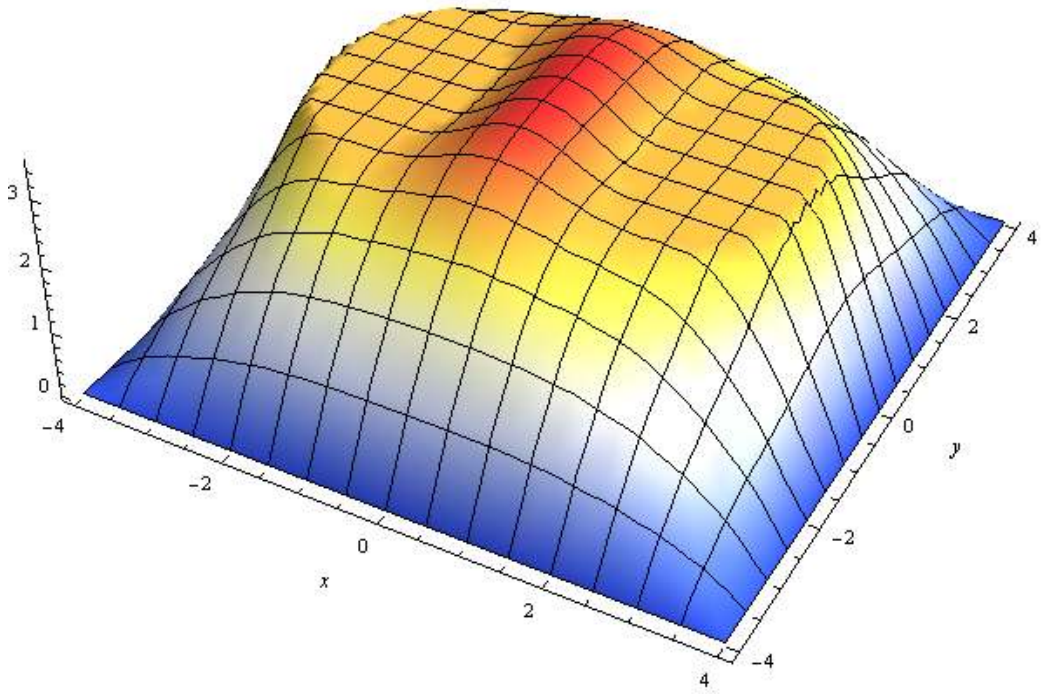

Figure 3.37 3-D Temperature profile for the PTE in the TIP.

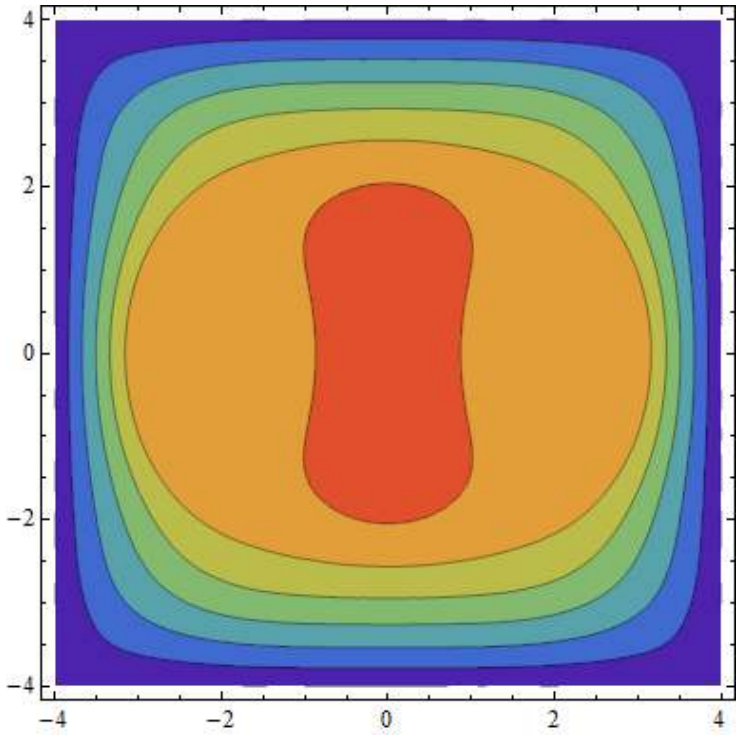

Figure 3.38 Temperature contour plot for the PTE in the TIP.

Table 3.10 Summary of the convergence study of the temperature solution for the TIP

Order	N	λ_1	c_1	$T(x,y)$ at $(x=0, y=0)$
8	13	0.60441	7.27765	1.88318
10	43	0.46414	7.05351	2.42385
12	90	0.39375	6.85924	3.40924
14	149	0.39159	6.27685	3.49690

Table 3.11 Comparison between the EEM and FEM solutions for the TIP

$T(x,y)$ at $(x=0, y=0)$			
Inclusion Aspect Ratio	EEM Solution	FEM Solution	Percentage Diff.
0.667	3.4939	3.4603	1.05771

The results of the parametric study of the effect on the temperature field due to variation in the geometrical and material constants for the single inclusion problem could very well be applied to two inclusion problems; and a similar trend can be observed. However, for the two inclusion problem, an interesting study would be to observe as to how the temperature field behaves as the distance between the inclusions is varied. In this dissertation, two such scenarios will be explored; one in which the distance between the inclusions, w, is varied such that the distance from the origin to the two inclusions remains the same, hence preserving the symmetry of the geometry of the heterogeneous medium about the y-axis; and the other in which the location of one of inclusions (on the left) is fixed while the position of the other inclusion (on the right) is varied along the x- axis, thus inducing an unsymmetrical geometry about the y-axis. With regard to the afore-mentioned scenarios, Figures 3.39 and 3.40 and the

accompanying Table 3.12 demonstrates and compare the effect of the varying inclusion positions along the x- axis on the resulting temperature fields, in a self-explanatory fashion.

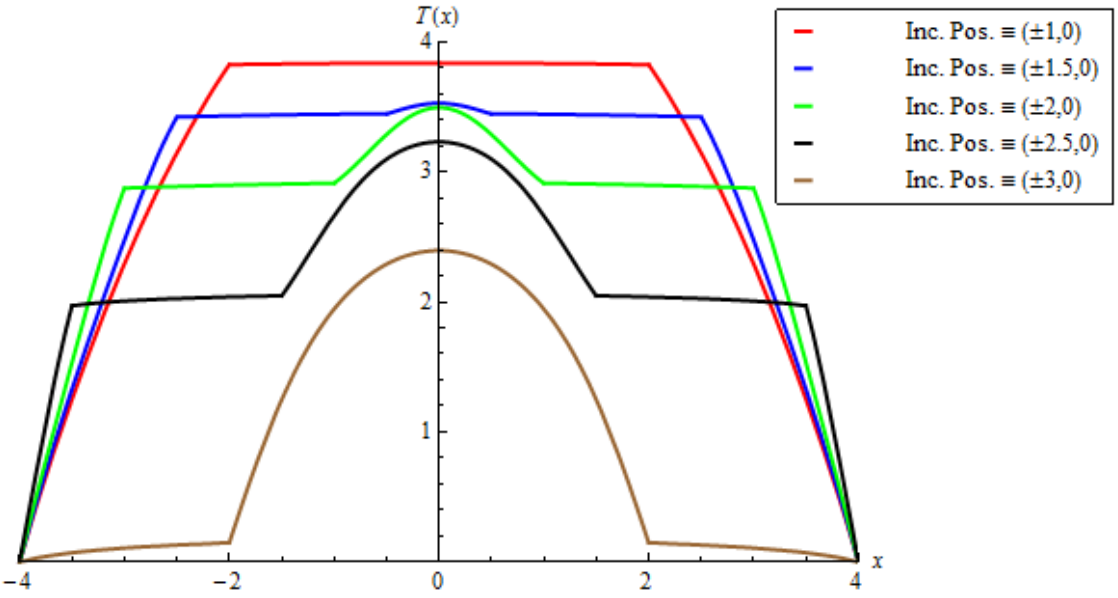

Figure 3.39 Effect of symmetrically varying inclusion position on the temperature field for TIP.

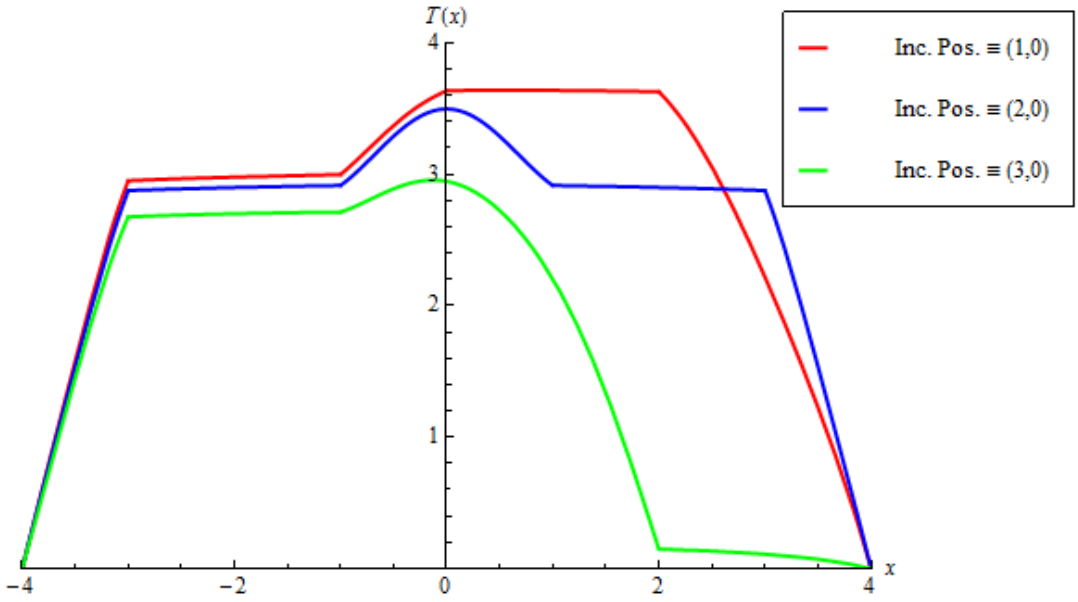

Figure 3.40 Effect of unsymmetrically varying inclusion position on the temperature field for TIP.

Table 3.12 Effect of varying distance between the inclusions on the temperature field for the TIP

Constant parameters for the Inclusion					Symmetrically located inclusions			
a/b	a	b	$\pi\ a\ b$	k_1/k_2	(x_1, y_1)	(x_2, y_2)	w	T_{max}
$\frac{2}{3}$	1	1.5	$\frac{3\pi}{2}$	$\frac{100}{1}$	$(0,0)$	$(0,0)$	0	3.84063
					$(-1,0)$	$(1,0)$	2	3.53878
					$(-2,0)$	$(2,0)$	4	3.49690
					$(-2.5,0)$	$(2.5,0)$	5	3.23259
					$(-3,0)$	$(3,0)$	6	2.39948
					Unsymmetrically located inclusions			
					$(-2,0)$	$(1,0)$	3	3.64655
					$(-2,0)$	$(2,0)$	4	3.49690
					$(-2,0)$	$(3,0)$	5	2.95604

CHAPTER 4

STRESS EQUILIBRIUM EQUATION IN HETEROGENEOUS MATERIALS

This chapter forms the crux of this study into engineering fields in heterogeneous materials; the motivation derived from J.D. Eshelby's pioneering work that has shaped the field of micromechanics of heterogeneous materials. Specifically, his work on ellipsoidal inclusions [7, 8, 9], that has widely been used to analyze the microstructure of elastic solids with inclusions for the last sixty years, laid down the framework for this investigation. However, a major limitation of micromechanics is the difficulty in accurately representing general heterogeneous materials due to certain unrealistic assumptions. Firstly it is presumed that a representative volume element (one that represents the microcosm of the entire material system) is sufficient enough to approximate the complete structural configuration of the material under consideration, which in turn translates into a uniformly distributed system on a macroscopic scale. Secondly, with regard to the works of J.D. Eshelby and that of others which followed, the heterogeneous medium is assumed to be infinitely extended i.e. no boundaries. However, practicality dictates the converse.

The afore-mentioned questionable premises were counteracted by the semi-analytical approach presented in this dissertation; that clearly distinguishes the inclusion and the matrix as two distinct phases and accommodates the existence of a finite boundary. The analytical derivation of the permissible functions that satisfy the boundary conditions and continuity conditions, deployment of a suitable approximation method to obtain a set of undetermined coefficients (as in the Galerkin or the Rayleigh-Ritz method) or independent non-trivial solutions (as in EEM), and formulation of the final solution as a linear combination of the permissible functions or eigenfunctions, epitomizes the approach. As an illustration, in the previous chapter, the 2-D Poisson type equation with homogeneous Dirichlet boundary conditions was considered

that governs the steady-state heat conduction in a square-shaped matrix medium with two elliptical inclusions. For chosen values of geometrical parameters and material constants, the results of the temperature profile from the semi-analytical approach were favorably compared with those obtained from FEM; thus establishing the potency of the approach.

Motivated by the results from the 2-D Poisson equation, the same approach is now extended to solve the 2-D elasticity equilibrium equations for displacement fields, in heterogeneous materials. It should be noted that unlike the Poisson type equation which is a scalar relation, the stress equilibrium equation (SEQ) is a vector relation which makes the solution process more involved than imagined. The complexity and the relevant adjustments made to the solution process will be demonstrated in due course. However, the method remains structurally intact hence providing a unified methodology for solving BVPs of this nature. The first three sections of this chapter constitute certain derivations such as an expression for the stress vector (or traction vector) in terms of the stress tensor, the basic form of the stress equilibrium equation and its equivalent form in terms of the displacement fields using the strain displacement relation. In the fourth section, single elliptical inclusion problems will be solved which will provide an understanding of the mathematical alterations made to the previously discussed solution process. Additionally, for completeness, the results for the displacement fields for homogeneous materials are also presented in this section. The final section deals with solving the displacement fields for a geometry that contains two elliptical inclusions embedded in a finite matrix. A comparative and parametric study is also presented for each of the two heterogeneous cases.

4.1 Understanding The 2-D Stress Equilibrium Equation

4.1.1 State Of Stress

The state of stress on a plane $A-A$ that passes through a point P within a body, subjected to a system of body forces and surface forces - $\boldsymbol{F}_1$, $\boldsymbol{F}_2$, $\boldsymbol{F}_3$ and $\boldsymbol{F}_4$, can be defined by means of the stress vector (or traction vector) $\boldsymbol{t}$, which in turn is a function of the position vector

$\boldsymbol{x}$ and the normal $\boldsymbol{n}$ to the plane $A-A$ that passes through P. This plane can be imagined to be a surface cutting through the body thus dividing it into two segments $S_1$and S_2, on one of which (say S_1) lies P. If one was to imagine an elemental area ΔA around P, then the influence of S_2 on S_1can be interpreted as a force $\Delta \boldsymbol{F}$. Thus, at the point P, the state of stress on a plane can be defined in terms of $\boldsymbol{t}$ as

$$\boldsymbol{t}(P(\boldsymbol{x}),\boldsymbol{n}) = \lim_{\Delta A \to 0} \frac{\Delta \boldsymbol{F}}{\Delta A}. \tag{4.1}$$

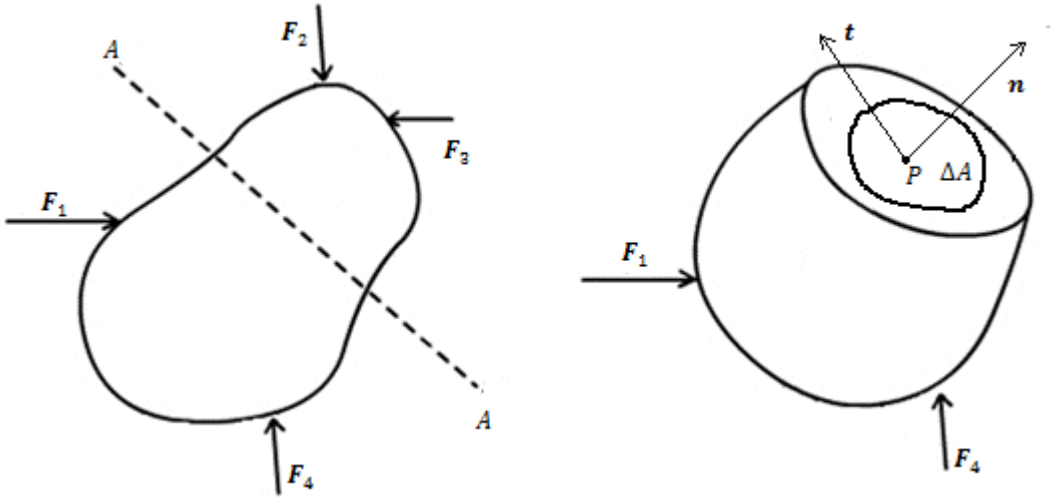

Figure 4.1 State of stress at a point on a plane.

Hence using the above relation, the stress on any given plane can be defined. However, from Figure 4.1 it is evident that there could be an infinite number of planes that can pass through the point P and hence defining the stress at a particular point of interest becomes a seemingly cumbersome task, but when the planes are well defined in terms of a coordinate system, the state of stress at any point can be expressed conveniently in terms of a stress tensor σ_{ij} (second rank tensor), in which i represents the plane and j represents the direction. Hence stress can either be interpreted as a first rank tensor (traction vector),$\boldsymbol{t}$, that defines the state of stress on a plane or as a second rank tensor (stress tensor), σ_{ij}, that defines the state

of stress at a point; and a relationship between these two tensors can be established using the Cauchy tetrahedron which is based on the *Cauchy's second law* which states that all possible traction vectors at a point corresponding to all possible slicing planes passing through that point can be found from the knowledge of the traction vector on three mutually orthogonal planes in three dimensions.

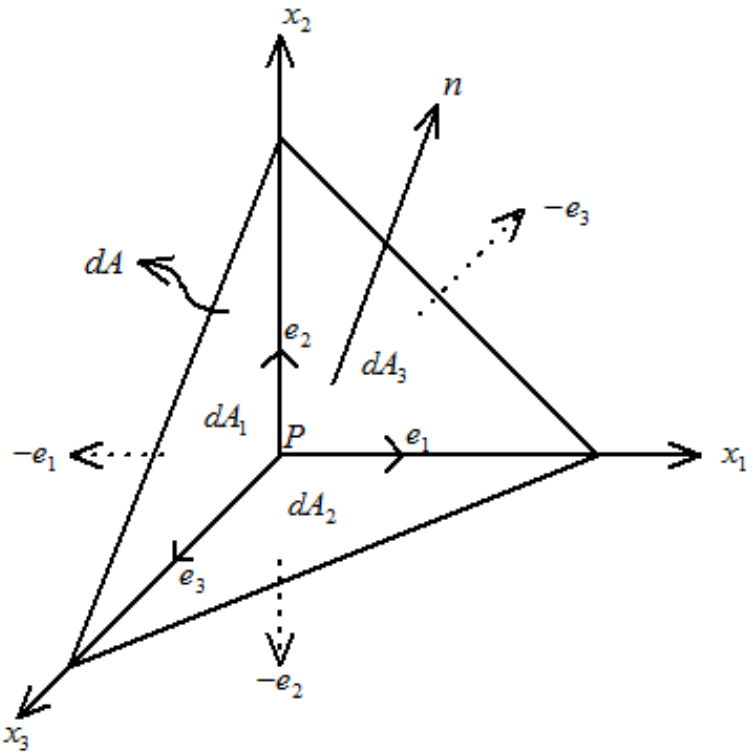

Figure 4.2 Cauchy Tetrahedron.

The Cauchy tetrahedron essentially comprises of four planes as depicted in Figure 4.2 with the dA_1, dA_2, and dA_3 planes perpendicular to the axes x_1, x_2, and x_3, respectively, and an inclined plane dA which is an arbitrary slicing plane in close proximity to the point P at which the state of stress needs to be determined. The quantities $\boldsymbol{e_1}, \boldsymbol{e_2}$, and $\boldsymbol{e_3}$, represent the unit vectors (or base vectors) in the x_1, x_2, and x_3 directions, respectively with $-\boldsymbol{e_1}, -\boldsymbol{e_2}$, and $-\boldsymbol{e_3}$ representing the outward unit vectors to the planes dA_1, dA_2, and dA_3, respectively; and the

symbol $\boldsymbol{n}$ is the outward unit normal to the slicing plane dA. The traction vector on each of the three mutually perpendicular faces dA_1, dA_2, and dA_3 is given by

$$\boldsymbol{t_i} = \boldsymbol{t}(-\boldsymbol{e_i}).$$

where $\boldsymbol{t}$ denotes the traction vector on dA; furthermore, the faces dA_1, dA_2, and dA_3 can be expressed in terms of the principal slicing plane dA as

$$dA_i = n_i dA,$$

where n_i represents the components of the outward unit normal $\boldsymbol{n}$. Hence the total force acting on each of the three mutually perpendicular faces can be summarized as

$$dA_i\ \boldsymbol{t_i} = n_i dA\ \ \boldsymbol{t}(-\boldsymbol{e_i}).$$

Hence the total surface force $\boldsymbol{F_s}$ acting on the tetrahedron element is

$$\boldsymbol{F_s} = \left(\sum_{i=1}^{3} n_i dA\ \ \boldsymbol{t}(-\boldsymbol{e_i})\right) + dA\ \boldsymbol{t}(\boldsymbol{n}),$$

where the term $dA\ \boldsymbol{t}(\boldsymbol{n})$ corresponds to the total surface force acting on dA. The total force acting throughout the body, $\boldsymbol{F_b}$ can be expressed as

$$\boldsymbol{F_b} = \ \boldsymbol{b} \times \frac{dA\ h}{3},$$

where $\boldsymbol{b}$ is the body force per unit volume and h denotes the height of the tetrahedron or the distance between the point P and the inclined plane dA; and this distance being considerably small results in $\boldsymbol{F_b} \to 0$ as $h \to 0$. Hence, the body force can be neglected. Now, for the tetrahedron to be in equilibrium, the vector sum of all the forces acting should be zero. Hence

$$dA\big(n_1\ \boldsymbol{t}(-\boldsymbol{e_1}) + n_2\ \boldsymbol{t}(-\boldsymbol{e_2}) + n_3\ \boldsymbol{t}(-\boldsymbol{e_3}) + \ \boldsymbol{t}(\boldsymbol{n})\big) = 0.$$

Further, applying *Cauchy's first law* i.e., $\boldsymbol{t}(-\boldsymbol{e_1}) = -\boldsymbol{t}(\boldsymbol{e_1})$ to the above expression results in

$$\boldsymbol{t}(\boldsymbol{n}) = n_1\, \boldsymbol{t}(\boldsymbol{e_1}) + n_2\, \boldsymbol{t}(\boldsymbol{e_2}) + n_3\, \boldsymbol{t}(\boldsymbol{e_3}).$$

Resolving the above traction vectors yields

$$\begin{pmatrix} t_1 \\ t_2 \\ t_3 \end{pmatrix} = n_1 \begin{pmatrix} t_1(\boldsymbol{e_1}) \\ t_2(\boldsymbol{e_1}) \\ t_3(\boldsymbol{e_1}) \end{pmatrix} + n_2 \begin{pmatrix} t_1(\boldsymbol{e_2}) \\ t_2(\boldsymbol{e_2}) \\ t_3(\boldsymbol{e_2}) \end{pmatrix} + n_3 \begin{pmatrix} t_1(\boldsymbol{e_3}) \\ t_2(\boldsymbol{e_3}) \\ t_3(\boldsymbol{e_3}) \end{pmatrix}.$$

In terms of the stress tensor components, the above expression can be rewritten as

$$\begin{pmatrix} t_1 \\ t_2 \\ t_3 \end{pmatrix} = n_1 \begin{pmatrix} \sigma_{11} \\ \sigma_{12} \\ \sigma_{13} \end{pmatrix} + n_2 \begin{pmatrix} \sigma_{21} \\ \sigma_{22} \\ \sigma_{23} \end{pmatrix} + n_3 \begin{pmatrix} \sigma_{31} \\ \sigma_{32} \\ \sigma_{33} \end{pmatrix}.$$

Using tensor notation, the above expression can be succinctly represented as

$$t_i = \sigma_{ji}\, n_j. \tag{4.2}$$

Equation (4.2) represents the most basic expression of the traction vector. In relation to the above equation, the stress tensor σ_{ji} can now be construed to be the i^{th} component of the traction vector acting on the j^{th} surface (or a surface whose normal is along the j-axis). Furthermore, by establishing the symmetric nature of the stress tensor, the above equation yields a more widely accepted expression of the traction vector. This will be illustrated at a later point in this chapter.

4.1.2 Fundamental Model Of The SEQ

The elasticity equilibrium equation can be derived in a manner similar to that of the expression for the traction vector derived above; thus its formulation is based on the balance of forces. However, the difference lies in the consideration of the body forces. Here, the body forces will be included which makes the resulting stress equilibrium equation valid at every point in the body. Figure 4.3 shows a body subjected to a system of body and surface forces. The

body force $\boldsymbol{b}$ is represented as acting throughout an elemental volume dV and the surface force (or traction) $\boldsymbol{t}$ is shown as acting on an elemental area dA.

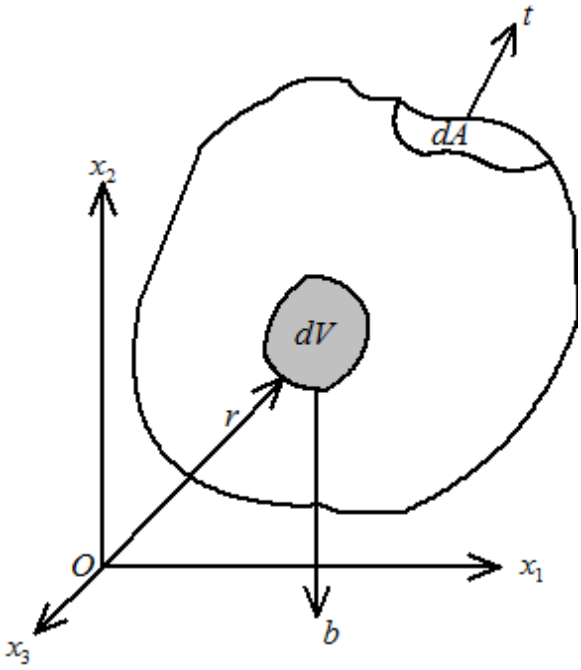

Figure 4.3 A body subjected to a system of forces.

As mentioned earlier, for the body to be in equilibrium, the vector sum of all the forces acting on and throughout the body must be zero i.e.,

$$\oint_{\partial V} \boldsymbol{t}\, dA + \int_{V} \boldsymbol{b}\, dV = 0,$$

where the symbols ∂V and V represent the volume of the body and the boundary of the volume respectively. The above equation can be expressed in the tensor form as

$$\oint_{\partial V} t_i\, dA + \int_{V} b_i\, dV = 0.$$

Substitution of Equation (4.2) into the above relation yields

$$\oint_{\partial V} \sigma_{ji}\, n_j \; dA \; + \int_V \; b_i \, dV = 0. \tag{4.3}$$

Equation (4.3) contains two terms, one of which is a surface integral and the other a volume integral. This inconsistency can be rectified by employing the Gauss divergence theorem that will facilitate the shift from a surface to a volume integral. Mathematically, the theorem states

$$\oint_{\partial V} \omega_j \, n_j \; dA = \int_V \; \omega_{j,j} \, dV, \tag{4.4}$$

where ω is a continuous vector field defined in the vicinity of the volume V. Application of Equation (4.4) to Equation (4.3) yields

$$\int_V \; \sigma_{ji,j} \; dV + \int_V \; b_i \, dV = 0.$$

Further simplification of the above relation results in

$$\int_V \; \left(\sigma_{ji,j} + b_i\right) dV = 0.$$

The above expression represents the stress equilibrium equation for a body as depicted in Figure 4.3. It also suggests that for a body to be in equilibrium the integral kernel must be valid (or equal to zero) for any arbitrary volume element (or at any point) of the body. Thus, the final basic form of the stress equilibrium equation can be expressed as

$$\sigma_{ji,j} + b_i = 0. \tag{4.5}$$

4.1.3 Symmetricity Of The Stress Tensor

Though not a necessary condition for a body to be in equilibrium, the balance of moments provides useful corollaries in various engineering practices. The symmetricity of the stress tensor is one such inference and can be considered to be one of the most essential

characteristics of the stress tensor that results in six independent components (instead of the expected nine components). This intrinsic property of the stress tensor can be established by imposing the balance of moments i.e., by taking the algebraic sum of the moments of all the forces about a certain point to be zero. In Figure 4.3, dV represents an infinitesimal volume element with $\boldsymbol{r}$ as its position vector. Before taking the moments about the origin O, it is convenient to introduce a vector operation, namely, the cross product of two vectors, which will facilitate the balance of moments about a point. In indical notations, the cross product between two vectors is expressed as

$$(\boldsymbol{\alpha} \times \boldsymbol{\beta})_i = \epsilon_{ijk}\alpha_j\beta_k, \tag{4.6}$$

where $\boldsymbol{\alpha}$ and $\boldsymbol{\beta}$ are arbitrary vectors and ϵ_{ijk} represents the permutation symbol defined as

$$\epsilon_{ijk} = \begin{cases} 1 & (ijk) = (123), (231), (312), \\ -1 & (ijk) = (321), (213), (132), \\ 0 & \text{otherwise.} \end{cases} \tag{4.7}$$

Balancing the moments about the point O yields

$$\oint_{\partial V} (\boldsymbol{r} \times \boldsymbol{t})\ dA + \int_V (\boldsymbol{r} \times \boldsymbol{b})\, dV = 0.$$

Incorporating the definition from Equation (4.6), the above relation can be expressed as

$$\oint_{\partial V} \epsilon_{ijk} r_j t_k\ dA\ + \int_V \epsilon_{ijk} r_j b_k\, dV = 0.$$

Substituting the basic expression for traction from Equation (4.2) into the above expression and subsequently applying the Gauss divergence theorem to the surface integral yields

$$\int_V \epsilon_{ijk}\left(r_j \sigma_{lk}\right)_{,l}\ dV + \int_V \epsilon_{ijk} r_j b_k\, dV = 0.$$

Compiling the integrands and administering the product rule for differentiation leads to

$$\int_V \epsilon_{ijk}\left[r_j(\sigma_{lk,l} + b_k) + r_{j,l}\,\sigma_{lk}\right] dV = 0.$$

Imposing the mathematical formulation of the stress equilibrium equation i.e. Equation (4.5) to the above expression and doing away with the volume integral due to reasons mentioned earlier, results in

$$\epsilon_{ijk}\, r_{j,l}\sigma_{lk} = 0.$$

The term $r_{j,l}$ is replaced with the Kronecker delta function δ_{jl}. This function further interacts with the stress tensor σ_{lk} to give σ_{jk}; and hence the final form of the balance of moments equation is

$$\epsilon_{ijk}\, \sigma_{jk} = 0.$$

Applying the definition of the permutation symbol from Equation (4.7) leads to an expression that represents the symmetry of the stress tensor; a generalized version of which reads

$$\sigma_{ji} = \sigma_{ij}. \tag{4.8}$$

In view of the above property of the stress tensor, the expression for the traction vector from Equation (4.2) and the stress equilibrium equation from Equation (4.5) can be rewritten as

$$t_i = \sigma_{ij}\, n_{j.} \tag{4.9}$$

$$\sigma_{ij,j} + b_i = 0. \tag{4.10}$$

4.2 2-D Strain-Displacement Relation

As illustrated in Figure 4.4, pq is an infinitesimal line segment, of length dx_i, in an elastic body with a coordinate system represented by x_1-x_2-x_3, and $p'q'$ is the same line segment after deformation, of length $d\xi_i$, in a coordinate system denoted by ξ_1-ξ_2-ξ_3. However,

it is assumed that the new coordinate system corresponding to the deformation i.e. ξ_1-ξ_2-ξ_3 can be expressed in terms of the original un-deformed coordinate system x_1-x_2-x_3 such that

$$\xi_i = \xi_i(x_1, x_2, x_3\ ).$$

The vector $\boldsymbol{u}$ represents the displacement of the point p to p' and $\boldsymbol{u} + d\boldsymbol{u}$ is the displacement of the point q to q'. If $d\boldsymbol{u} = 0$, then line element pq is merely displaced to $p'q'$ without any deformation. To facilitate the derivation of the strain tensor, the square of the length of pq and $p'q'$ are defined as ds^2 and ds'^2; and the these quantities can be tensorially expressed as

$$ds^2 = dx_i\ dx_i = \delta_{ij}\ dx_i\ dx_j,$$

$$ds'^2 = d\xi_\alpha\ d\xi_\alpha = \delta_{\alpha\beta}\ d\xi_\alpha\ d\xi_\beta.$$

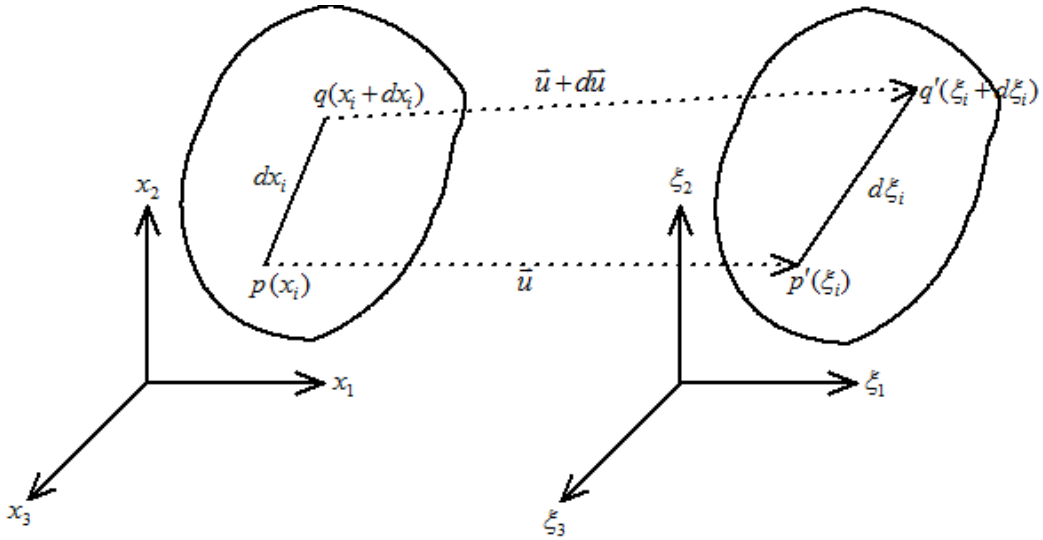

Figure 4.4 Deformation of an elastic body.

Further, based on the earlier assumption that the deformed coordinate system is a function of the un-deformed coordinate system, ds'^2 can be rewritten in terms of the original system as

$$ds'^2 = \delta_{\alpha\beta}\,\frac{\partial \xi_\alpha}{\partial x_i}\,\frac{\partial \xi_\beta}{\partial x_j}\,dx_i\,dx_j.$$

From the above geometry, it is also clear that

$$u_i = \xi_i - x_i.$$

Based on the above identity, the quantity ds' now takes the form:

$$ds'^2 = \delta_{\alpha\beta}\left(\frac{\partial u_\alpha}{\partial x_i} + \delta_{i\alpha}\right)\left(\frac{\partial u_\beta}{\partial x_j} + \delta_{j\beta}\right)dx_i\,dx_j.$$

Expanding the above expression and imposing the properties of the Kronecker delta yields

$$ds'^2 = \left(u_{i,j} + u_{j,i} + u_{k,i}\,u_{k,j} + \delta_{ij}\right)dx_i\,dx_j.$$

The difference between the squares of the length elements ds^2 and ds'^2 gives

$$ds^2 - ds'^2 = \left(u_{i,j} + u_{j,i} + u_{n,i}\,u_{n,j}\right)dx_i\,dx_j.$$

The strain tensor can now be defined by

$$ds^2 - ds'^2 = 2\,E_{ij}\,dx_i\,dx_j,$$

where E_{ij} is called the Green's strain tensor and is mathematically defined as

$$E_{ij} = \frac{1}{2}\left(u_{i,j} + u_{j,i} + u_{k,i}\,u_{k,j}\right). \tag{4.11}$$

Further, under the assumption that the strains are infinitesimally small i.e. $u_{k,i}\,u_{k,j} << 1$, the strain tensor is now defined by the following relation

$$ds^2 - ds'^2 = 2\,\varepsilon_{ij}\,dx_i\,dx_j,$$

where ε_{ij} is called the infinitesimal strain tensor and is given by

$$\varepsilon_{ij} = \frac{1}{2}\left(u_{i,j} + u_{j,i}\right). \tag{4.12}$$

Furthermore, like the stress tensor, both the strain tensors E_{ij} and ε_{ij} are also symmetric. However, as is the usual practice in most structural engineering applications, from here on, the infinitesimal strain tensor ε_{ij} will serve as the primary definition of strain.

4.3 The SEQ In Terms Of the Displacement Fields

Having derived the basic form of the stress equilibrium equation as in Equation (4.10) and the strain-displacement relation as in Equation (4.12), the stage is now set to establish an expression for the equilibrium equation in terms of the displacement fields. After all, it's the study of the displacement fields that shapes the core of this dissertation. First and foremost, the constitutive relation, that defines the relationship between the stress and strain in an elastic solid, is considered which essentially states that the stress tensor σ_{ij} is linearly proportional to the strain tensor ε_{kl}; with the proportionality constant denoted by C_{ijkl} referred to as the elastic moduli and by nature is a fourth rank tensor (following the quotient rule of tensors). In the tensorial form, the constitutive relation reads

$$\sigma_{ij} = C_{ijkl}\,\varepsilon_{kl}. \tag{4.13}$$

In essence, C_{ijkl} relates the (ij) component of stress with the (kl) component of strain; and as a fourth rank tensor it represents 81 components. However due to the symmetry of the stress and strain tensors, it can be shown that

$$C_{ijkl} = C_{jikl} = C_{ijlk} = C_{klij}. \tag{4.14}$$

The above identity results in C_{ijkl} having only 21 independent components. Further, by introducing the simplifying premise of material isotropy, the number of independent constants further reduces to two. A physical interpretation of an isotropic material would be one whose mechanical property is uniform (or invariant) in all directions. A more rigorous clarification of

isotropy can be made using the constitutive relation as described by Equation (4.13) in which the constitutive relation as such remains unaltered under orthogonal transformations such as rotation and reflection of the coordinate axes due to isotropy. In general, any fourth rank isotropic tensor P_{ijkl} has three independent constants A, B, and C; and can be represented as a combination of Kronecker's delta functions as

$$P_{ijkl} = A\,\delta_{ij}\delta_{kl} + B\delta_{ik}\delta_{jl} + C\delta_{il}\delta_{jk}.$$

However, for C_{ijkl}, due to its stress tensor induced symmetry, it can be shown that $B = C$; and hence the number of independent constants is reduced to two; and further by replacing A and B with the Lamé constants λ and μ, the elastic tensor can be written as

$$C_{ijkl} = \lambda\,\delta_{ij}\delta_{kl} + \mu\left(\delta_{ik}\delta_{jl} + \delta_{il}\delta_{jk}\right), \tag{4.15}$$

where μ is identified as the shear modulus G, and λ is a linear combination of the shear modulus G and the bulk modulus K. The Lamé constants are related to the more commonly used elastic constants, namely the Young's modulus E and the Poisson's ratio ν as

$$\lambda = \frac{\nu\,E}{(1+\nu)(1-2\,\nu)} = K - \frac{2\,G}{3}, \tag{4.16}$$

$$\mu = \frac{E}{2\,(1+\nu)} = G, \tag{4.17}$$

Substituting Equation (4.15) into Equation (4.13) yields

$$\sigma_{ij} = \lambda\,\delta_{ij}\delta_{kl}\,\varepsilon_{kl} + \mu\left(\delta_{ik}\delta_{jl} + \delta_{il}\delta_{jk}\right)\varepsilon_{kl}.$$

Further, imposing the properties of the Kronecker's delta to the above expression results in

$$\sigma_{ij} = \lambda\,\delta_{ij}\,\varepsilon_{kk} + 2\,\mu\,\varepsilon_{ij}. \tag{4.18}$$

Equation (4.18) is also more commonly referred to as the Hooke's law for an isotropic elastic solid. Since the objective is to solve the 2-D stress equilibrium equations for the displacement fields, it would only be more sensible and convenient to express the right hand side of the above expression in terms of the displacement fields, rather than the strain components. This transition can be accomplished by applying the formerly derived strain-displacement relation from Equation (4.12) to Equation (4.18). This substitution yields the equivalent form of the stress tensor in terms of displacements as

$$\sigma_{ij} = \lambda\, \delta_{ij}\, u_{k,k} + \mu\, (u_{i,j} + u_{j,i}), \tag{4.19}$$

Substituting Equation (4.19) into Equation (4.10) yields

$$\left(\lambda\, \delta_{ij}\, u_{k,k} + \mu\, (u_{i,j} + u_{j,i})\right)_{,j} + b_i = 0.$$

Expanding the above expression leads to

$$\lambda\, \delta_{ij}\, u_{k,kj} + \mu\, (u_{i,jj} + u_{j,ij}) + b_i = 0.$$

Further tensor manipulation and regrouping yields the final form of the stress equilibrium equation in terms of the displacement fields as

$$\mu\, u_{i,jj} + (\lambda + \mu) u_{j,ij} + b_i = 0. \tag{4.20}$$

In general, Equation (4.20) represents a vector equation that can be expressed explicitly as two equations in the x and y directions (for $i = 1,2$ respectively) as

$$\mu \left(\frac{\partial^2 u}{\partial x^2} + \frac{\partial^2 u}{\partial y^2}\right) + (\lambda + \mu)\left(\frac{\partial^2 u}{\partial x^2} + \frac{\partial^2 v}{\partial x\, \partial y}\right) + b_x = 0, \tag{4.21}$$

$$\mu \left(\frac{\partial^2 v}{\partial x^2} + \frac{\partial^2 v}{\partial y^2}\right) + (\lambda + \mu)\left(\frac{\partial^2 u}{\partial x\, \partial y} + \frac{\partial^2 v}{\partial y^2}\right) + b_y = 0, \tag{4.22}$$

where u and v denote the displacement fields; and b_x and b_y represent the body forces in the x and y directions, respectively.

4.4 Solution Methodology For The 2-D SEQ In Heterogeneous Materials

Though the structure of the semi-analytical approach essentially remains the same as in the methodology adopted for the 2-D Poisson type equation, certain disparities arise in the solution process for the displacement fields due to the nature of the governing equation and the physical fields of interest. First of all, the 2-D Poisson type equation is an equation that involves a scalar physical field, namely temperature; and hence for each individual phase of the heterogeneous medium, if N represents the dimension of the resulting linear system, then N permissible functions are needed to provide an approximate solution for the temperature field. However, the 2-D elasticity equilibrium equation is a vector equation that forks out into two equations as shown in Equations (4.21) and (4.22), with a vector physical field, namely displacement that involves two components in the x and y directions. Hence, for each phase of the heterogeneous medium, it becomes imperative to define $2N$ permissible functions to account for the displacement vector components in the the x and y directions.

Secondly, the two equations that result from the general elasticity equilibrium equation are not independent of each other, i.e. Equation (4.21) contains the displacement component in both the x and y directions; and the same holds true for Equation (4.22). This renders the Galerkin technique ineffective when imposed on such equations; and this limitation of the Galerkin method will be demonstrated in due course. However, the Rayleigh-Ritz method works out to be a suitable candidate to solve equations of this nature and the intricacies involved with such an approximation technique will also be presented in this section. Besides the above mentioned differences in the solution technique, other factors that contribute to the complexity of solving the stress equilibrium equation in heterogeneous materials, in comparison with the Poisson type equation, are the complex nature of the governing differential equation itself, and the increased number of material constants as well as the continuity conditions across the

interface. As before, the heterogeneous medium under consideration is a square-shaped matrix with two elliptical inclusions subjected to homogeneous Dirichlet boundary conditions (or zero displacement at the boundaries). However for the purpose of plainness in explaining the solution process, first an isotropic homogeneous medium, as shown in Figure 4.5, is considered, after which, the solution methodology can be conveniently extended to suit single and multiple inclusion problems.

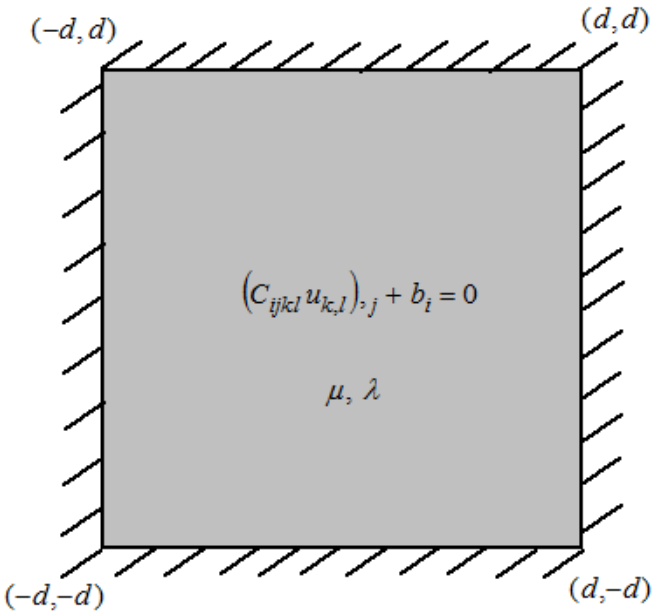

Figure 4.5 Elasticity equilibrium equation in an isotropic homogeneous medium.

To begin with, an analogy is drawn between the Equation (4.18) and the basic form of a governing differential equation as suggested by Equation (2.20) as

$$(L[u])_i + b_i = 0, \tag{4.23}$$

where

$$(L[u])_i = \mu\, u_{i,jj} + (\lambda + \mu) u_{j,ij}, \tag{4.24}$$

In a more basic and succinct form, Equation (4.24) can be express as

$$(L[u])_i = \left(C_{ijkl}\, u_{k,l}\right)_{,j}. \tag{4.25}$$

Under general circumstances, for each phase of a given system, two sets of displacement trial functions corresponding to the displacement components in the x and y directions need to be defined. However, for the given isotropic homogeneous system (Figure 4.5), due to the geometry and boundary conditions being symmetrical about the x and y axes, a single set of permissible functions are sufficient to represent the given system. Also, the permissible functions can be directly obtained by multiplying each element of the 2-D Pascal triangle with a function, in x and y, that unqualifiedly satisfies the homogeneous boundary conditions. A generalized expression for such a set of permissible functions reads

$$g_i(x,y) = h_i(x,y) = (x^2 - d^2)(y^2 - d^2)\, x^{j-i}\, y^i \qquad (i = 0, 1, 2, \dots \dots j), \tag{4.26}$$

where g_i and h_i are permissible functions corresponding to the x and y components of displacment. The permissible functions are now subjected to a suitable approximation technique to obtain the displacement fields. Initially, as a default choice, the possibility of employing the Galerkin method was explored. Presented below are the results of this investigation. To start with, the displacement fields, u and v, are approximated as a series combination of the analytically derived permissible functions as

$$u(x,y) = \sum_{i=1}^{N} \alpha_i\, g_i(x,y), \tag{4.27}$$

$$v(x,y) = \sum_{i=N+1}^{2N} \alpha_i\, h_i(x,y), \tag{4.28}$$

where α_i 's are the coefficients associated with the approximated displacement fields in the x and y directions. Further, Equations (4.21) and (4.22), can be expressed in a concise form as

$$\mu\,(\Delta u) + (\lambda + \mu)\big(u_{,xx} + v_{,xy}\big) + b_x = 0, \tag{4.29}$$

$$\mu\,(\Delta v) + (\lambda + \mu)\big(u_{,xy} + v_{,yy}\big) + b_y = 0. \tag{4.30}$$

Substituting Equations (4.27) and (4.28) into Equations (4.29) and (4.30) yields

$$\mu\left(\sum_{i=1}^{N} \alpha_i\,\Delta g_i\right) + (\lambda + \mu)\left(\sum_{i=1}^{N} \alpha_i\, g_{i,xx} + \sum_{i=1}^{N} \beta_i\, h_{i,xy}\right) + b_x = 0, \tag{4.31}$$

$$\mu\left(\sum_{i=1}^{N} \beta_i\,\Delta h_i\right) + (\lambda + \mu)\left(\sum_{i=1}^{N} \alpha_i\, g_{i,xy} + \sum_{i=1}^{N} \beta_i\, h_{i,yy}\right) + b_y = 0. \tag{4.32}$$

It can be observed from Equations (4.29) and (4.30) that the displacement fields are coupled; and hence in order to determine the unknown coefficients, α_i, using the Galerkin method, Equation (4.31) should by multiplied by g_j and h_j separately; and the same applies to Equation (4.32). This generates $4N$ equations with $2N$ unknowns; hence suggesting an over-specified system of equations without a unique solution for the unknown coefficients. Thus, the Galerkin method fails to produce a solution for the elasticity equilibrium equation.

As the next method of choice, the Rayleigh-Ritz method is examined which, as discussed in Chapter 2, is also an approximation technique that reduces a continuous system to a discretized model. In structural engineering applications, the Rayleigh-Ritz Method (RRM) is a widely used approximation technique that is based on the principle of minimum potential energy which states that – for conservative systems, of all the kinematically admissible displacement fields, those corresponding to equilibrium extremize the total potential energy, Π, and if the extremum condition is minimum, the equilibrium state is stable. In other words, the displacement field that makes Π take an extremum value is the one that satisfies the equilibrium equation. For the conservative system under deliberation (Figure 4.5), its potential energy Π can be expressed as

$$\Pi = U + (-W), \tag{4.33}$$

where U represents the strain energy defined as

$$U = \frac{1}{2}\int_V \sigma_{ij}\,\varepsilon_{ij}\,dV, \tag{4.34}$$

and W is the work potential and the negative sign indicates the potential that is lost by the system upon the action of external forces. In general, external agents include body forces, surface loads and point loads. However, for the current system, the only external force is the body force; and hence this system's work potential takes the form

$$W = \int_V b_i\,u_i\,dV. \tag{4.35}$$

Based on the above definitions, Equation (4.33) can be rewritten as

$$\Pi = \frac{1}{2}\int_V (\sigma_{ij}\,\varepsilon_{ij} - 2\,b_i\,u_i)\,dV. \tag{4.36}$$

The first term of the integrand in Equation (4.36) is expanded as follows:

$$\begin{aligned}
\sigma_{ij}\,\varepsilon_{ij} &= \left(C_{ijkl}\,\varepsilon_{kl}\right)\varepsilon_{ij} \\
&= \left(\lambda\,\delta_{ij}\,\epsilon_{kk} + 2\,\mu\,\epsilon_{ij}\right)\varepsilon_{ij} \\
&= \lambda\,\varepsilon_{kk}\,\varepsilon_{ll} + 2\,\mu\,\varepsilon_{ij}\,\varepsilon_{ij} \\
&= \lambda\,u_{k,k}\,u_{l,l} + \frac{\mu}{2}\left(u_{i,j} + u_{j,i}\right)\left(u_{i,j} + u_{j,i}\right) \\
&= \lambda\,u_{k,k}\,u_{l,l} + \frac{\mu}{2}\left(u_{i,j}\,u_{i,j} + u_{i,j}\,u_{j,i} + u_{j,i}\,u_{i,j} + u_{j,i}\,u_{j,i}\right) \\
&= \lambda\,u_{k,k}\,u_{l,l} + \mu\left(u_{i,j}\,u_{i,j} + u_{i,j}\,u_{j,i}\right) \\
&= \lambda\left(u_{,x} + v_{,y}\right)\left(u_{,x} + v_{,y}\right) + \mu\left(2\,u_{,x}\,u_{,x} + u_{,y}\,u_{,y} + v_{,x}\,v_{,x} + v_{,x}\,u_{,y} + u_{,y}\,v_{,x} + 2\,v_{,y}\,v_{,y}\right) \\
&= \lambda\left(u_{,x} + v_{,y}\right)^2 + \mu\left(2\,u_{,x}{}^2 + 2\,v_{,y}{}^2 + u_{,y}{}^2 + v_{,x}{}^2 + 2\,u_{,y}\,v_{,x}\right).
\end{aligned}$$

Rearranging the terms in the above expression and substituting it into Equation (4.36) results in

$$\Pi = \frac{1}{2}\int_V \Big((2\,\mu + \lambda)\left(u_{,x}{}^2 + v_{,y}{}^2\right) + \mu\left(u_{,y} + v_{,x}\right)^2 + 2\,\lambda\, u_{,x}\, v_{,y} - 2\, b_x\, u - 2\, b_y\, v \Big)\, dV. \tag{4.37}$$

Equation (4.37) represents the generalized expression for the potential energy of a homogeneous system. The unknown coefficients, α_i, can now be determined by applying the previously discussed principle of minimum potential energy as

$$\frac{\partial \Pi}{\partial \alpha_i} = 0 \qquad (i = 1, 2, \ldots\ldots\ldots, 2N). \tag{4.38}$$

Equation (4.38) results in an algebraic system of $2N$ equations with $2N$ unknowns, hence providing a unique solution set for the unknown coefficients α_i that are substituted back into Equations (4.27) and (4.28) to obtain approximate solutions to the displacement fields, $u(x, y)$ and $v(x, y)$. Presented below are the results for the stress equilibrium equation (SEQ) in a homogeneous medium with $\mu = 1$, $\lambda = 1$, $b_x = b_y = 1$, and $d = 4$. Table 4.1 provides a convergence study of RRM by varying the order of the polynomials used for the approximation; and its comparison with the FEM solution. It can be seen that a 10th order polynomial is sufficient to provide a more than reasonable solution.

Table 4.1 Convergence of the RRM solution for the SEQ in a homogeneous medium

Order	N	Rayleigh-Ritz Solution		FEM Solution	
		u_{max}	v_{max}	u_{max}	v_{max}
4	6	2.3993	2.3993	2.5071	2.5071
6	15	2.4413	2.4413		
8	28	2.4282	2.4282		
10	45	2.4349	2.4349		
12	66	2.4315	2.4315		
14	91	2.4337	2.4337		

Figures 4.6 and 4.7 show the cross-sectional displacement profiles for $u(x,y)$ and $v(x,y)$ along the x and y axes, respectively, and their comparison with the respective FEM solutions. Figures 4.8 and 4.9 depict the 3-D displacement profiles along the x and y directions, respectively. Furthermore, the displacement contour plots for $u(x,y)$ and $v(x,y)$ are also presented as shown in Figures 4.10 and 4.11. All of the above mentioned pictorial representations (Figures 4.6 - 4.11) conform to a 10^{th} order approximation.

The FEM model was constructed in ANSYS using PLANE183 elements characterized by their two dimensional geometry with 8 nodes. The material constants, namely the Young's modulus E and the Poisson's ratio ν, were calculated from the Lamé constants using Equations (4.16) and (4.17) to be $E = 2.5$ and $\nu = 0.25$ corresponding to $\mu = 1$ and $\lambda = 1$. In order to accommodate the application of body forces, the system was modeled as a plane stress representation with thickness such that the volume of the system $(8 \times 8 \times 0.015625)$ equals one unit. The density ρ and the acceleration due to gravity g were also chosen to be one unit each, so that the body force $(\rho \times V \times g)$ equals one unit, as chosen for the semi-analytical model.

Hence, the FEM model, so constructed, only serves as a reasonable approximation to the original 2-D stress equilibrium equation. This explains the slim disparity in the solutions obtained from the FEM model to that procured from the semi-analytical solution; and the same trend will be observed for the heterogeneous cases as well. However, it should be noted that the FEM solutions only serve to corroborate the semi-analytical solutions in terms of the behavior of the displacement profiles which can be noticed, from the cross-sectional plots depicted below, to be consistent with those obtained from the semi-analytical model; and do not serve as the ultimate basis of comparison.

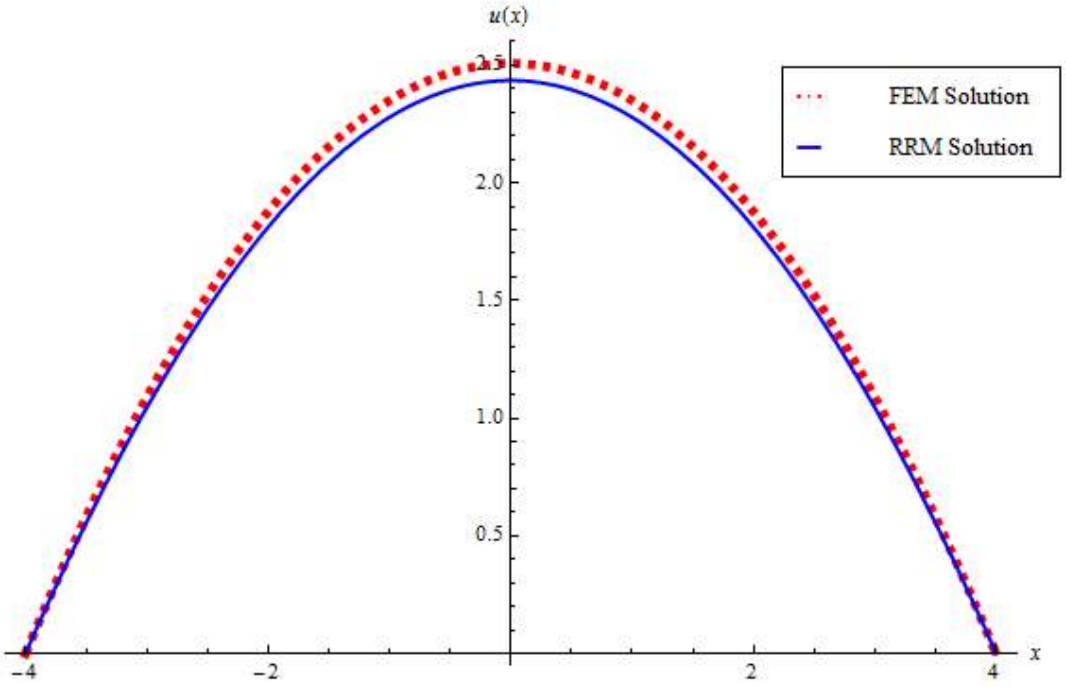

Figure 4.6 Comparison between the RRM solution and FEM solution for the x-component of displacement in a homogeneous medium.

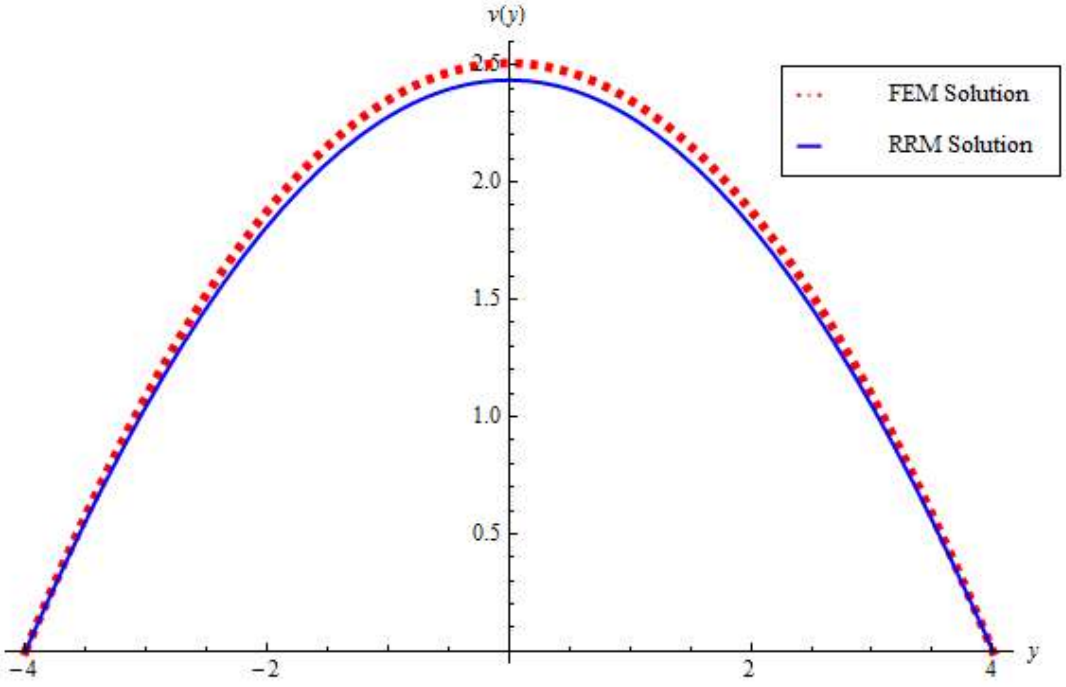

Figure 4.7 Comparison between the RRM solution and FEM solution for the y-component of displacement in a homogeneous medium.

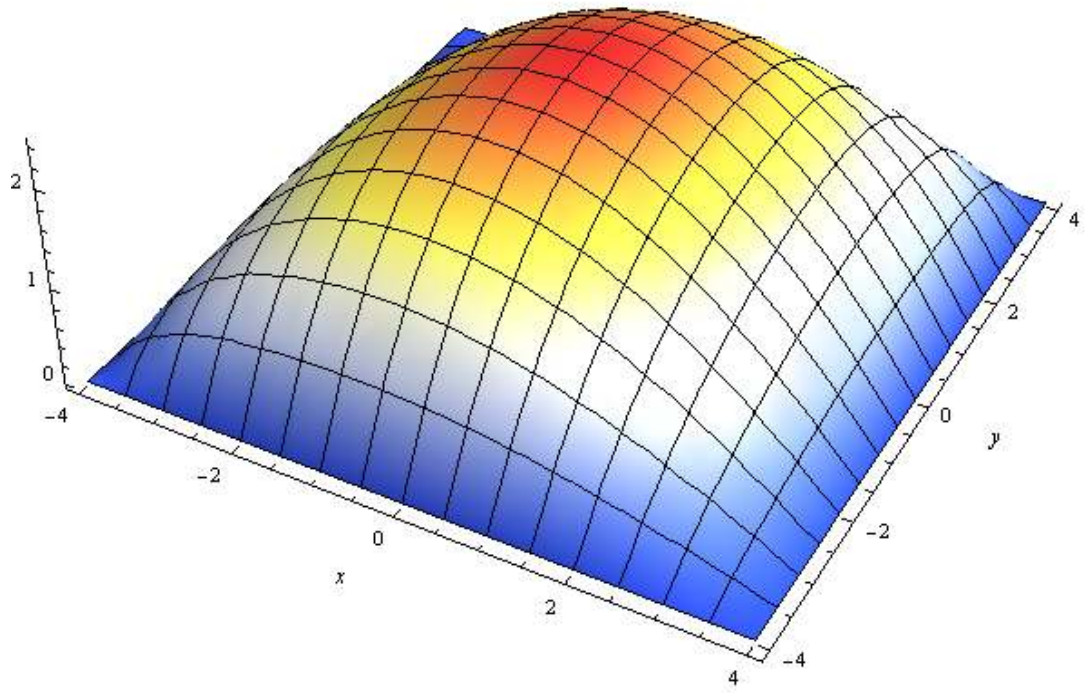

Figure 4.8 3-D profile for $u(x, y)$ in the homogeneous medium.

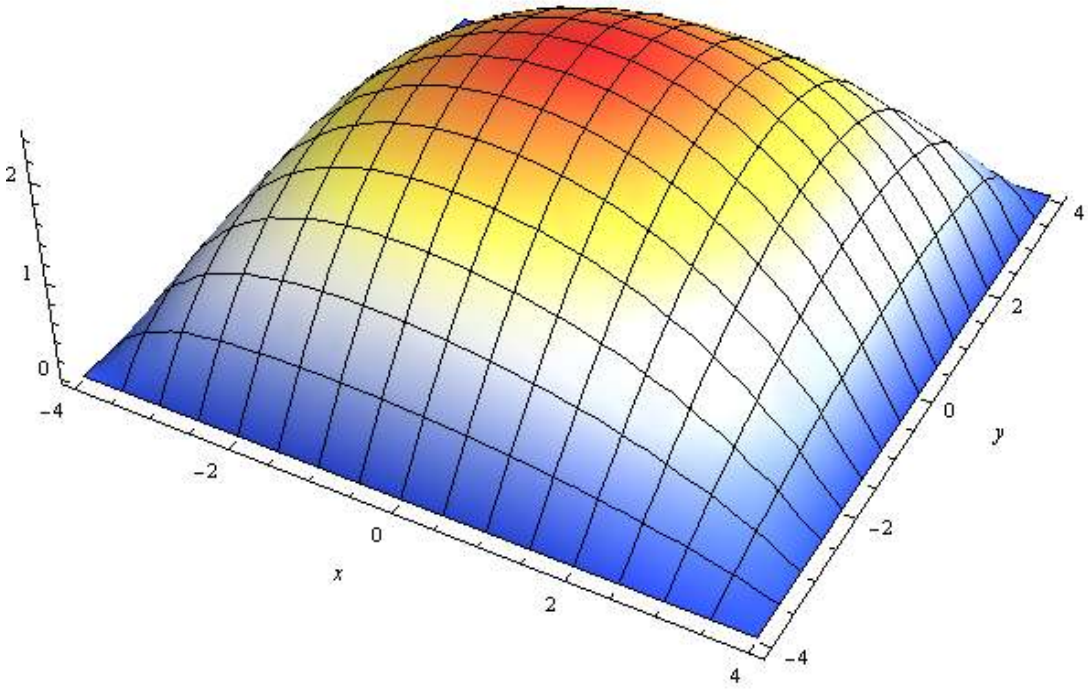

Figure 4.9 3-D profile for $v(x, y)$ in the homogeneous medium.

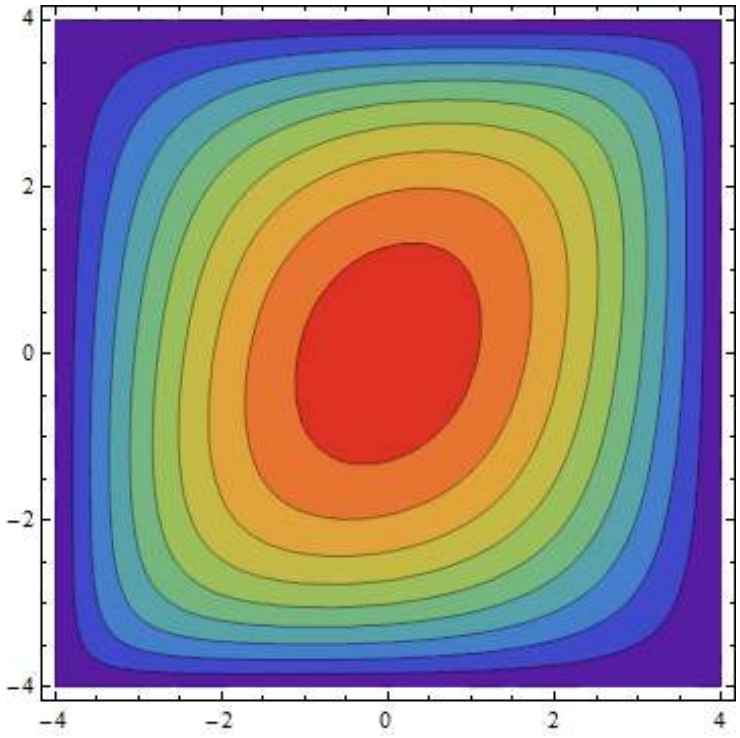

Figure 4.10 Contour plot of $u(x, y)$ in the homogeneous medium.

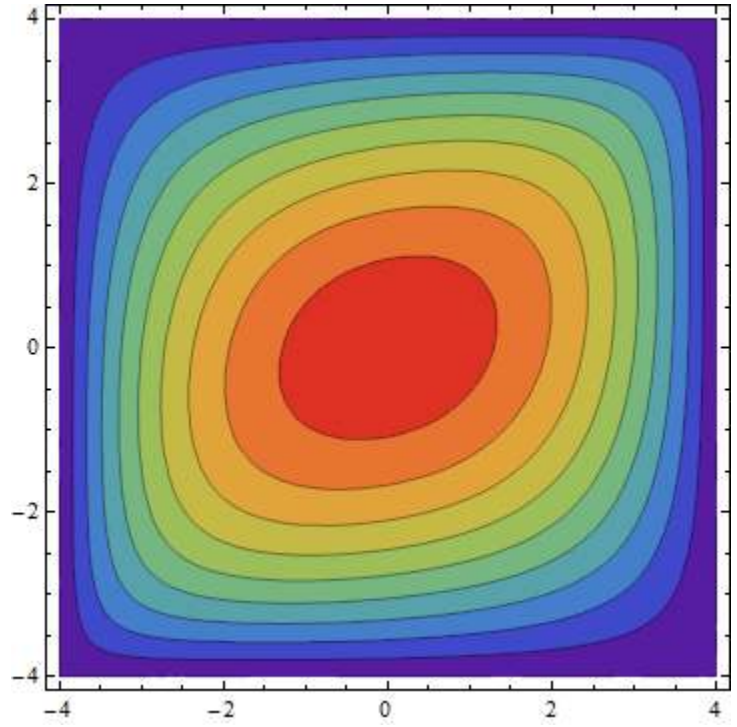

Figure 4.11 Contour plot of $v(x, y)$ in the homogeneous medium.

4.4.1 Stress Equilibrium Equation In SIPs

The heterogeneous medium under consideration is depicted in Figure 4.12. The governing equation, as in the homogeneous case, is of the form:

$$\left(C_{ijkl}\, u_{k,l}\right)_{,j} + b_i = 0. \tag{4.39}$$

The geometry constitutes a centrally located elliptical inclusion (with Lamé constants μ_1 and λ_1) embedded in a square-shaped matrix medium (with Lamé constants μ_2 and λ_2) subjected to zero displacement boundary conditions (homogeneous Dirichlet boundary conditions).

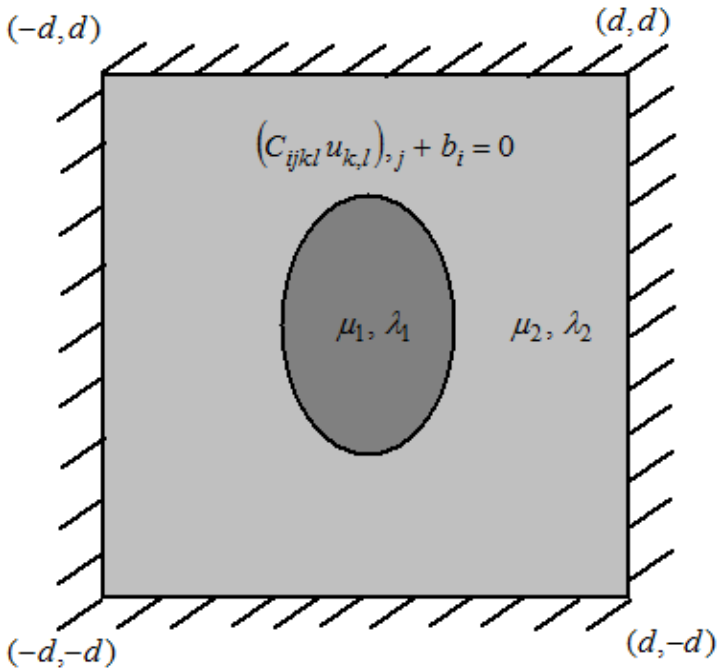

Figure 4.12 Elasticity equilibrium equation for a SIP.

Four sets of displacement trial functions corresponding to the two distinct phases as well as displacement components in the x and y directions are defined as

$$(f_x(x,y))_1 = c_0 + c_1(x) + c_2(y) + c_3(x^2) + c_4(xy) + c_5(y^2) + \ldots\ldots\ldots + c_{k-1}(\ldots), \tag{4.40}$$

$$\left(f_y(x,y)\right)_1 = c_k + c_{k+1}(x) + c_{k+2}(y) + c_{k+3}(x^2) + c_{k+4}(xy) + \ldots\ldots\ldots + c_{2k-1}(\ldots), \quad (4.41)$$

$$(f_x(x,y))_2 = (x^2 - d^2)(y^2 - d^2)\,(c_{2k} + c_{2k+1}(x) + c_{2k+2}(y) + \ldots\ldots\ldots + c_{3k-1}(\ldots)), \quad (4.42)$$

$$\left(f_y(x,y)\right)_2 = (x^2 - d^2)(y^2 - d^2)(c_{3k} + c_{3k+1}(x) + c_{3k+2}(y) + \ldots\ldots\ldots + c_{4k-1}(\ldots)), \quad (4.43)$$

where c_0, c_1,…, c_{4k-1} are the coefficients associated with the trial functions. Equations (4.40) and (4.41) represent the displacement trial functions for the inclusion phase along the x and y directions, respectively, while Equations (4.42) and (4.43) are the displacement trial functions for the matrix phase in the x and y directions. The trial functions so defined categorically satisfy the homogeneous boundary conditions. For heterogeneous materials, the trial functions also need to satisfy the continuity conditions of displacement and traction at the interface as

$$(f_i(x,y))_1|_{interface} = (f_i(x,y))_2|_{interface}, \quad (4.44)$$

$$(t_i(x,y))_1|_{interface} = (t_i(x,y))_2|_{interface.} \quad (4.45)$$

Equation (4.44) represents the continuity conditions of displacement; and for $i = 1, 2$, the displacement continuity conditions in the x and y directions can be written as

$$(f_x(x,y))_1|_{interface} = (f_x(x,y))_2|_{interface} \quad (4.46)$$

$$(f_y(x,y))_1|_{interface} = (f_y(x,y))_2|_{interface} \quad (4.47)$$

Equation (4.45) describes the continuity conditions of traction at the interface that need to be expressed in terms of the trial functions in the x and y directions. To facilitate this transition, the definition of traction from Equation (4.9) is expanded as

$$t_x = \sigma_{xx}\, n_x + \sigma_{xy}\, n_{y,} \quad (4.48)$$

$$t_y = \sigma_{xy}\, n_x + \sigma_{yy}\, n_{y,} \tag{4.49}$$

where t_x and t_y, and n_x and n_y, are the traction components and the normalized surface normal components, in the x and y directions, respectively, with σ_{xx} and σ_{yy} representing the normal stresses in the x and y directions, and σ_{xy} denoting the shear stress on the $x-y$ plane. The stress components are further expanded using Equation (4.19) as

$$\sigma_{xx} = 2\,\mu\,\varepsilon_{xx} + \lambda\left(\varepsilon_{xx} + \varepsilon_{yy}\right) = 2\,\mu\,\frac{\partial f_x}{\partial x} + \lambda\left(\frac{\partial f_x}{\partial x} + \frac{\partial f_y}{\partial y}\right),$$

$$\sigma_{yy} = 2\,\mu\,\varepsilon_{yy} + \lambda\left(\varepsilon_{xx} + \varepsilon_{yy}\right) = 2\,\mu\,\frac{\partial f_y}{\partial y} + \lambda\left(\frac{\partial f_x}{\partial x} + \frac{\partial f_y}{\partial y}\right),$$

$$\sigma_{xy} = 2\,\mu\,\varepsilon_{xy} = 2\,\mu\,\frac{1}{2}\left(\frac{\partial f_x}{\partial y} + \frac{\partial f_y}{\partial x}\right).$$

Rearranging the terms in the above equations results in

$$\sigma_{xx} = (2\,\mu + \lambda)\frac{\partial f_x}{\partial x} + \lambda\left(\frac{\partial f_y}{\partial y}\right), \tag{4.50}$$

$$\sigma_{yy} = (2\,\mu + \lambda)\frac{\partial f_y}{\partial y} + \lambda\left(\frac{\partial f_x}{\partial x}\right), \tag{4.51}$$

$$\sigma_{xy} = \mu\left(\frac{\partial f_x}{\partial y} + \frac{\partial f_y}{\partial x}\right). \tag{4.52}$$

Substituting Equations (4.50), (4.51), and (4.52) into Equations (4.48) and (4.49) and exercising the definition of the surface normal for an elliptical interface, from Equation (2.10) yields

$$t_x = \left((2\,\mu + \lambda)\frac{\partial f_x}{\partial x} + \lambda\left(\frac{\partial f_y}{\partial y}\right)\right)\frac{x/a^2}{\sqrt{\frac{x^2}{a^4} + \frac{y^2}{b^4}}} + \mu\left(\frac{\partial f_x}{\partial y} + \frac{\partial f_y}{\partial x}\right)\frac{y/b^2}{\sqrt{\frac{x^2}{a^4} + \frac{y^2}{b^4}}}, \tag{4.53}$$

$$t_y = \mu \left(\frac{\partial f_x}{\partial y} + \frac{\partial f_y}{\partial x}\right) \frac{x/a^2}{\sqrt{\frac{x^2}{a^4} + \frac{y^2}{b^4}}} + \left((2\,\mu + \lambda)\frac{\partial f_y}{\partial y} + \lambda \left(\frac{\partial f_x}{\partial x}\right)\right) \frac{y/b^2}{\sqrt{\frac{x^2}{a^4} + \frac{y^2}{b^4}}}. \tag{4.54}$$

For explicitness, each component of traction along the x and y directions for the inclusion (subscript 1) and matrix (subscript 2), is illustrated below:

$$(t_x)_1 = \left((2\,\mu_1 + \lambda_1)\frac{\partial (f_x)_1}{\partial x} + \lambda_1 \frac{\partial (f_y)_1}{\partial y}\right)\frac{x}{a^2} + \mu_1 \left(\frac{\partial (f_x)_1}{\partial y} + \frac{\partial (f_y)_1}{\partial x}\right)\frac{y}{b^2}, \tag{4.55}$$

$$(t_x)_2 = \left((2\,\mu_2 + \lambda_2)\frac{\partial (f_x)_2}{\partial x} + \lambda_2 \frac{\partial (f_y)_2}{\partial y}\right)\frac{x}{a^2} + \mu_2 \left(\frac{\partial (f_x)_2}{\partial y} + \frac{\partial (f_y)_2}{\partial x}\right)\frac{y}{b^2}, \tag{4.56}$$

$$(t_y)_1 = \mu_1 \left(\frac{\partial (f_x)_1}{\partial y} + \frac{\partial (f_y)_1}{\partial x}\right)\frac{x}{a^2} + \left(\lambda_1 \frac{\partial (f_x)_1}{\partial x} + (2\,\mu_1 + \lambda_1)\frac{\partial (f_y)_1}{\partial y}\right)\frac{y}{b^2}, \tag{4.57}$$

$$(t_y)_2 = \mu_2 \left(\frac{\partial (f_x)_2}{\partial y} + \frac{\partial (f_y)_2}{\partial x}\right)\frac{x}{a^2} + \left(\lambda_2 \frac{\partial (f_x)_2}{\partial x} + (2\,\mu_2 + \lambda_2)\frac{\partial (f_y)_2}{\partial y}\right)\frac{y}{b^2}. \tag{4.58}$$

Substituting the above equations into Equation (4.45) will yield the final form of the continuity conditions for traction at the elliptical interface; and in combination with Equations (4.46) and (4.47), the continuity conditions are all set to be solved for the unknown coefficients, c_i, where $i = 0, 1, 2, \ldots\ldots\ldots\ldots, (4k-1)$ to obtain two separate sets of permissible functions for the inclusion and matrix phases that are essentially dependent on the geometrical and material parameters of the heterogeneous medium; with each set comprising of the permissible functions in the x and y directions. As in the case of the homogeneous system, the permissible functions are now subjected to the Rayleigh-Ritz method, during the course of which an expression for the potential energy is obtained based on the schematic depicted below.

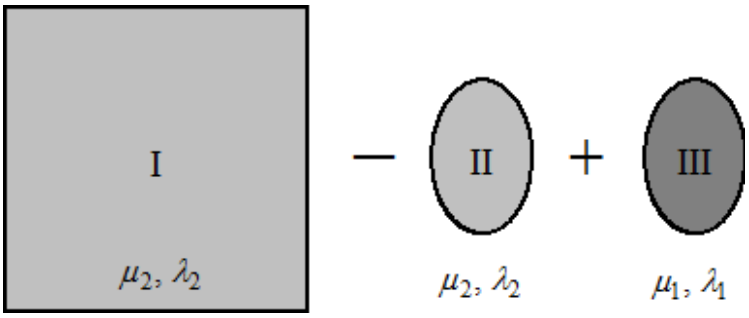

Figure 4.13 Geometrical decomposition of the SIP into its constituent phases

The potential energy of a system corresponding to the square-shaped region I is given by

$$\Pi_{\mathrm{I}} = \frac{1}{2}\iint_{\mathrm{I}} \Big((2\,\mu_2 + \lambda_2)\left({u_2}_{,x}{}^2 + {v_2}_{,y}{}^2\right) + \mu_2\left(u_{2,y} + v_{2,x}\right)^2 + 2\,\lambda_2\, u_{2,x}\, v_{2,y} - 2\left(b_x u_2 - b_y\, v_2\right)\Big)\, dx\; dy, \tag{4.59}$$

Similarly, for the elliptical regions II and III, their respective potential energies Π_{II} and Π_{III} are

$$\Pi_{\mathrm{II}} = \frac{1}{2}\iint_{\mathrm{II}} \Big((2\,\mu_2 + \lambda_2)\left({u_2}_{,x}{}^2 + {v_2}_{,y}{}^2\right) + \mu_2\left(u_{2,y} + v_{2,x}\right)^2 + 2\,\lambda_2\, u_{2,x}\, v_{2,y} - 2\left(b_x u_2 - b_y\, v_2\right)\Big)\, dx\; dy, \tag{4.60}$$

$$\Pi_{\mathrm{III}} = \frac{1}{2}\iint_{\mathrm{III}} \Big((2\,\mu_1 + \lambda_1)\left({u_1}_{,x}{}^2 + {v_1}_{,y}{}^2\right) + \mu_1\left(u_{1,y} + v_{1,x}\right)^2 + 2\,\lambda_1\, u_{1,x}\, v_{1,y} - 2\left(b_x u_1 - b_y\, v_1\right)\Big)\, dx\; dy, \tag{4.61}$$

where u_1 and v_1 are approximate assumed solutions of the displacements in the x and y directions, respectively, for the inclusion phase, with u_2 and v_2 representing the corresponding displacement solutions for the matrix phase, and these quantities are defined as

$$u_1(x,y) = \sum_{i=1}^{N} \alpha_i\, g_{1i}(x,y), \tag{4.62}$$

$$v_1(x,y) = \sum_{i=N+1}^{2N} \alpha_i \, h_{1i}(x,y), \tag{4.63}$$

$$u_2(x,y) = \sum_{i=1}^{N} \alpha_i \, g_{2i}(x,y), \tag{4.64}$$

$$v_2(x,y) = \sum_{i=N+1}^{2N} \alpha_i \, h_{2i}(x,y), \tag{4.65}$$

where $g_{1i}(x,y)$ and $h_{1i}(x,y)$, are the displacement permissible functions along the x and y directions for the inclusion phase while $g_{2i}(x,y)$, and $h_{2i}(x,y)$ are the corresponding displacement permissible functions for the matrix phase. In general, a permissible function e_i depends on the geometrical and material parameters that constitute the given heterogeneous system, and is of the form:

$$e_i = e_i(a,b,d,\mu_1,\lambda_1,\mu_2,\lambda_2,x,y). \tag{4.66}$$

Combining Equations (4.59), (4.60), and (4.61), as per the schematic depicted in Figure 4.13, yields the potential energy of the entire heterogeneous system, Π, as

$$\Pi = \Pi_{\mathrm{I}} - \Pi_2 + \Pi_3. \tag{4.67}$$

Equation (4.67) is now subjected to the principle of minimum potential energy as described in Equation (4.38) to solve for the $2N$ unknown coefficients, α_i, that in turn are substituted back into Equations (4.62 – 4.65) to obtain approximate solutions to the displacement fields. Furnished below are the results of the stress equilibrium equation in terms of the displacement fields for the single elliptical inclusion problem with material constants, $\mu_1 = 30$, $\lambda_1 = 40$, $\mu_2 = 1$, $\lambda_2 = 1$; and the size of the elliptical inclusion being defined by $a = 1$ and $b = 1.5$ with dimensions of the square-shaped matrix characterized by $d = 4$. Also, the

body forces in the x and y directions are chosen to be $b_x = b_y = 1$. Furthermore, the results for a single circular inclusion problem are also presented retaining the same material and geometrical parameters as indicated above with the exception that $b = 1$.

Figures 4.14 and 4.15 depict the cross-sectional displacement plots for $u(x, y)$ and $v(x, y)$ along the x-axis and y-axis, respectively, for the single elliptical inclusion problem. The corresponding FEM solutions are also provided on the same plots. Figures 4.16 – 4.19 present the 3-D displacement profiles and the displacement contour plots for the same problem. Figures 4.20 - 4.25 demonstrate a similar study of the displacement fields for the single circular inclusion problems. It can be observed that the semi-analytical solution is well corroborated by the purely numerical solution, for both types of problems. The table below (Table 4.2) provides a documentation of the results for the displacement fields in SCIP and SEIP.

Table 4.2 Comparison between the RRM and FEM displacement solutions for the SIPs

Order	N	Dimensions of the Inclusion			RRM Solution		FEM Solution	
		a	b	Area (πab)	u_{max}	v_{max}	u_{max}	v_{max}
10	80	1	1.5	1.5π	2.2385	2.1938	2.3192	2.2806
	88	1	1	π	2.3064	2.3064	2.3789	2.3789
	88	0	0	0	2.4349	2.4349	2.5071	2.5071

The maximum displacement values displayed in Table 4.2 correspond to the following material constants - $E_1 = 540/7,\ \nu_1 = 1/7,\ E_2 = 2.5,$ and $\nu_2 = 0.25$. Among the three sets of results tabulated above, the case when $a = 0$ and $b = 0$ exhibits the largest of displacements; and this conforms to the homogeneous system, solved for earlier. However, with the existence of an inclusion ($a \neq 0,\ b \neq 0$), the resulting heterogeneous system experiences a noticeable reduction in displacement compared to its homogeneous counterpart. In an engineering sense, this is a valid occurrence since the inclusion material is almost 25 times stiffer than its

surrounding matrix, thus making it less susceptible to deformation. Also, a further reduction in displacement is observed as the surface area of the inclusion increases. Figures 4.26 and 4.27 provide a graphical interpretation of Table 4.2, reiterating the effect of the inclusion area on the resulting displacement fields in the x and y directions.

A similar study is carried out to investigate the effect of varying aspect ratios of the inclusion and material constants of the individual phases on the displacement fields. In the first instance (Figures 4.28 and 4.29), the aspect ratios of the inclusion are varied while retaining a constant inclusion surface area. It is interesting to observe that as the aspect ratios become larger, the displacements become smaller irrespective of the inclusion area being a constant. Also, it can be seen that the decrease in displacement is more pronounced in $u(x)$ than in $v(y)$. This can be attributed to the geometry and orientation of the elliptical inclusion i.e. $a > b$ and also that a lies along the x-axis. In the second case (Figures 4.30 and 4.31), while retaining the same geometrical parameters throughout, only the material properties of the inclusion and the matrix are varied. Here, a noticeable feature is the profound effect on the displacement field due to the change in the material constants of the matrix phase, compared to the change in the material properties of the inclusion. Tables 4.3 and 4.4 summarize the results of the afore-mentioned sensitivity analyses. It is worth mentioning that this kind of analysis can be easily administered due to the ready availability of the analytically derived permissible functions.

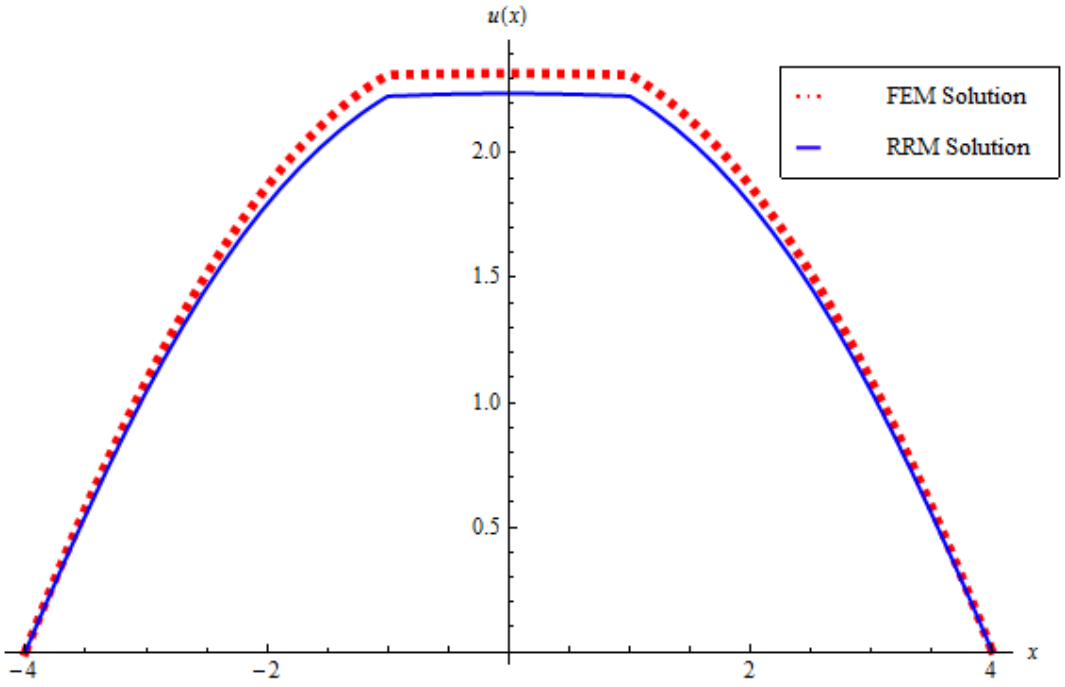

Figure 4.14 Comparison between the RRM and FEM solution for the x-component of displacement in the SEIP.

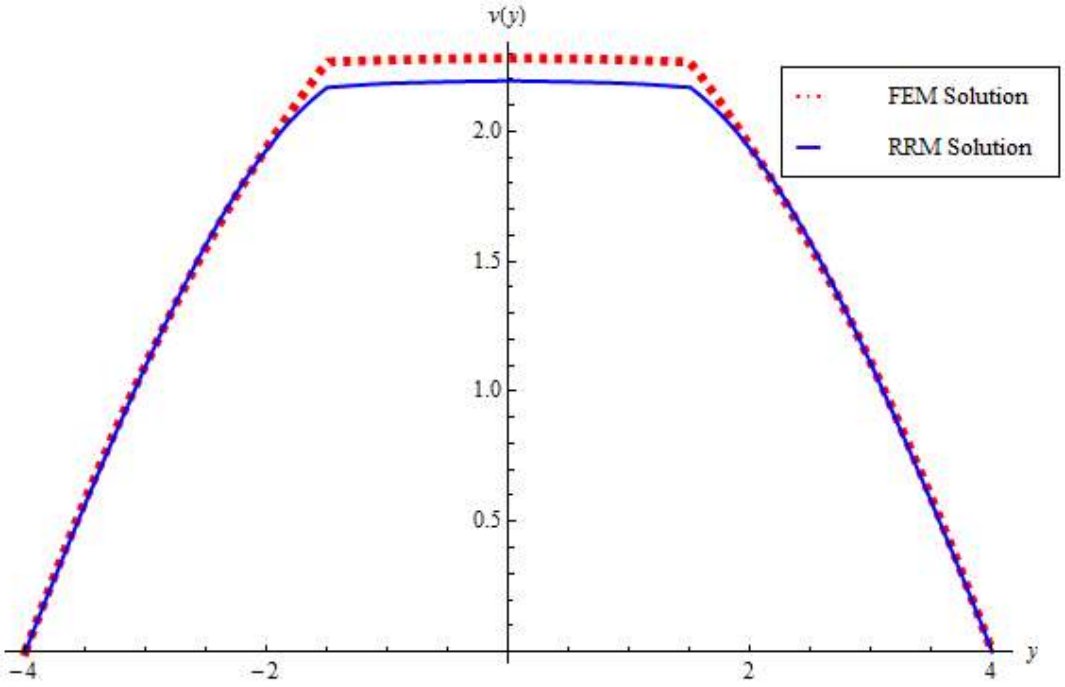

Figure 4.15 Comparison between the RRM and FEM solution for the y-component of displacement in the SEIP.

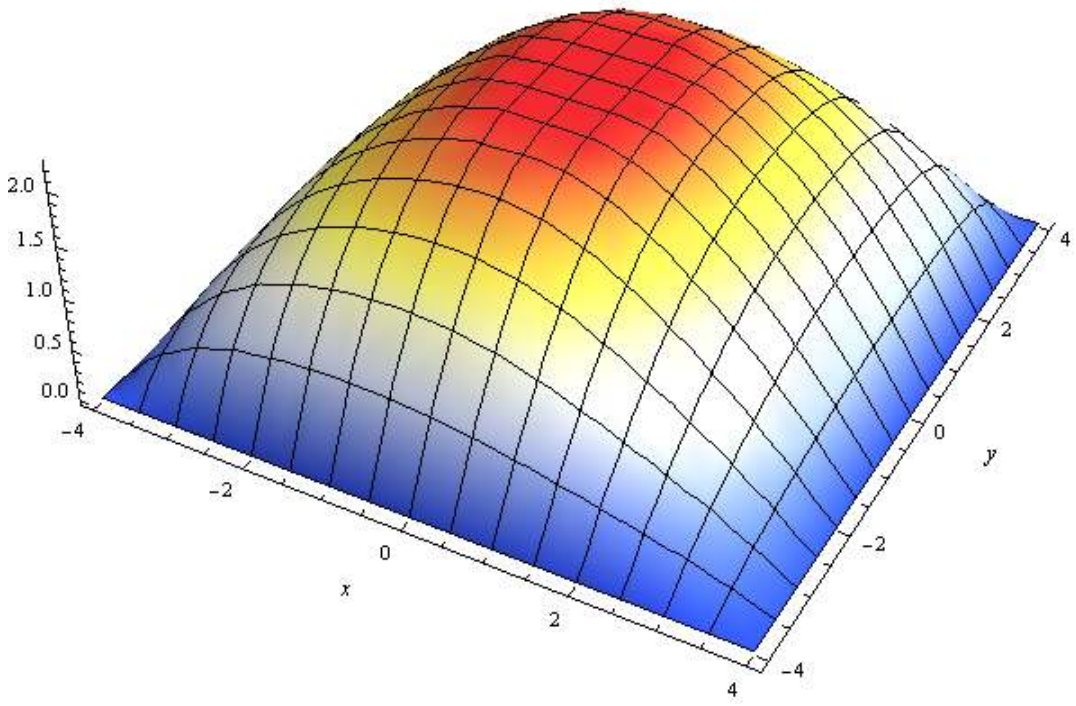

Figure 4.16 3-D profile of the x-component of displacement for the SEIP.

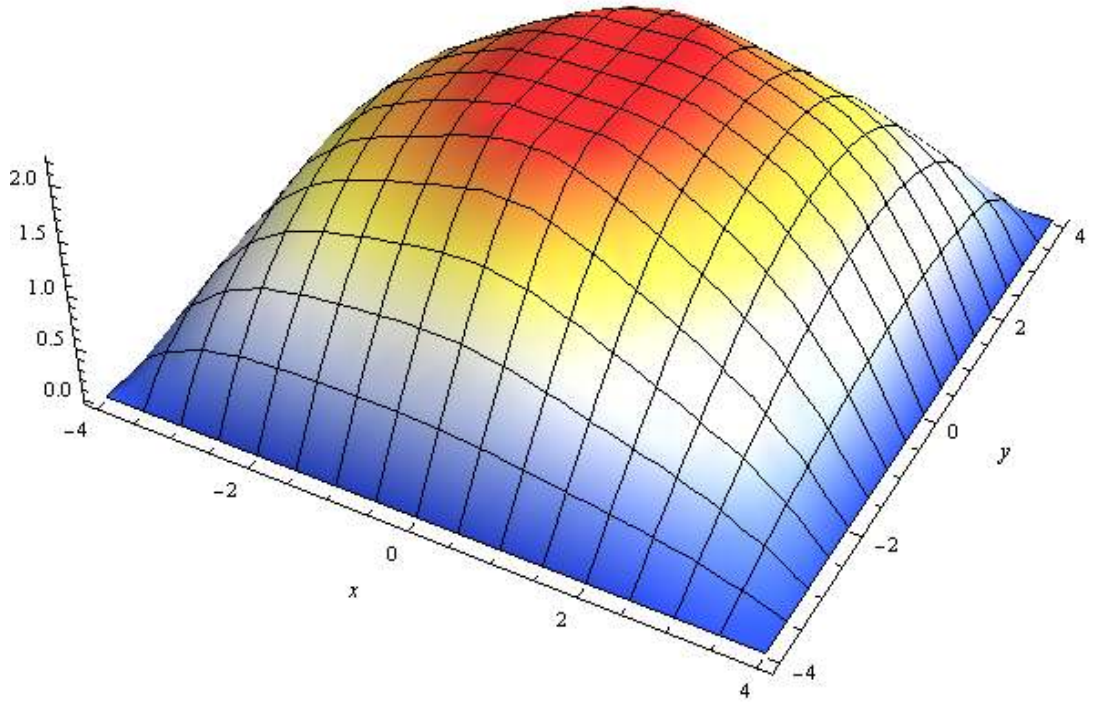

Figure 4.17 3-D profile of the y-component of displacement for the SEIP.

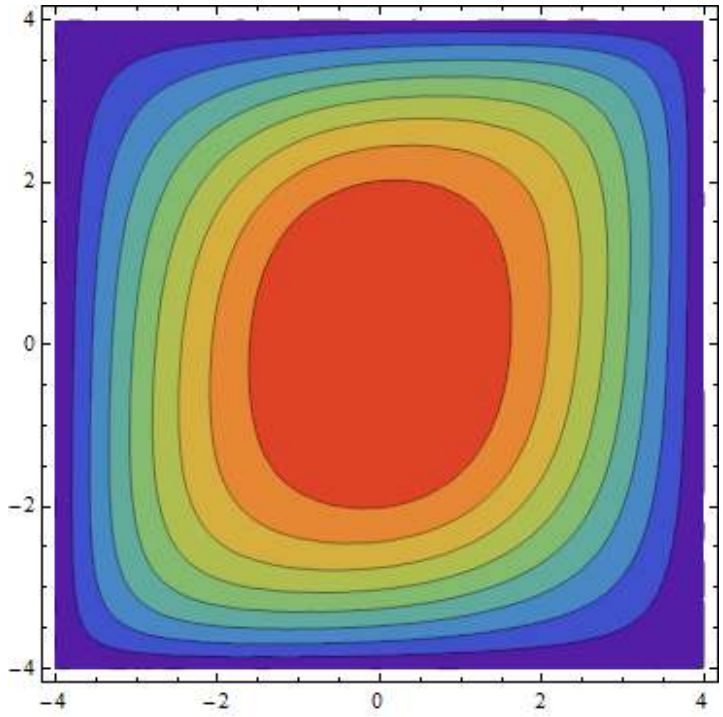

Figure 4.18 Contour plot of the x-component of displacement for the SEIP.

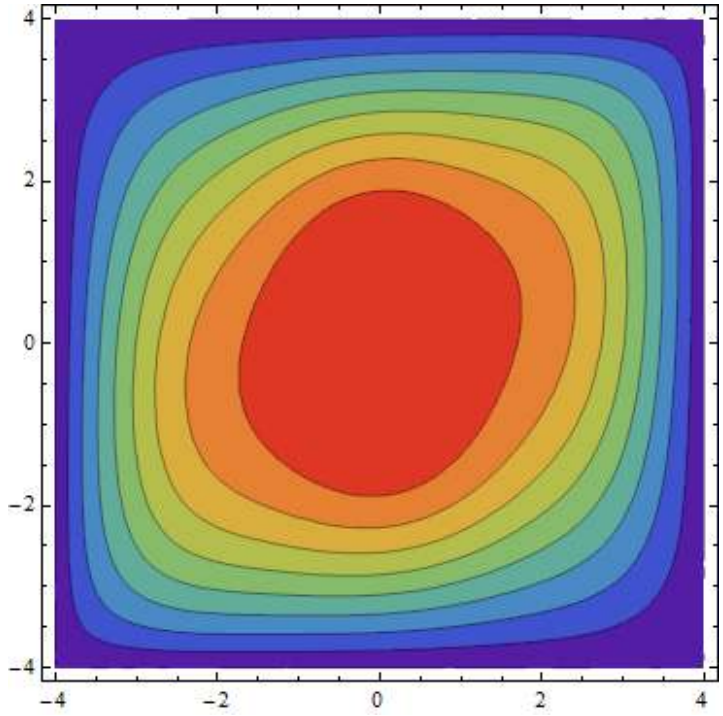

Figure 4.19 Contour plot of the y-component of displacement for the SEIP.

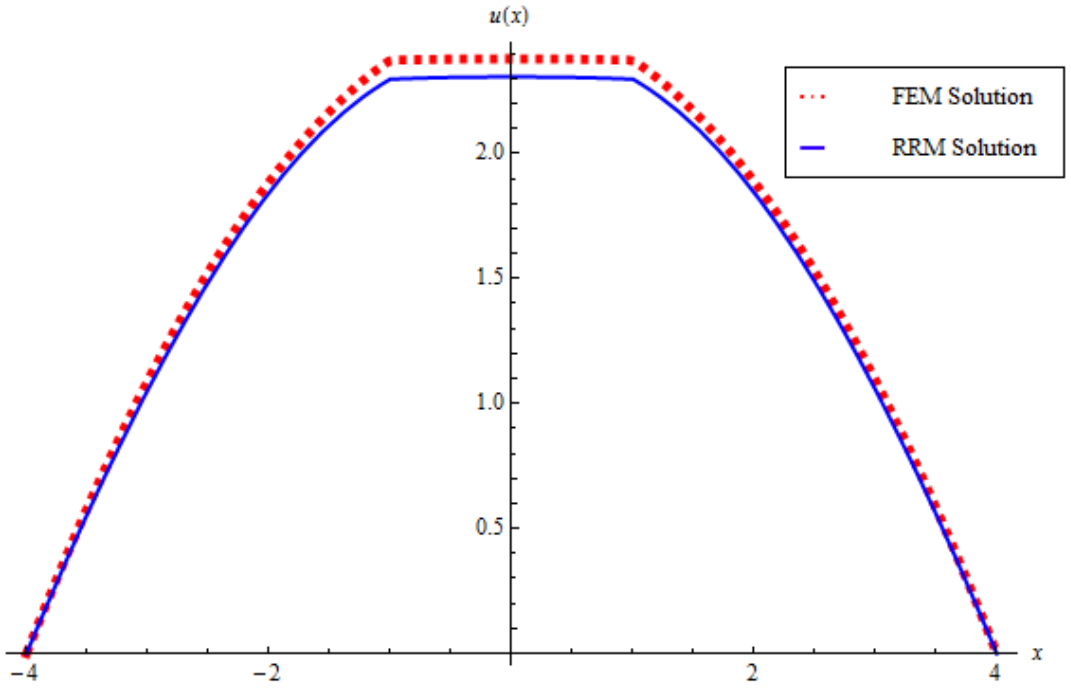

Figure 4.20 Comparison between the RRM and FEM solution for the x-component of displacement in the SCIP.

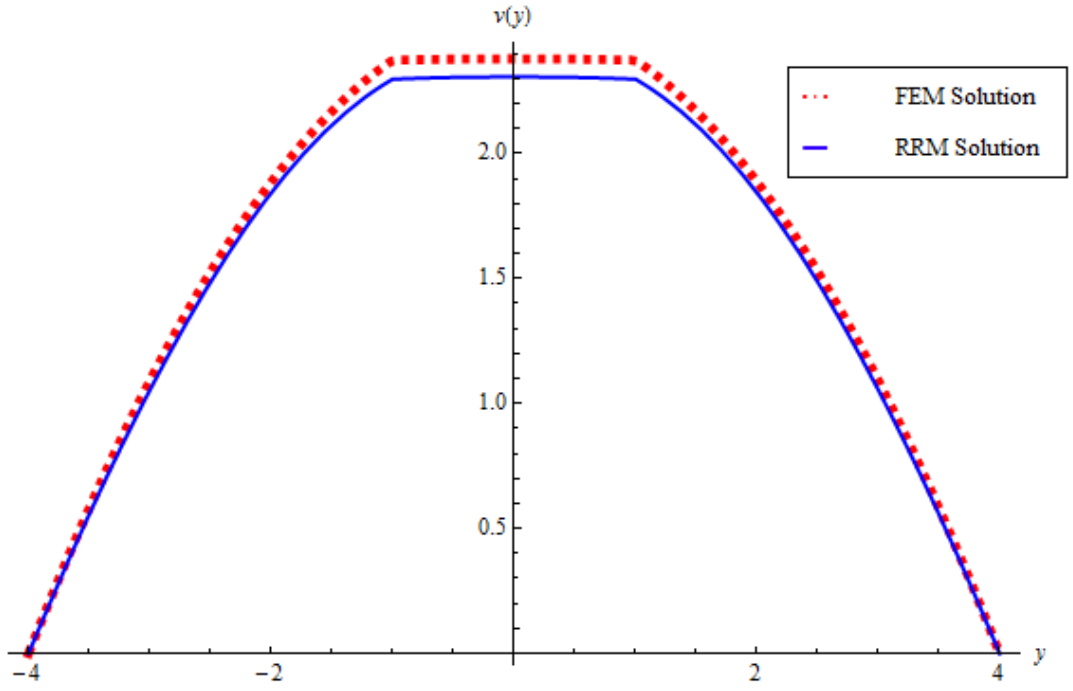

Figure 4.21 Comparison between the RRM and FEM solution for the y-component of displacement in the SCIP.

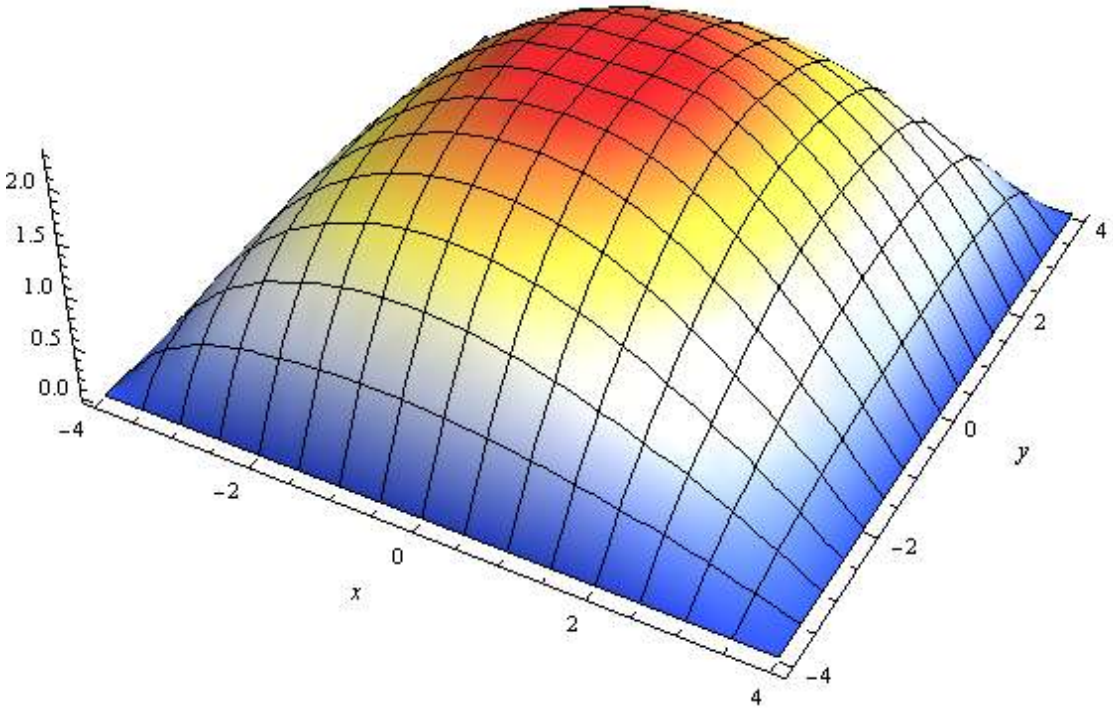

Figure 4.22 3-D profile of the x-component of displacement for the SCIP.

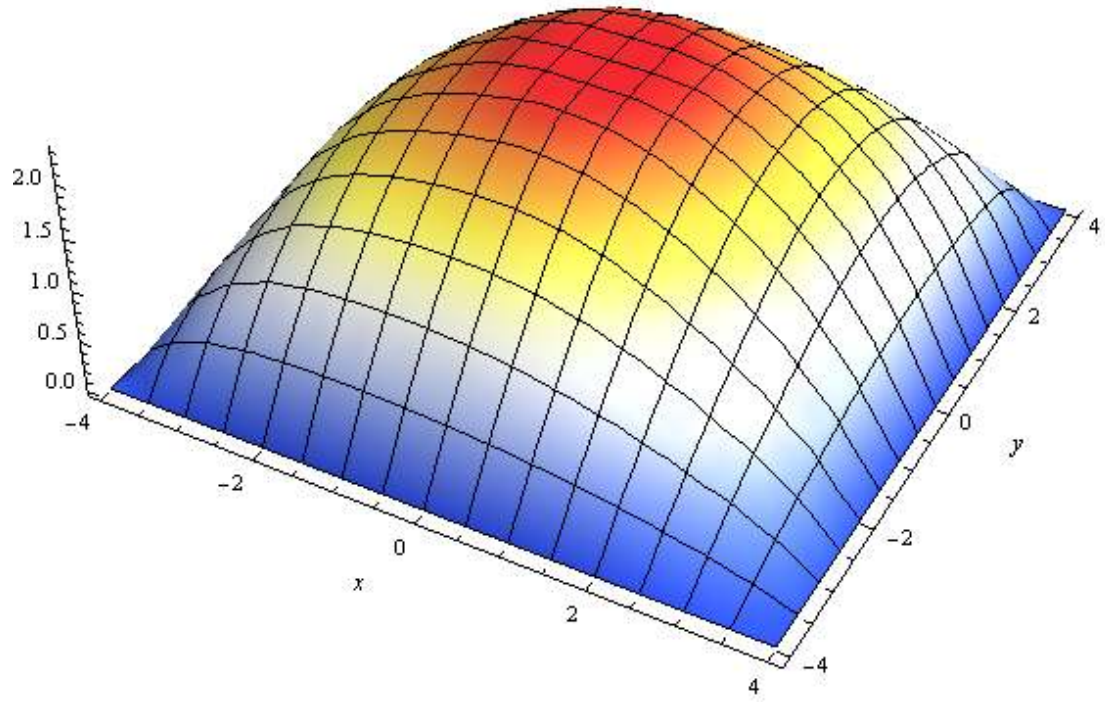

Figure 4.23 3-D profile of the y-component of displacement for the SCIP.

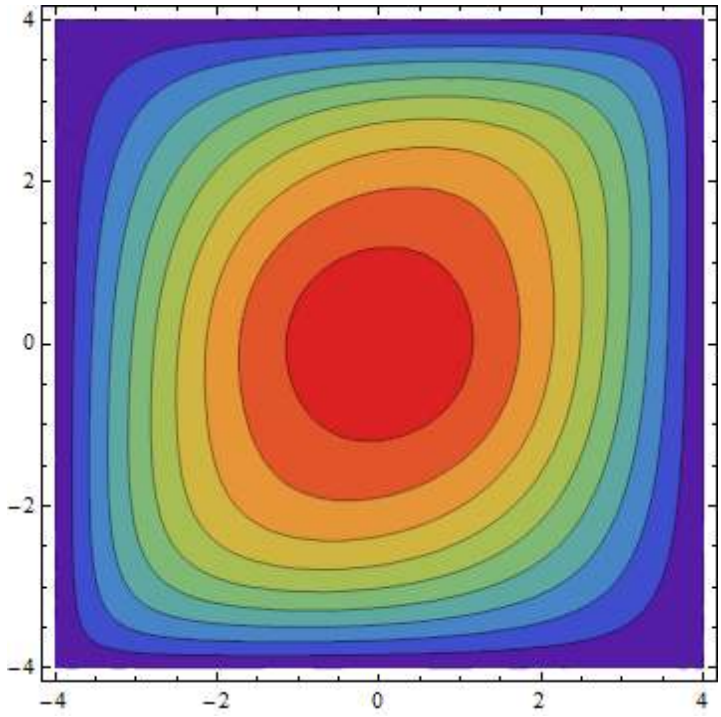

Figure 4.24 Contour plot of the x-component of displacement for the SCIP.

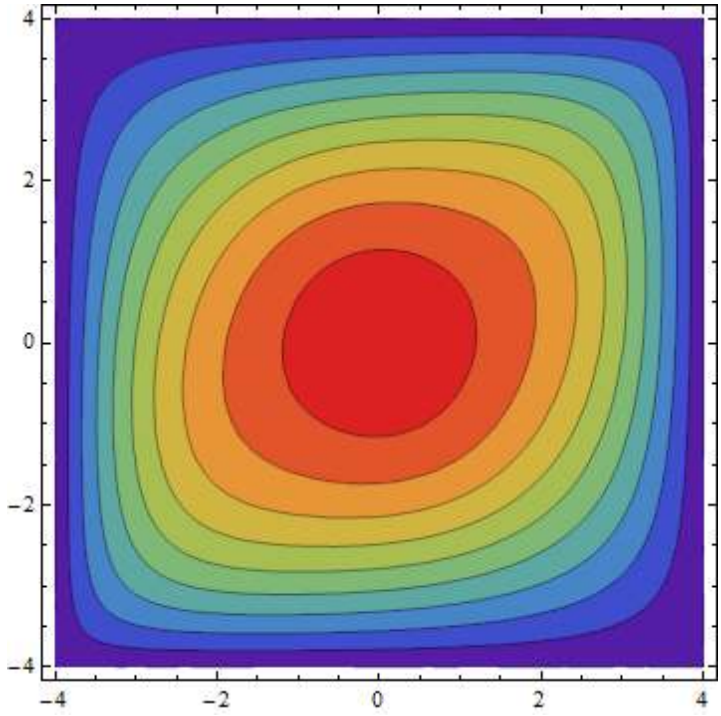

Figure 4.25 Contour plot of the y-component of displacement for the SCIP.

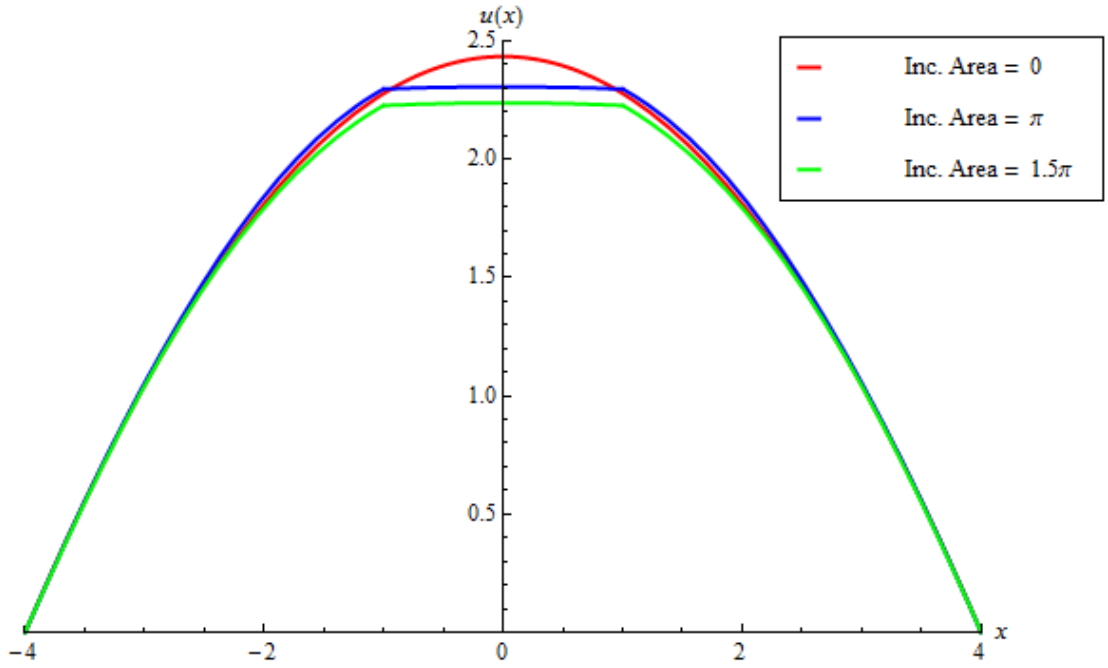

Figure 4.26 Effect of varying inclusion surface areas on the x-component of displacement for the SIPs.

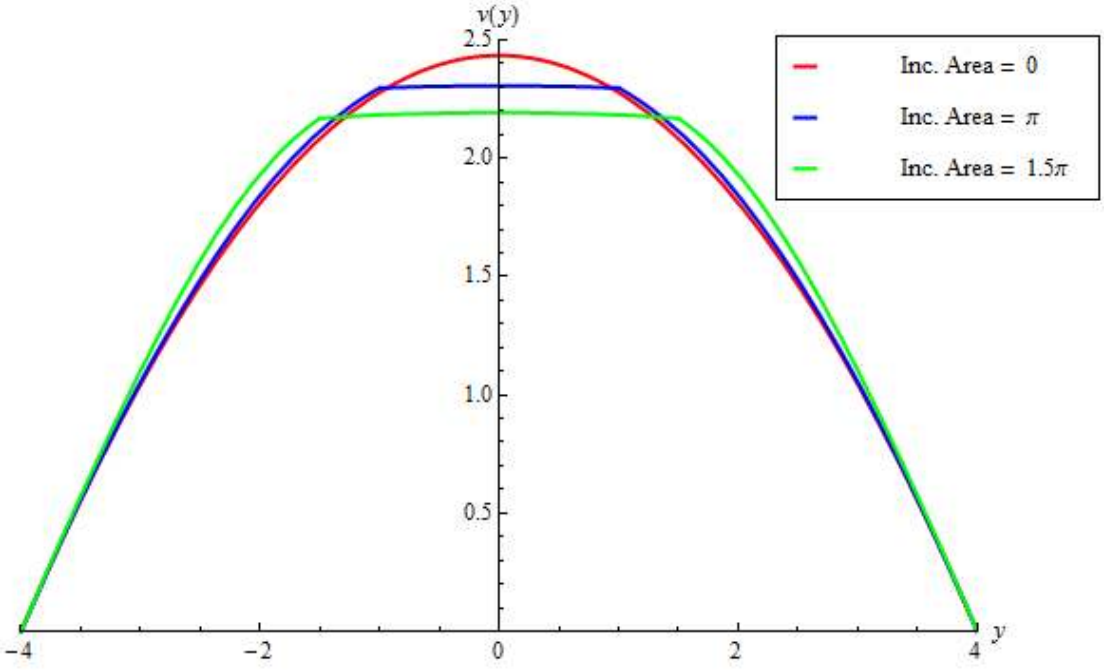

Figure 4.27 Effect of varying inclusion surface areas on the y-component of displacement for the SIPs.

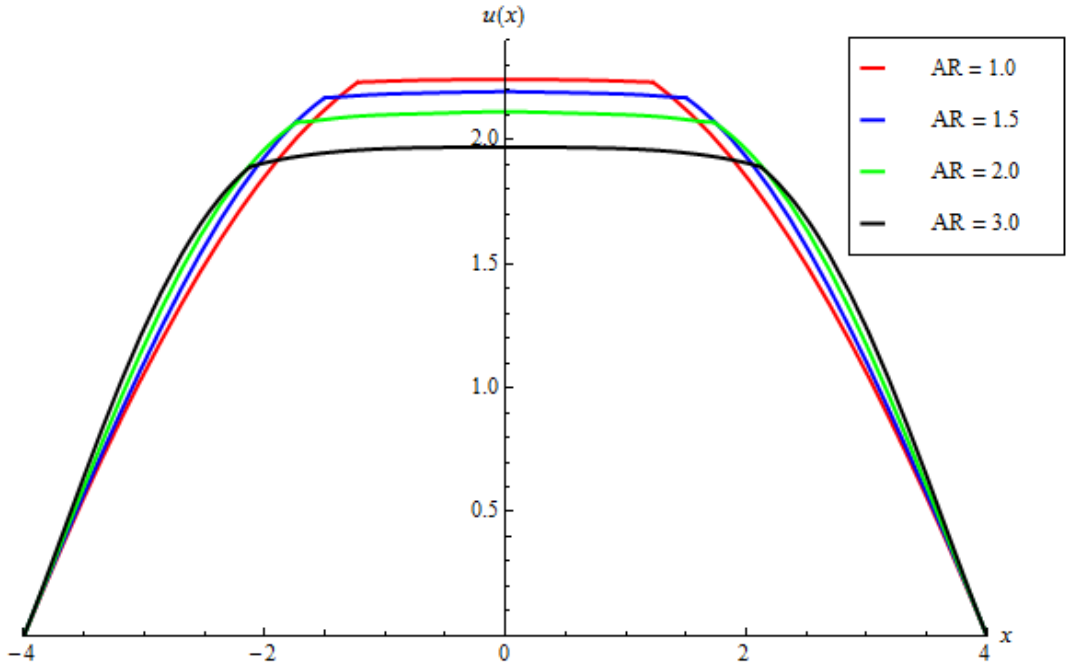

Figure 4.28 Effect of varying aspect ratios of the inclusion on the x-component of displacement for the SIPs.

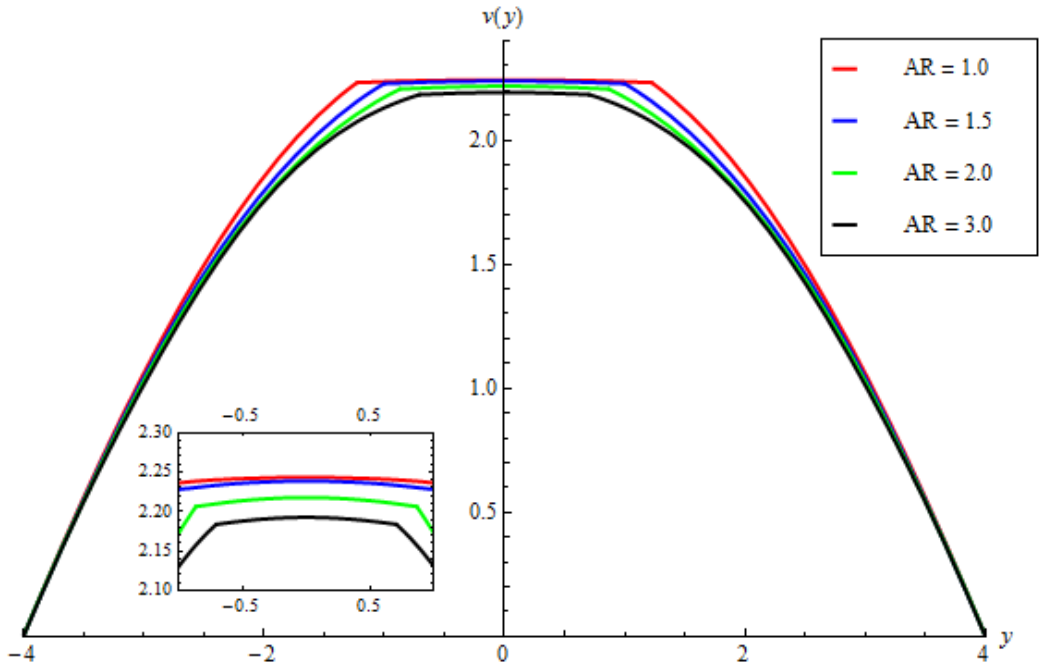

Figure 4.29 Effect of varying aspect ratios of the inclusion on the y-component of displacement for the SIPs.

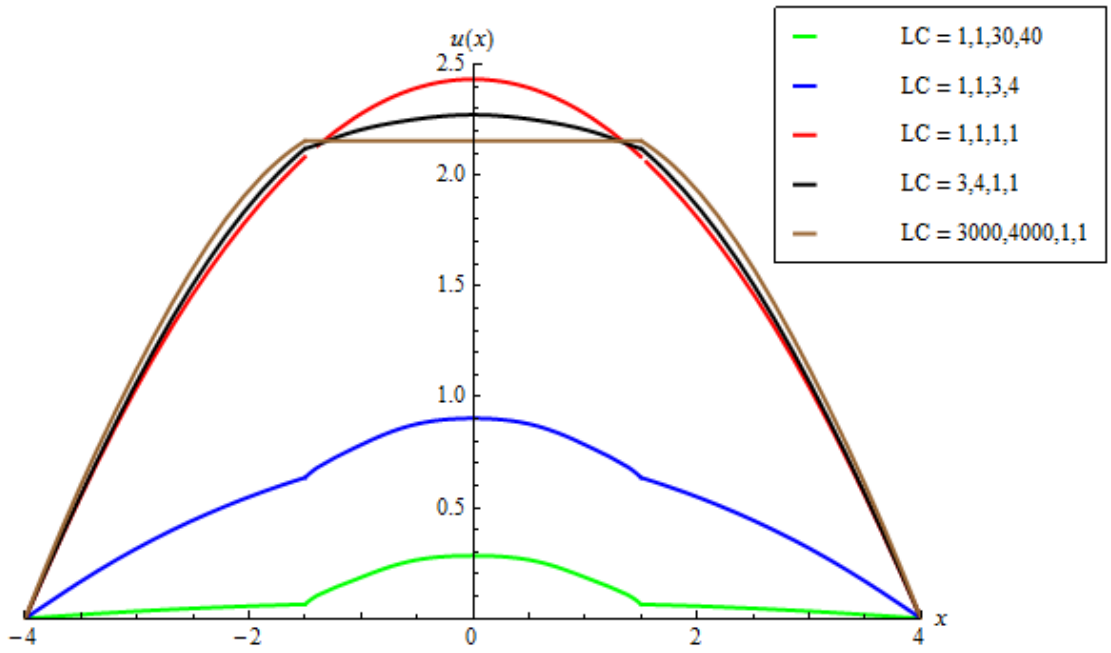

Figure 4.30 Effect of varying material constants of the constituent phases on the x-component of displacement for the SIPs.

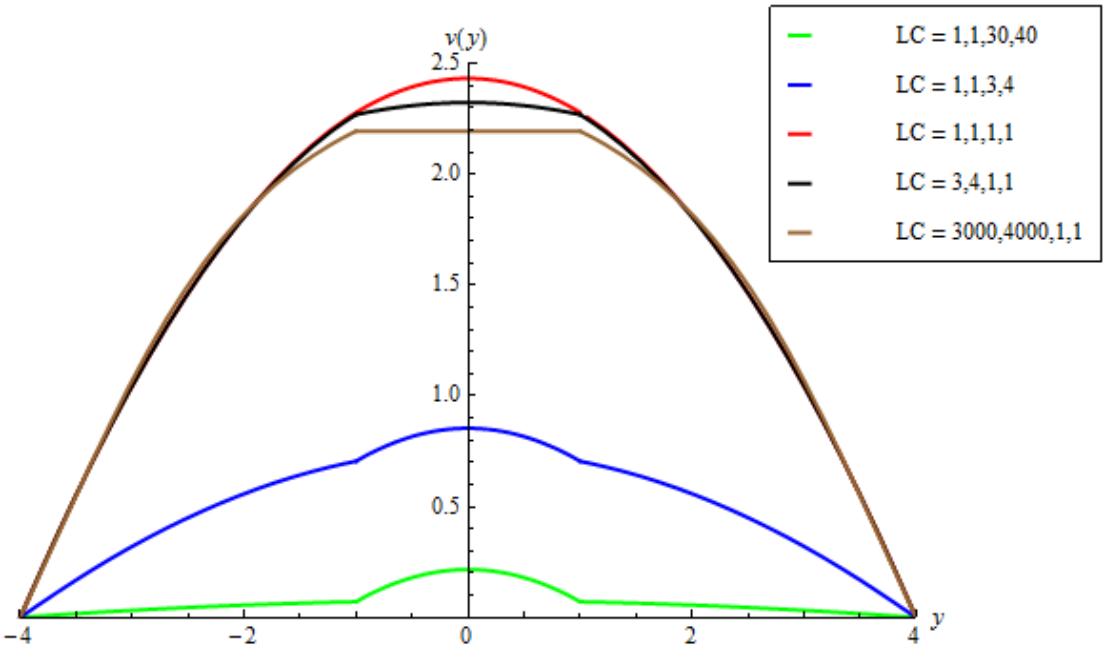

Figure 4.31 Effect of varying material constants of the constituent phases on the y-component of displacement for the SIPs.

Table 4.3 Effect of varying inclusion aspect ratios on the displacement fields for the SIPs

Constant Parameters for the inclusion						Varying Parameters for the inclusion			Displacements	
$\pi\ a\ b$	(x_1, y_1)	μ_1	λ_1	μ_2	λ_2	a	b	a/b	u_{max}	v_{max}
$\frac{3\pi}{2}$	$(0,0)$	30	40	1	1	$\sqrt{\frac{3}{2}}$	$\sqrt{\frac{3}{2}}$	1	2.24326	2.24326
						$\frac{3}{2}$	1	$\frac{3}{2}$	2.19375	2.23853
						$\sqrt{3}$	$\frac{\sqrt{3}}{2}$	2	2.11284	2.21761
						$\frac{3}{\sqrt{2}}$	$\frac{1}{\sqrt{2}}$	3	1.97011	2.19249

Table 4.4 Effect of varying material constants on the displacement fields for the SIPs

Constant Parameters for the Inclusion					Varying Parameters for the inclusion				Displacements	
a/b	a	b	$\pi\ a\ b$	(x_1, y_1)	μ_1	λ_1	μ_2	λ_2	u_{max}	v_{max}
$\frac{3}{2}$	$\frac{3}{2}$	1	$\frac{3\pi}{2}$	$(0,0)$	3	4	1	1	2.27259	2.32332
					3000	4000	1	1	2.15595	2.19496
					1	1	1	1	2.43321	2.43245
					1	1	3	4	0.90275	0.85351
					1	1	30	40	0.28303	0.21614

4.4.2 Stress Equilibrium Equations In MIPs

Multiple inclusion problems (MIPs) are characterized by two or more inclusions surrounded by a matrix medium. As in the case of the single inclusion problems (SIPs), the matrix and inclusion phases exhibit different material properties. Each of the inclusions can further possess properties different from each other. Figure 4.32 represents a rather basic geometrical model of a multiple inclusion problem with a square-shaped matrix (with Lamè

constants μ_3, λ_3) encompassing two elliptical inclusions (with Lamè constants μ_1, λ_1 and μ_2, λ_2 respectively). The boundary value problem comprises of the governing equation i.e., the stress equilibrium equation as described by Equation (4.39), and homogeneous Dirichlet boundary conditions i.e. zero displacement conditions at the boundary.

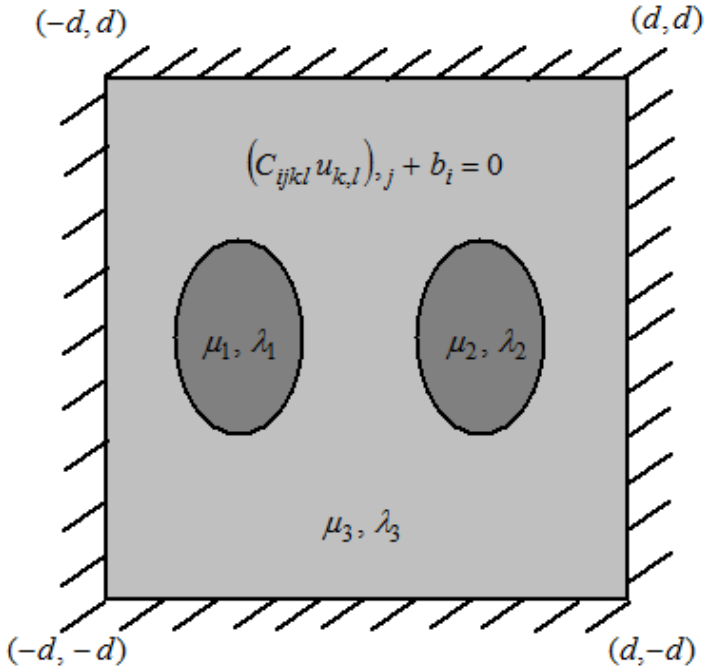

Figure 4.32 Elasticity equilibrium equation for a TIP.

As discussed earlier, six trial functions are defined, corresponding to the x and y components of displacement and the three distinct phases of the given medium, as follows:

$$(f_x(x,y))_1 = c_0 + c_1(x) + c_2(y) + c_3(x^2) + c_4(xy) + c_5(y^2) + \ldots\ldots\ldots + c_{k-1}(\ldots), \quad (4.68)$$

$$\left(f_y(x,y)\right)_1 = c_k + c_{k+1}(x) + c_{k+2}(y) + c_{k+3}(x^2) + c_{k+4}(xy) + \ldots\ldots\ldots + c_{2k-1}(\ldots), \quad (4.69)$$

$$(f_x(x,y))_2 = c_{2k} + c_{2k+1}(x) + c_{2k+2}(y) + c_{2k+3}(x^2) + \ldots\ldots\ldots + c_{3k-1}(\ldots), \quad (4.70)$$

$$\left(f_y(x,y)\right)_2 = c_{3k} + c_{3k+1}(x) + c_{3k+2}(y) + c_{3k+3}(x^2) + \ldots\ldots\ldots + c_{4k-1}(\ldots), \quad (4.71)$$

$$(f_x(x,y))_3 = (x^2 - d^2)(y^2 - d^2)\,(c_{4k} + c_{4k+1}(x) + c_{4k+2}(y) + \ldots\ldots\ldots + c_{5k-1}(\ldots)), \quad (4.72)$$

$$\left(f_y(x,y)\right)_3 = (x^2 - d^2)(y^2 - d^2)(c_{5k} + c_{5k+1}(x) + c_{5k+2}(y) + \ldots\ldots\ldots + c_{6k-1}(\ldots)), \quad (4.73)$$

where $c_0,\ c_1,\ldots,\ c_{6k-1}$ are the coefficients associated with the trial functions. Equations (4.68), (4.69), (4.70) and (4.71) are the trial functions associated with the two inclusions (starting from the left), while Equations (4.72) and (4.73) are the trial functions corresponding to the matrix phase that also satisfy the zero displacement boundary conditions. The trial functions, so defined, are subject to the continuity conditions of displacement and traction that read

$$(f_i(x,y))_j|_{interface} = (f_i(x,y))_3|_{interface}, \qquad (i = x,y), \qquad (j = 1,2), \quad (4.74)$$

$$(t_i(x,y))_j|_{interface} = (t_i(x,y))_3|_{interface,} \qquad (i = x,y), \qquad (j = 1,2), \quad (4.75)$$

where i indicates the direction (or displacement component) and j represents the constituent phases. Equation (4.74) forks out into four equations of continuity, and so does Equation (4.75). This results in eight continuity conditions that are solved to obtain expressions for the unknown coefficients, $c_0,\ c_1,\ldots,\ c_{4k-1}$, that are substituted back into the trial functions from which the permissible functions can be obtained by extracting the polynomials associated with the residual coefficients. Three sets permissible functions result corresponding to the three distinct phases, with each set consisting of displacement permissible functions in the x and y directions. As in SIPs, the permissible functions are obtained in terms of the geometrical and material constants of the heterogeneous medium, and in a compact form, read

$$e_i = e_i(a,b,d,\mu_1,\lambda_1,\mu_2,\lambda_2,\mu_3,\lambda_3,x_1,x_2,x,y). \quad (4.76)$$

where x_1 and x_2 are the positions of the inclusions along the x-axis. As before, the analytically derived permissible functions are treated using the RRM based on following schematic:

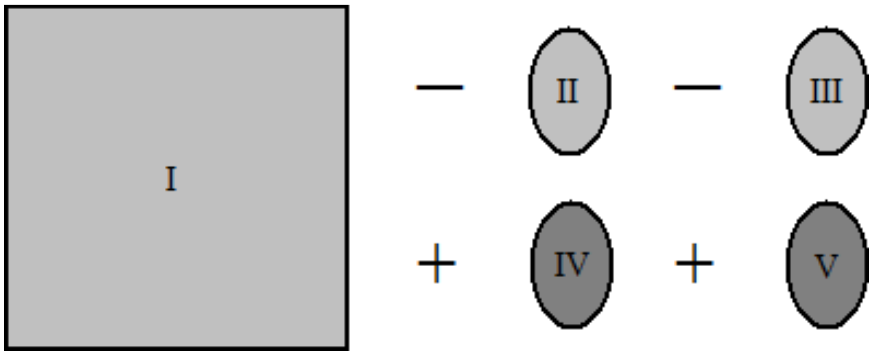

Figure 4.33 Geometrical decomposition of the TIP into its constituent phases.

To begin with, the displacements associated with each of the regions (I, II, III, IV, and V) are approximated, with $u_3(x,y)$ and $v_3(x,y)$ representing the approximate assumed displacement solutions in the x and y directions, respectively, for the matrix phase (regions I, II, and III); $u_1(x,y)$ and $v_1(x,y)$ denoting the corresponding displacement solutions for the inclusion on the left (region IV), while $u_2(x,y)$ and $v_2(x,y)$ are the associated displacement solutions for inclusion on the right (region V). The quantities, $u_1(x,y), v_1(x,y), u_2(x,y)$, and $v_2(x,y)$, are described by Equations (4.62), (4.63), (4.64), and (4.65), respectively, wherein $g_{1i}(x,y)$ and $h_{1i}(x,y)$, and $g_{2i}(x,y)$ and $h_{2i}(x,y)$, now represent the permissible functions, in the x and y directions, that correspond to the inclusions on the left and right, respectively. The quantities, $u_3(x,y)$ and $v_3(x,y)$, are defined as

$$u_3(x,y) = \sum_{i=1}^{N} \alpha_i \, g_{3i}(x,y), \tag{4.77}$$

$$v_3(x,y) = \sum_{i=N+1}^{2N} \alpha_i \, h_{3i}(x,y), \tag{4.78}$$

where $g_{3i}(x,y)$ and $h_{3i}(x,y)$, are the displacement permissible functions along the x and y directions, respectively, for the matrix phase. Next, the expressions for the potential energy associated with each of the regions, namely Π_{I}, Π_{II}, Π_{III}, Π_{IV}, Π_{V} are evaluated as

$$\Pi_i = \frac{1}{2}\iint_i \Big((2\,\mu_3 + \lambda_3)\left({u_3}_{,x}{}^2 + {v_3}_{,y}{}^2\right) + \mu_3\left(u_{3,y} + v_{3,x}\right)^2 + 2\,\lambda_3\, u_{3,x}\, v_{3,y} - 2\left(b_x u_3 - b_y\, v_3\right)\Big)\, dx\; dy, \qquad (i = \mathrm{I}, \mathrm{II}, \mathrm{III}), \tag{4.79}$$

$$\Pi_{\mathrm{IV}} = \frac{1}{2}\iint_{\mathrm{IV}} \Big((2\,\mu_1 + \lambda_1)\left({u_1}_{,x}{}^2 + {v_1}_{,y}{}^2\right) + \mu_1\left(u_{1,y} + v_{1,x}\right)^2 + 2\,\lambda_1\, u_{1,x}\, v_{1,y} - 2\left(b_x u_1 - b_y\, v_1\right)\Big)\, dx\; dy, \tag{4.80}$$

$$\Pi_{\mathrm{V}} = \frac{1}{2}\iint_{\mathrm{V}} \Big((2\,\mu_2 + \lambda_2)\left({u_2}_{,x}{}^2 + {v_2}_{,y}{}^2\right) + \mu_2\left(u_{2,y} + v_{2,x}\right)^2 + 2\,\lambda_2\, u_{2,x}\, v_{2,y} - 2\left(b_x u_2 - b_y\, v_2\right)\Big)\, dx\; dy. \tag{4.81}$$

Combining Equations (4.79), (4.80), and (4.81) according to the schematic depicted above, the potential energy of the entire heterogeneous system, Π, is obtained as

$$\Pi = \Pi_{\mathrm{I}} - \Pi_2 - \Pi_3 + \Pi_4 + \Pi_5. \tag{4.82}$$

Equation (4.82) is further subjected to the principle of minimum potential energy that results in the determination of the unknown coefficients, α_i.

Presented henceforth are the approximate displacement solutions (that conform to a 10$^{\text{th}}$ order approximation with $N = 86$) for the following chosen values of the geometrical and material constants: $a = 1$, $b = 1.5$, $d = 4$, $\mu_1 = \mu_2 = 30$, $\lambda_1 = \lambda_2 = 40$, $\mu_3 = 1$, and $\lambda_3 = 1$, with $b_x = b_y = 1$. Figures (4.34) and (4.35) illustrate the cross-sectional displacement profiles for

$u(x,y)$ along the x-axis, and $v(x,y)$ along the y-axis, respectively. The afore-mentioned cross-sectional plots also display the corresponding displacement solutions obtained from *Ansys*. It is observed that the profile obtained using the suggested semi-analytical approach is consistent with that obtained from a purely numerical scheme.

Figures (4.36) and (4.37) depict the 3-D displacement profile, while Figures (4.38) and (4.39) show the displacement contour plots for $u(x,y)$ and $v(x,y)$, respectively. Furthermore, three cases, namely, a homogeneous medium, a heterogeneous medium with a single centrally located elliptical inclusion, and a heterogeneous medium with two elliptical inclusions (symmetrically located about the y-axis) positioned at $(x_1,y_1) \equiv (-2,0)$ and $(x_2,y_2) \equiv (2,0)$, are compared to study the effect on the displacement fields due to the number of inclusions. Figures (4.40) and (4.41) present the results of this investigation in the form of cross-sectional plots for $u(x,y)$ along the x-axis, and $v(x,y)$ along the y-axis, respectively. Table 4.5 provides a self-explanatory inference of this study by comparing the maximum displacements in each of the three scenarios.

Also, a study is carried out to investigate the effect of varying the distance between the two inclusions, on the displacement fields. Figures (4.42) and (4.43) offer the results of this study, with Table 4.6 summarizing this study by comparing the maximum displacements for each of the cases. It can be seen that as the inclusions move away from each other towards the periphery of the matrix, there is a decrease in the maximum displacement, thus rendering increased stiffness to the overall heterogeneous system.

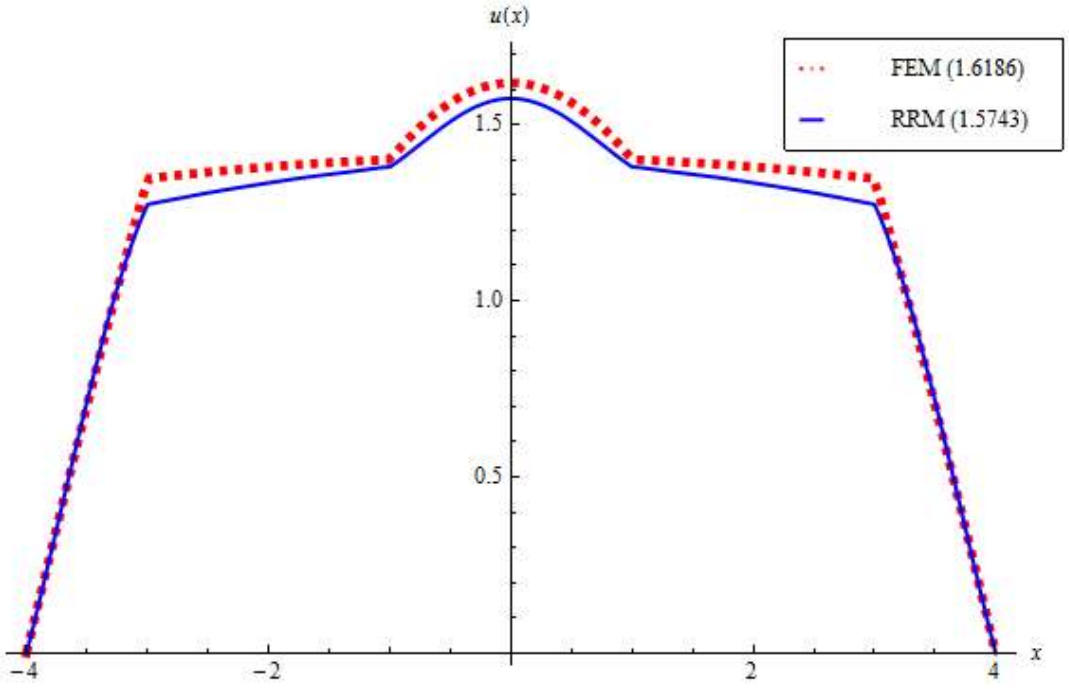

Figure 4.34 Comparison between the RRM and FEM solution for the x-component of displacement in the TIP.

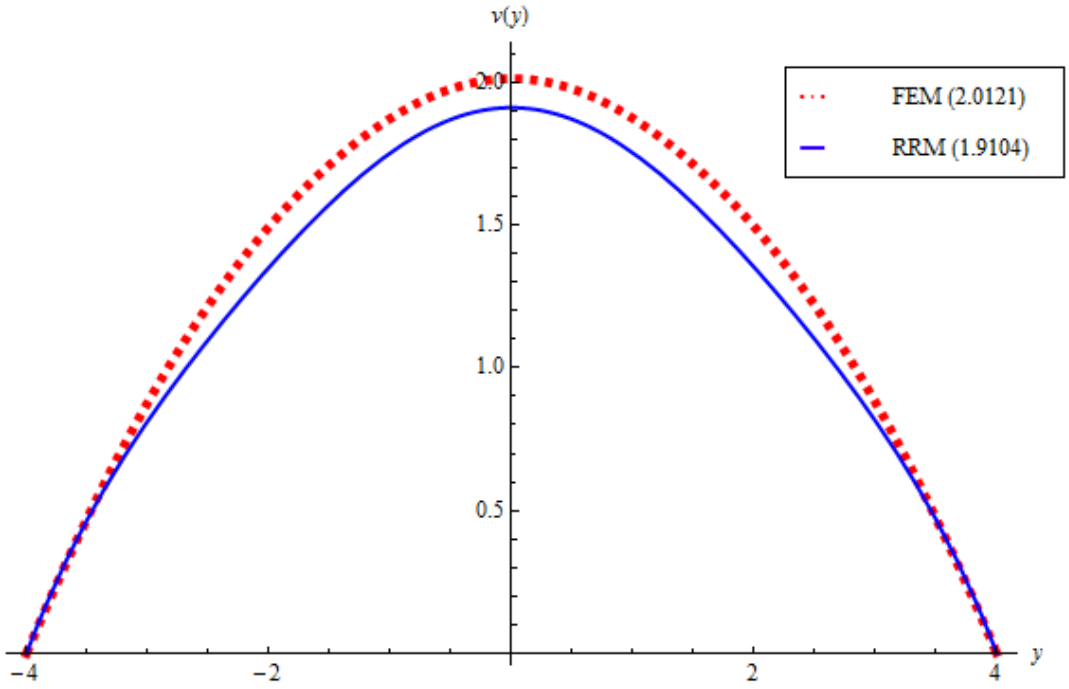

Figure 4.35 Comparison between the RRM and FEM solution for the y-component of displacement in the TIP.

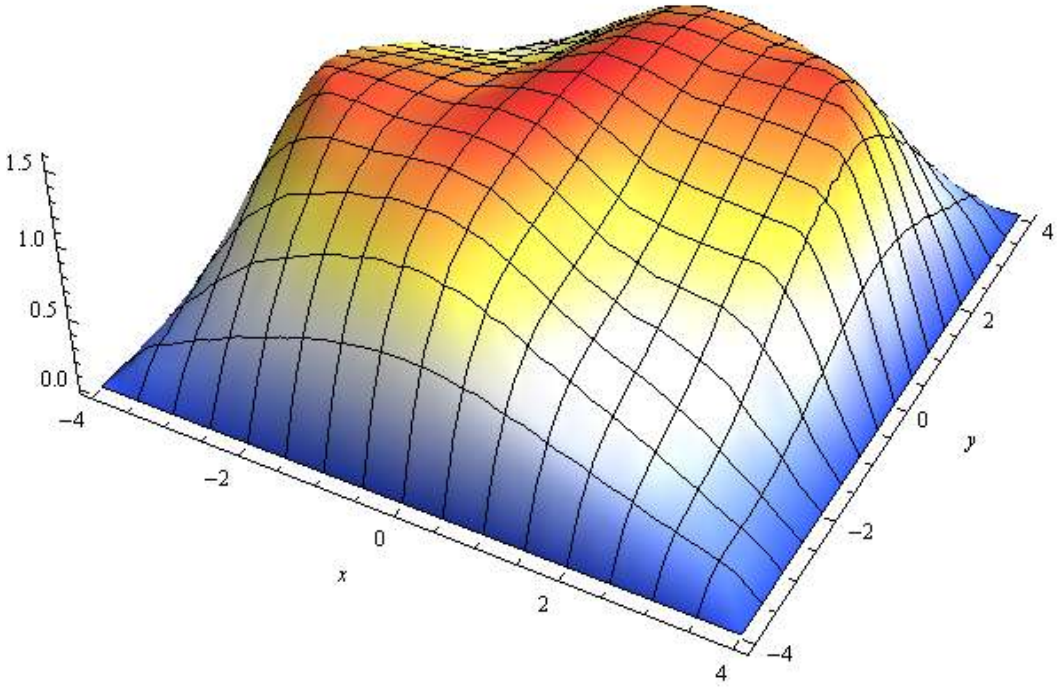

Figure 4.36 3-D profile of the x-component of displacement for the TIP.

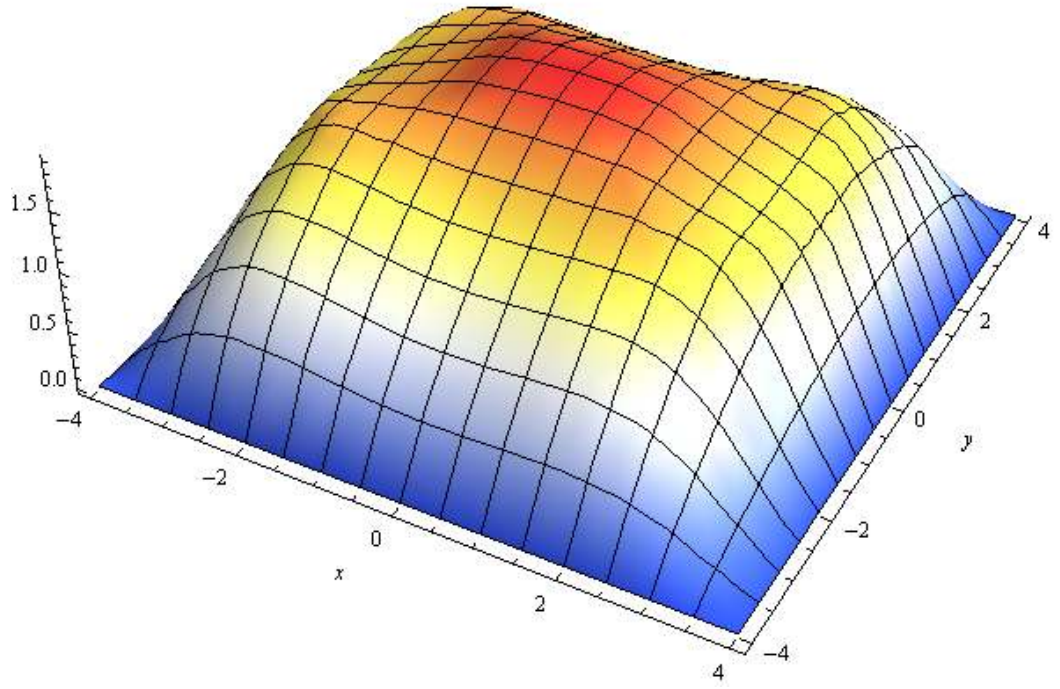

Figure 4.37 3-D profile of the y-component of displacement for the TIP.

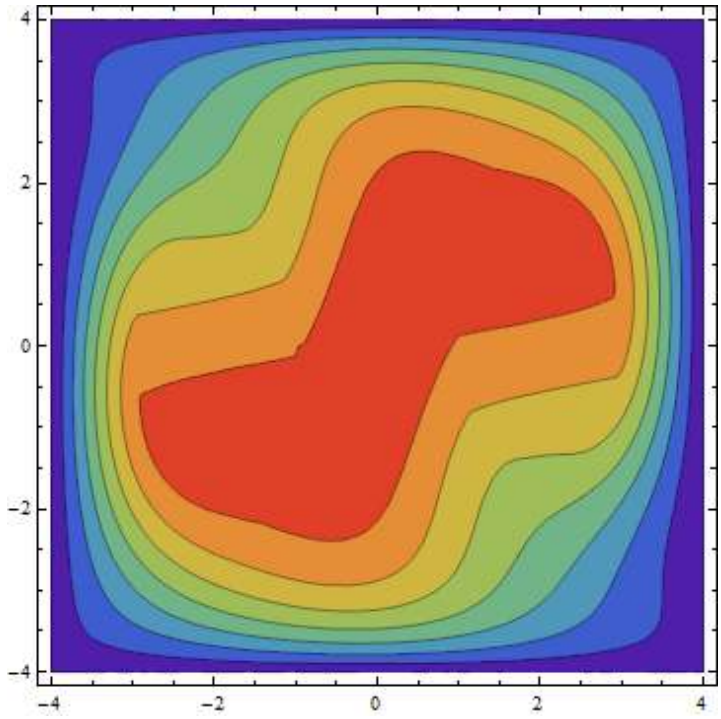

Figure 4.38 Contour plot of the x-component of displacement for the TIP.

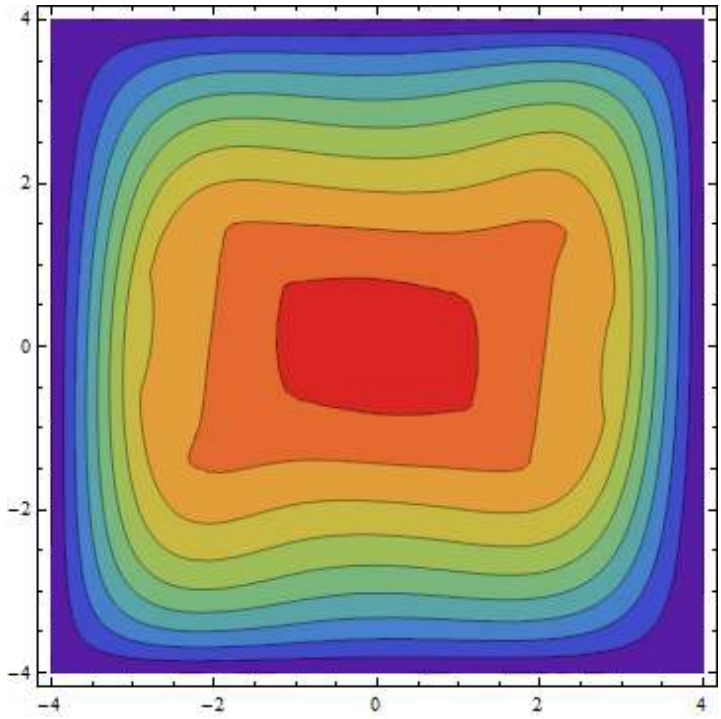

Figure 4.39 Contour plot of the y-component of displacement for the TIP.

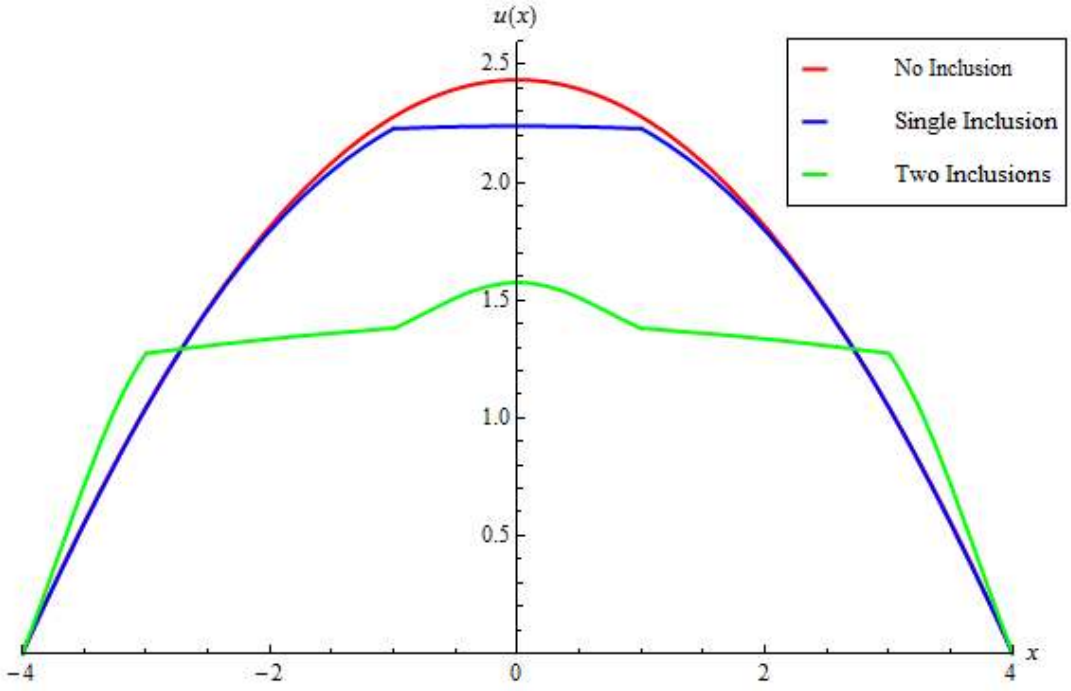

Figure 4.40 Effect of varying the number of inclusions on the x-component of displacement.

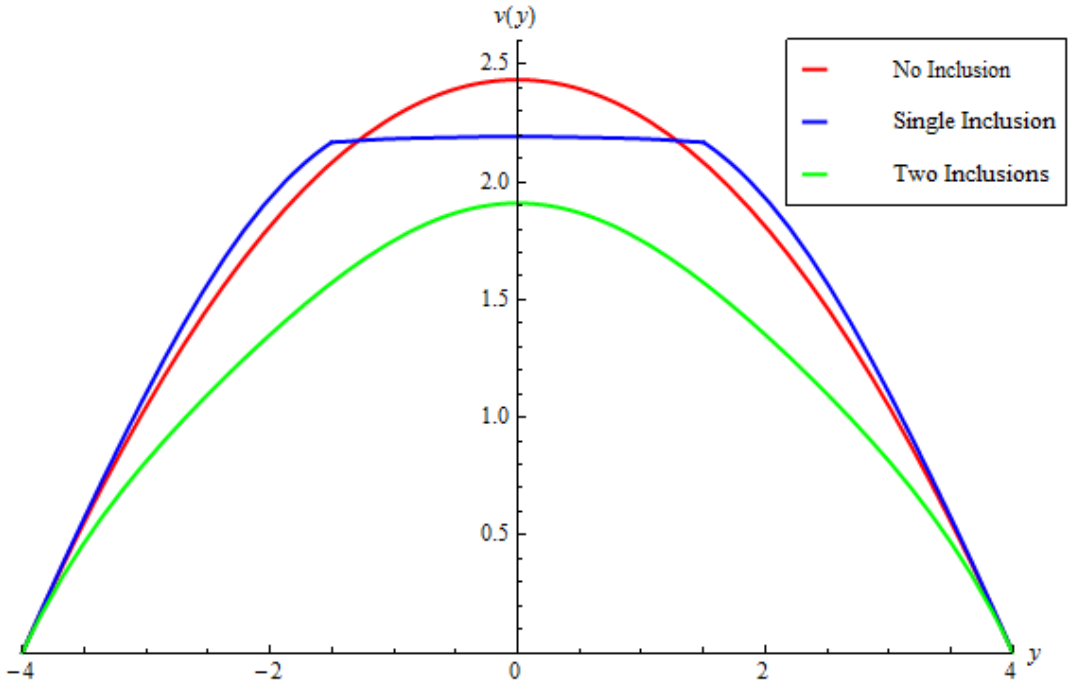

Figure 4.41 Effect of varying the number of inclusions on the y-component of displacement.

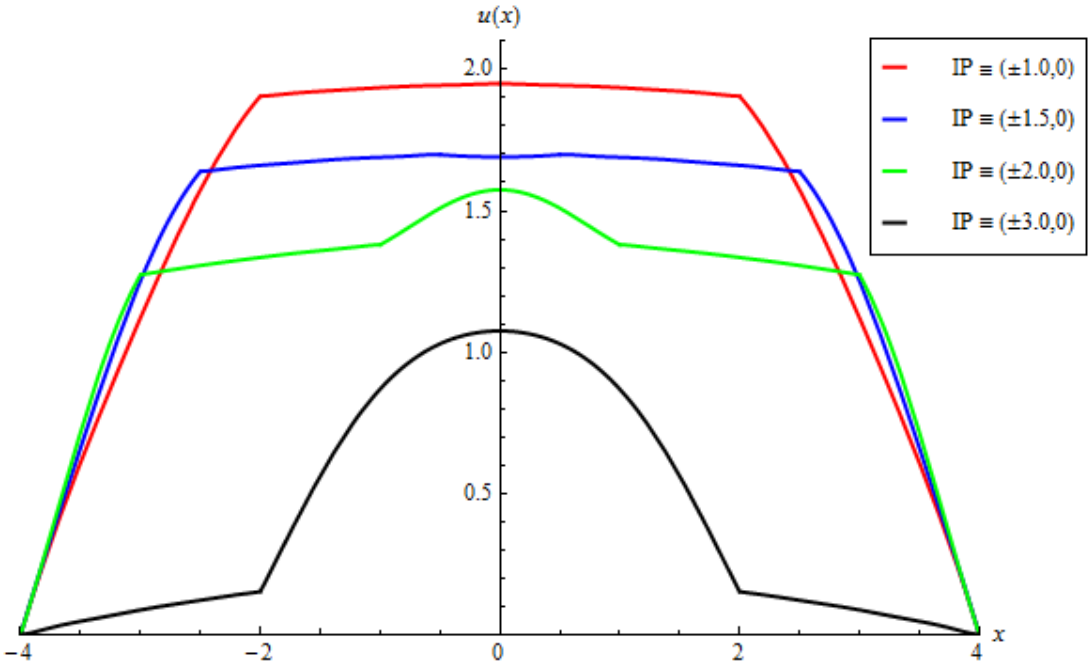

. Figure 4.42 Effect of symmetrically varying the inclusion positions on the x-component of displacement for the TIP.

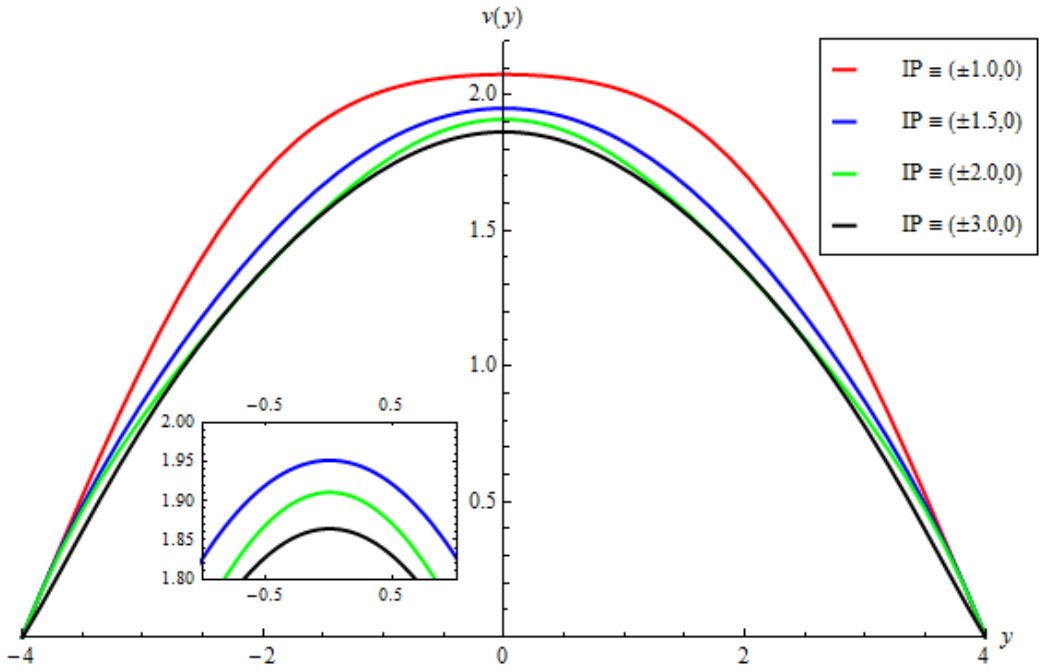

Figure 4.43 Effect of symmetrically varying the inclusion positions on the y-component of displacement for the TIP.

Table 4.5 Effect of varying the number of inclusions on the displacement fields for the TIP

Number of inclusions	Inclusion position		Displacement fields	
	(x_1, y_1)	(x_2, y_2)	u_{max}	v_{max}
0	NA		2.4349277	2.4349277
1	$(0,0)$		2.2385314	2.1937528
2	$(-2,0)$	$(2,0)$	1.5743422	1.9104285

Table 4.6 Effect of varying the inclusion positions on the displacement fields for the TIP

Constant parameters for the inclusion										Inclusion positions			Displacement fields	
a/b	a	b	$\pi\ a\ b$	μ_1	μ_2	μ_3	λ_1	λ_2	λ_3	(x_1, y_1)	(x_2, y_2)	w	u_{max}	v_{max}
$\frac{2}{3}$	1	1.5	$\frac{3\pi}{2}$	30	30	1	40	40	1	$(-1, 0)$	$(1, 0)$	2	1.9503	2.0761
										$(-1.5, 0)$	$(1.5, 0)$	3	1.6907	1.9511
										$(-2, 0)$	$(2, 0)$	4	1.5743	1.9104
										$(-3, 0)$	$(3, 0)$	6	1.0748	1.8641

CHAPTER 5

CONCLUSION

In this dissertation, a semi-analytical approach was presented to solve 2-D boundary value problems for heterogeneous materials, in an effort to obtain and study their physical fields. It was J.D. Eshelby's pioneering work (1957) in the field of micromechanics, specifically his work on ellipsoidal inclusions, which provided the rudimentary thought behind this treatise. Sixty years later, the domain of micromechanics is still an extensively researched area with various methods being introduced, time and again, reiterating its effectiveness in analyzing and treating inhomogeneity problems. However, due to its inability to accurately model heterogeneous materials, and also due to the analytically intractable nature of some of the closed formed integrals, there is always an increasing thirst to formulate efficient techniques that counteract these concerns. Furthermore, analytical solutions are almost impossible to obtain for such open-ended problems, and with numerical techniques being computationally expensive, semi-analytical methods are highly sought after. With the afore-mentioned factors, serving as a backdrop, this dissertation was aimed at developing a versatile semi-analytical approach that clearly distinguishes the inclusion and matrix as two distinct phases and accommodates the existence of a finite boundary. The approach basically involves analytically deriving a set of continuous permissible functions in terms of geometrical and material constants, that satisfy the boundary conditions and continuity conditions at the matrix-inclusion interface, and employing suitable approximation techniques to obtain an expression for the physical fields of interest.

In order to validate the potency of the approach, two case studies were presented. One of them was the 2-D Poisson type equation that essentially translates into the 2-D steady state heat equation with internal heat generation, in a heterogeneous medium characterized by two

elliptical inclusions embedded in a square-shaped matrix medium with different material properties and subjected to homogeneous Dirichlet boundary conditions. As a primer to the two inclusions problem, two subcases were dealt with. In the first example, the same BVP was solved for a homogeneous medium and the resulting temperature field was compared with the readily available Fourier series solution and further corroborated by a finite element solution. In the second instance, a centrally located elliptical inclusion was introduced into the homogeneous medium, thus rendering a heterogeneous setup, for which an approximate expression for the temperature field was obtained using the suggested approach and subsequently compared with the corresponding FEM solution. A parametric study/sensitivity analysis is carried out for each of the heterogeneous media described above so as to study the effect of varying geometrical and material parameters on the resulting temperature field. For the Poisson type equation, the eigenfunction expansion method was the suggested approximation technique in which the Galerkin method was employed to obtain a set of orthonormal eigenfunctions, a linear combination which yields the temperature solution.

The other case study was the 2-D stress equilibrium equation with body forces in heterogeneous media, which in essence forms the crux of this dissertation. Once again, three cases are considered - a homogeneous medium, a heterogeneous medium with a single inclusion and finally a matrix medium with two inclusions, subjected to zero displacement boundary conditions. With the Galerkin technique proving ineffective, the Rayleigh-Ritz method, based on the principle of minimum potential energy, was used and successfully incorporated, to obtain the expressions for the displacement fields. For all of the above scenarios, expressions for the displacement fields were determined and corroborated with their respective FEM solutions, and a parametric study was conducted to investigate the effect of altering the aspect ratios, positions and elastic constants of the inclusion on the resulting displacement fields. It should be noted that the FEM solutions were used only to check for the consistency of the semi-analytical solution profiles and do not serve as the ultimate basis of comparison.

Besides the fact that the semi-analytical approach was successfully employed to treat BVPs in a heterogeneous medium, the effectiveness of the approach can also be measured through the analytically derived continuous permissible functions that are obtained in terms of the geometrical and material constants that characterize the heterogeneous system. One such computer generated displacement permissible function is illustrated below:

$$-\frac{(a^2-x^2-y^2)(\mu_1^2+6\lambda_1\mu_2+4\mu_1\mu_2)}{3\big(\mu_1(-3\lambda_2+\mu_1-\mu_2)+\lambda_1(\mu_1+2\mu_2)\big)}+\frac{(5a^2-x^2-y^2)\mu_1\mu_2}{3\big(\mu_1(-3\lambda_2+\mu_1-\mu_2)+\lambda_1(\mu_1+2\mu_2)\big)}$$

$$-\frac{(a^2-x^2-y^2)\mu_1(3\lambda_1+2\mu_1)}{3\big(\mu_1(-3\lambda_2+\mu_1-\mu_2)+\lambda_1(\mu_1+2\mu_2)\big)}$$

$$+\frac{\big(4a^2-3(x^2+y^2)\big)\mu_1(3\lambda_2+2\mu_2)}{3\big(\mu_1(-3\lambda_2+\mu_1-\mu_2)+\lambda_1(\mu_1+2\mu_2)\big)},$$

where a is the radius of the circular inclusion, d is the parameter that describes the size of the square-shaped matrix, μ and λ represent the material constants and the indices, 1 and 2, represent the inclusion and matrix phase, respectively. Having the permissible functions readily available in the form of analytic expressions, as shown above, facilitates parametric investigations with relative ease. Furthermore, the availability of permissible functions also imparts versatility to the semi-analytical approach. This tendency was observed during the solution process of the 2-D stress equilibrium equation. While the Galerkin method worked well for the 2-D Poisson type equation, it was rendered ineffective when imposed on the displacement permissible functions of the stress equilibrium equation. However, the flexibility of the permissible functions made it possible for them to be applied in a different approximation scheme, namely the Rayleigh-Ritz method. Thus, in totality, the semi-analytical approach offers a unified methodology to solve general boundary value problems in heterogeneous media. Now is a good time as any to mention that analytically deriving the permissible functions was a very tedious and time consuming process. This was facilitated with the help of *Mathematica*.

During the course of this dissertation, the semi-analytical solutions were superposed with the FEM solutions to check for consistency in the solution profiles. It was also observed that the semi-analytical and the purely numerical solutions were in favorable agreement with each other. So, a question that surfaces is why a semi-analytical method, when a reasonable solution can be obtained using FEM. Firstly, for a heterogeneous system that contains multiple inclusions, purely numerical methods can turn out to be a computationally expensive enterprise. In addition, if the heterogeneous medium contains very small inclusions, finite element meshing can be a daunting task. However, the semi-analytical approach can be conveniently extended to solve multiple inclusion problems as well as limiting cases, wherein the size of the inclusions is infinitesimally small. Presented below are the results of one such investigation. The problem under deliberation is the 2-D Poisson type equation in a heterogeneous medium comprising of a single, centrally located, circular inclusion, of radius a, embedded in a square-shaped matrix medium of length $2d$ with its center positioned at the origin, and subjected to homogeneous Dirichlet boundary conditions. The radius of the inclusion is varied from $a = 1$ to $a = 1/10^6$, and its effect on the resulting temperature field is documented. Table 5.1 provides a summary of the results, in which the minor variations in the maximum temperature (as $a \to 0$) can be observed.

Table 5.1 Effect of varying radius of the inclusion on the temperature field for the SIPs

Constant parameters of the inclusion		Varying parameters for the inclusion	
(x_1, y_1)	k_1/k_2	a	Maximum Temperature
$(0,0)$	$\frac{100}{1}$	1	4.4648697601
		10^{-2}	4.7066726999
		10^{-4}	4.7066963497
		10^{-6}	4.7066963520

Besides the afore-mentioned reasons, another primary reason for adopting semi-analytical methods over their numerical counterparts is that it offers an expression for the

physical field of interest. As an illustration, for the BVP discussed above, presented below is a part of the expression of the resulting temperature field (for $a = 1$) that corresponds to an 8th order approximation:

$$-0.0000106892 \times \text{If}[x^2 + y^2 \leq 1,\ 1.56447 - 12.4432\, x^2 + 20.7597\, x^4 - 9.69242\, x^6 - 12.4432\, y^2 + 41.5217\, x^2 y^2 - 29.0788\, x^4 y^2 + 20.7597\, y^4 - 29.0788\, x^2 y^4 - 9.69242\, y^6,\ 0.315205 - 0.147223\, x^2 + 0.0218467\, x^4 - 0.00129672\, x^6 + 0.0000268393\, x^8 - 0.147223\, y^2 + 0.0449248\, x^2 y^2 - 0.00438828\, x^4 y^2 + 0.000161563\, x^6 y^2 - 1.67746\times10^{-6}\, x^8 y^2 + 0.0218467\, y^4 - 0.00438828\, x^2 y^4 + 0.000269447\, x^4 y^4 - 5.03237\times10^{-6}\, x^6 y^4 - 0.00129672\, y^6 + 0.000161563\, x^2 y^6 - 5.03237\times10^{-6}\, x^4 y^6 + 0.0000268393\, y^8 - 1.67746\times10^{-6}\, x^2 y^8] + \ldots\ldots\ldots\ldots.$$

In all generality, the semi-analytical approach compounded with the versatility of the ellipsoidal geometry in approximating heterogeneities, can be extensively exercised in the accurate analysis of short fiber composites, as well as modeling of macroscopic (effective) properties of fiber reinforced and random fiber reinforced composites, among other applications in the fields of electronic packaging and metallurgy. Also, considering the versatility of this method in solving two dimensional BVPs, the approach could be extended to solve 3-D problems. Moreover, the suggested approach is based on concrete formulations that aid in explaining the solution process involved in obtaining the physical field, which in turn encourages the development of computationally efficient techniques. In this regard, the semi-analytical approach presented in this dissertation paves the way for future research towards obtaining permissible functions for more complex geometries as well as non-homogeneous boundary conditions, and improving the accuracy of the solution.

REFERENCES

[1] Larry C. Andrews, *Elementary Partial Differential Equations with Boundary Value Problems*, Academic Press, Inc., Orlando, FL, 1986.

[2] Haïm Brezis and Felix Browder, "Partial Differential Equations in the 20th Century," *Advances in Mathematics*, Vol. 135, Iss. 1, 1998, pp. 76-144.

[3] Y. C. Fung, *A First Course in Continuum Mechanics*, Prentice-Hall, Inc., Englewood Cliffs, NJ, 1977.

[4] Jianmin Qu and Mohammed Cherkaoui, *Fundamentals of Micromechanics of Solids*, John Wiley & Sons, Inc., Hoboken, NJ, 2006.

[5] Sia Nemat-Nasser and Muneo Hori, *Micromechanics: Overall Properties of Heterogeneous Materials*, Elsevier Science B.V., Amsterdam, The Netherlands, 1999.

[6] Valeriy Buryachenko, *Micromechanics of Heterogeneous Materials*, Springer Science+Business Media, LLC, New York, NY, 2007.

[7] J. D. Eshelby, "The determination of the elastic field of an ellipsoidal inclusion, and related problems," *Proceedings of the Royal Society of London, Series A, Mathematical and Physical Sciences*, Vol. 241, Iss. 1226, 1957, pp. 376-396.

[8] J. D. Eshelby, "The elastic field outside an ellipsoidal inclusion," *Proceedings of the Royal Society of London, Series A, Mathematical and Physical Sciences*, Vol. 252, Iss. 1271, 1959, pp. 561-569.

[9] J. D. Eshelby, "On The Elastic Interaction Between Inclusions," *Acta Metallurgica*, Vol. 14, Iss. 10, 1966, pp. 1306-1309.

[10] M. A. Jawson and R. D. Bhargava, "Two-dimensional elastic inclusion problems," *Mathematical Proceedings of the Cambridge Philosophical Society*, Vol. 57, Iss. 03, 1961, pp. 669-680.

[11] R. D. Bhargava and H. C. Radhakrishna, “Two-dimensional elliptic inclusions,” *Mathematical Proceedings of the Cambridge Philosophical Society*, Vol. 59, Iss. 04, 1963, pp. 811-820.

[12] R. D. List and J. P. O. Silberstein, “Two-dimensional elastic inclusion problems,” *Mathematical Proceedings of the Cambridge Philosophical Society*, Vol. 62, Iss. 02, 1966, pp. 303-311.

[13] F. J. Rizzo and D. J. Shippy, “A formulation and solution procedure for the general non-homogeneous elastic inclusion problem,” *International Journal of Solids and Structures*, Vol. 4, Iss. 12, 1968, pp. 1161-1179.

[14] R. D. List, “A two-dimensional circular inclusion problem,” *Mathematical Proceedings of the Cambridge Philosophical Society*, Vol. 65, Iss. 03, 1969, pp. 823-830.

[15] N. I. Muskhelishvili, *Some basic problems of the mathematical theory of elasticity*, P. Noordhoff, Groningen, The Netherlands, 1953.

[16] R. D. Bhargava and Raj Rani Bhargava, “Elastic circular inclusion in an infinite plane containing two cracks,” *International Journal of Engineering Science*, Vol. 11, Iss. 04, 1973, pp. 437-449.

[17] Toshio Mura, *Micromechanics of Defects in Solids*, Martinus Nijhoff Publishers, Dordrecht, The Netherlands, 1987.

[18] T. Mura, T. Mori and M. Kato, “The elastic field caused by a general ellipsoidal inclusion and the application to martensite formation,” *Journal of the Mechanics and Physics of Solids*, Vol.24, 1976, pp. 305 to 318.

[19] Minoru Taya and Tsu-Wei Chou, “On two kinds of ellipsoidal inhomogeneities in an infinite elastic body: an application to hybrid composite,” *International Journal of Solids and Structures*, Vol. 17, 1981, pp. 553-563.

[20] T. Iwakuma and S. Nemat-Nasser, “Composites with periodic microstructure,” *Computers & Structures*, Vol. 16, Iss. 1-4, 1983, pp. 13-19.

[21] Seiichi Nomura and Tsu-Wei Chou, “The viscoelastic behavior of short-fiber composite materials,” *International Journal of Engineering Science*, Vol. 23, No. 2, 1985, pp. 193-199.

[22] Nomura, S. and Oshima, N., “A method to estimate the overall behavior of fiber-reinforced hybrid composites,” *Journal of Composites Technology & Research*, Vol. 7, 1985, pp. 88-92.

[23] Hiroshi Hatta and Minoru Taya, “Equivalent inclusion method for steady state heat conduction in composites,” *International Journal of Engineering Science*, Vol. 24, No. 7, 1986, pp. 1159-1172.

[24] Gregory J. Rodin and Yuh-Long Hwang, “On the problem of linear elasticity for an infinite region containing a finite number of non-intersecting spherical inhomogeneities,” *International Journal of Solids and Structures*, Vol. 27, No. 2, 1991, pp. 145-159.

[25] Muneo Hori and Sia Nemat-Nasser, “Double-inclusion model and overall moduli of multi-phase composites,” *Mechanics of Materials*, Vol. 14, 1993, pp. 189-206.

[26] Gregory J. Rodin, “The overall elastic response of materials containing spherical inhomogeneities,” *International Journal of Solids and Structures*, Vol. 30, No. 14, 1993, pp. 1849-1863.

[27] H. Y. Yu, S. C. Sanday and C. I. Chang, “Elastic Inclusions and Inhomogeneities in Transversely Isotropic Solids”, *Proceedings: Mathematical and Physical Sciences*, Vol. 444, No. 1920, 1994, pp. 239-252.

[28] T. Mura, “The Determination of The Elastic Field of A Polygonal Star Shaped Inclusion,” *Mechanics Research Communications*, Vol. 24, No. 5, 1997, pp. 473-482.

[29] Han Xueli, Wang Tzuchiang, “Elastic fields of interacting elliptic inhomogeneities,” *International Journal of Solids and Structures*, Vol. 36, 1999, pp. 4523-4541.

[30] Muneo Hori, Sia Nemat-Nasser, “On two micromechanics theories for determining micro-macro relations in heterogeneous solids,” *Mechanics of Materials*, Vol. 31, 1999, pp. 667-682.

[31] S. Li, R. Sauer and G. Wang, “A circular inclusion in a finite domain I. The Dirichlet-Eshelby problem,” *Acta Mechanica*, Vol. 179, 2005, pp. 67-90.

[32] Nicolas Brusselaars, Sofia G. Mogilevskaya, Steven L. Crouch, “A semi-analytical solution for multiple circular inhomogeneities in one of two joined isotropic elastic half-planes,” *Engineering Analysis with Boundary Elements*, Vol. 31, 2007, pp. 692-705.

[33] Kevin D. Cole, James V. Beck, A. Haji-Sheikh, Bahman Litkouhi, *Heat Conduction Using Green’s Functions*, Taylor & Francis, Boca Raton, FL, 2011.

[34] C. A. J. Fletcher, *Computational Galerkin Methods*, Springer-Verlag, 1984.

[35] Stephen Wolfram, *The MATHEMATICA Book*, *Third Edition*, Wolfram Media, & Cambridge University Press, 1996.

[36] D.K. Choi and S. Nomura, “Application of symbolic computation to two-dimensional elasticity,” *Computers & Structures*, Vol. 43, No. 4, 1992, pp. 645-649.

[37] S. Nomura and D. L. Ball, “Stiffness reduction due to multiple microcracks in transverse isotropic media,” *Engineering Fracture Mechanics*, Vol. 48, No.5, 1994, pp. 649-653.

[38] R.E. Diaz-Contreras and S. Nomura, “Green’s function applied to solution of Mindlin plates,” *Computers & Structures*, Vol. 60, No. 1, 1996, pp. 41-48.

[39] R.E. Diaz-Contreras and S. Nomura, “Numerical Green’s function approach to finite-sized plate analysis,” *International Journal of Solids and Structures*, Vol. 33, No. 28, 1996, pp. 4215-4222.

BIOGRAPHICAL INFORMATION

The author secured his Ph.D in mechanical engineering from the University of Texas at Arlington in Spring 2013. His research dealt with providing semi-analytical solutions for physical fields in heterogeneous materials with emphasis on the 2-D Poisson type equation and the 2-D stress equilibrium equation.

His research interests include analysis of composite structures, micromechanics, and applied mathematics. He has worked on an array of projects during the course of his academic career, relating to heat transfer, CAD, and finite element analysis.

He intends to work in the aerospace industry as a structural analysis engineer, preferably for the research and development team for a few years after which he would like to setup his own firm that specializes in providing quality engineering solutions to industrial issues.